Jörg Danzer

Surfactant Transport and Coupled Transport of Polycyclic Aromatic Hydrocarbons (PAHs) in Natural Aquifer Material - Laboratory Experiments

Surfactant Transport and Coupled Transport of Polycyclic Aromatic Hydrocarbons (PAHs) in Natural Aquifer Material - Laboratory Experiments

Jörg Danzer

Lehrstuhl für Angewandte Geologie
Institut für Geologie und Paläontologie
Universität Tübingen
Sigwartstraße 10
72076 Tübingen
Germany

Surfactant Transport and Coupled Transport of Polycyclic Aromatic Hydrocarbons (PAHs) and Surfactants in Natural Aquifer Material - Laboratory Experiments

Jörg Danzer [1]

Abstract. Hydrophobic organic contaminants (HOCs) released from non-aqueous phase liquids (NAPLs) impose a serious risk on groundwater quality. The concentrations in groundwater of these toxic, cancerogenic and mutagenic compounds are at many sites far above legal limits. The time scale of contaminant emission could be centuries or longer due to their extremely low water solubility and the diffusion limited dissolution. Due to the same reasons conventional pump and treat remediation techniques can be not successful. Surface active agents (surfactants) are considered to overcome this limitations. Surfactants assemble at the solid-water interface as monomers, monolayers and bilayers (admicelles) depending on the bulk solution surfactant concentration. Above the critical micelle concentration (*CMC*) they form micelles in the aqueous phase due to their amphiphilic (hydrophilic-hydrophobic) properties. HOCs have a high affinity to the hydrophobic surfactant pseudophases created by the hydrophobic, oil-like moieties of the surfactant molecules either adsorbed to the solid (monolayer, bilayer) or mobile in the aqueous phase (monomers, micelles). The increase of the apparent water solubility of HOCs due to partitioning into micelles is known as solubilization. Analogous, the partitioning into adsorbed surfactant admicelles is known as adsolubilization. Thus, the surfactants can act either to enhance or reduce HOCs sorption to aquifer material from the aqueous solution depending on the surfactant concentration. An understanding of the processes influencing the transport of surfactant and the coupled transport of surfactants and HOCs in groundwater is an essential foundation for the design of surfactant enhanced subsurface remediation (SESR) technologies. Therefore, laboratory batch and column experiments were performed using phenanthrene as a chemical probe for the HOCs, different anionic, nonionic and cationic surfactants and different natural aquifer materials. The *CMC* and the surface area per molecule were determined from surface tension measurements. The results show that the *CMC* of the surfactants in the presence of electrolytes is decreased compared to the *CMC* in pure water. The surfactant sorption can be described by a typical nonlinear isotherm consisting of a linear part for concentrations below the *CMC* and an adsorption maximum q_{max} above the *CMC* where a complete surfactant bilayer is established. Different q_{max} values were found for different lithocomponents of the aquifer materials examined. Generally the sandstones show the highest values, followed by Triassic limestones, Jurassic limestones and quartzes. A surfactant specific surface area A_{surf} was calculated from q_{max} and compared to other specific surface areas. The external surface area A_{ext} assuming the aquifer grains as ideal, nonporous spheres shows no influence on A_{surf}, i.e. the grain size does not control surfactant adsorption. The comparison of A_{surf} with the cumulative surface area determined by N_2-adsorption (*BET*) and Hg-intrusion indicates that surfactants can access macropores (> 50 nm) but not mesopores (2 nm - 50 nm) and micropores (< 2 nm). A comparison of A_{surf} with *BET* indicates that in average about 2 % of the BET surface area can be "seen" by surfactants. The surfactant column experiments indicate that the surfactant transport is close to equilibrium and can be reasonably well predicted by the adsorption isotherm. The surfactant adsorption is completely reversible. The adsolubilization kinetics are fast and can be described by a first order process. To distinguish between the contributions to phenanthrene sorption of surfactant monolayers and bilayers the partitioning of phenanthrene onto the surfactant coated aquifer material was quantified over a wide range of surfactant loading. The bilayer partitioning coefficient (K_{bl}) was found to be a factor of 3 larger compared to monolayer partitioning coefficient (K_{bl}). The respective partitioning coefficients to the surfactant pseudophases in the mobile aqueous phase (K_{mic} and K_{mn}) are smaller. The different surfactants show different efficiencies in terms of sorbing phenanthrene from the aqueous phase. However, the coefficients (including literature data) are in a similar range. Thus, the transport behavior of phenanthrene depends strongly on the adsorption behavior of the surfactant present in the system. The retardation of phenanthrene in column experiments increases with increasing surfactant concentration below the *CMC* due to the increasing surfactant loading of the aquifer material (enhanced retardation). The phenanthrene retardation decreases again with further increasing surfactant concentration until a facilitated transport can be observed for surfactant concentrations well above the *CMC*. The phenanthrene distribution coefficients and thus the retardation factors in the presence of surfactants can be reasonably well predicted by a mass balance model. This denotes for the different surfactant pseudophases in the mobile (micelles and monomers) and the immobile (monolayers, bilayers) phase and the respective partitioning coefficients determined in independent equilibrium batch experiments.

[1] Dissertation at "Geowissenschaftliche Fakultät" of the University of Tübingen.
Author's Address: Jörg Danzer, Ludwig Krapf Str. 15, 72072 Tübingen, Germany.

Transport von Tensiden und gekoppelter Transport von polyzyklischen aromatischen Kohlenwasserstoffen (PAKs) und Tensiden in natürlichem Aquifermaterial - Laborexperimente

Jörg Danzer

Kurzfassung: Organische Flüssigkeiten, die nicht mit Wasser mischbar sind (Non-Aqueous Phase Liquids: NAPLs), wie z. B. Benzin, Hydrauliköl, Teeröl, Kreosot, chlorierte Lösemittel etc. gelangten an vielen Standorten (Tankstellen, Gaswerke, Flughäfen, Raffinerien, militärische Liegenschaften, Industrie etc.) in den Untergrund. Obwohl NAPLs als separate Flüssigphasen im Untergrund vorliegen, lösen sich aus ihnen Inhaltsstoffe, die z. T. giftig, krebserregend oder erbgutverändernd sind (z. B. Benzol oder polyzyklische aromatische Kohlenwasserstoffe), in das vorbeifließende Grundwasser und verursachen Schadstofffahnen im Abstrom. Die Konzentrationen dieser organischen Schadstoffe liegen häufig weit über den zulässigen Werten der Trinkwasserverordnung. NAPLs stellen deshalb eine große Gefahr für die Qualität des Grundwassers dar und können dieses für eine Nutzung als Trinkwasser unbrauchbar machen. Aufgrund der geringen Wasserlöslichkeit der NAPL-bürtigen Schadstoffe und der daraus resultierenden langsamen Lösung bleiben NAPLs und damit die Gefährdung Jahrzehnte bzw. Jahrhunderte bestehen. Die langsame Lösung ist auch dafür verantwortlich, daß konventionelle Sanierungsmaßnahmen, bei denen das Grundwasser zur Entfernung der Schadstoffe abgepumpt wird (pump and treat) in einem ökonomisch vertretbarem Zeitraum (< 10 Jahre) nicht erfolgreich sein können. Um diese Limitation zu überwinden, werden grenzflächenaktive Stoffe (Tenside) zur Boden- und Grundwassersanierung eingesetzt. Dabei macht man sich die Eigenschaft des Tensidmoleküls zu nutze, daß es aus einem hydrophilen ("wasseranziehenden") und einem hydrophoben ("wasserabstoßenden") Teil besteht. Aufgrund dieser amphiphilen Eigenschaft lagern sich Tenside vorallem an Grenz- und Oberflächen an. Tenside adsorbieren am Aquifermaterial konzentrationsabhängig als Monomere, in Monolagen oder Doppellagen (Admizellen). Oberhalb der sog. kritischen Mizellenkonzentration (*CMC*) bilden sie dreidimensionale, z.T. kugelförmige Aggregate die als Mizellen bezeichnet werden. Diese bestehen aus einer hydrophilen Hülle und einer hydrophoben Pseudophase im Inneren. Hydrophobe organische Schadstoffe haben eine hohe Affinität zu den hydrophoben Pseudophasen der Tenside, die mobil im Wasser (Monomere, Mizellen) oder sorbiert am Aquifermaterial (Mono- und Doppellagen) vorliegen. Die Wasserlöslichkeit von hydrophoben Schadstoffen wird durch die Tenside scheinbar erhöht was als Solubilisierung bezeichnet wird. Analog wird die Adsorption von hydrophoben Schadstoffen an sorbierten Tensiden als Adsolubilisierung bezeichnet. In Abhängigkeit der Tensidkonzentration kann also die Mobilität von hydrophoben Schadstoffen erhöht oder erniedrigt werden. Ein grundlegendes Verständnis der Prozesse die den Transport von Tensiden und den gekoppelten Transport von hydrophoben Schadstoffen und Tensiden in natürlichem Aquifermaterial kontrollieren ist unabdingbar, um tensidgestützte Boden- und Grundwassersanierungstechnologien optimal planen zu können. Deshalb wurden im Labor Schüttel- (Batch-) und Säulenversuche durchgeführt. Neben Phenanthren als repräsentativen Vertreter für hydrophobe organische Schadstoffe wurden verschiedene kationische, nichtionische und anionische Tenside sowie verschiedene natürliche Aquifermaterialien untersucht. Die *CMC* der Tenside und die Fläche, die ein Tensidmolekül an der Wasser-/Luftgrenzfläche einnimmt, wurde durch die Messung von Grenzflächenspannungen bestimmt. Die Adsorption der Tenside kann durch eine charakteristische nicht-lineare Isotherme beschrieben werden, die sich aus einem linearen Ast unterhalb der *CMC* (Sorption der Monomere) und einem Adsorptionsmaximum q_{max} oberhalb der *CMC* zusammensetzt. Die Lithokomponenten des Aquifermaterials zeigen unterschiedliche q_{max}-Werte. Diese liegen z.B. für Neckarsand für die Sandsteine am höchsten, gefolgt von Jurakalken, Muschelkalken und Quarzen. Aus den Adsorptionmaxima q_{max} wurden tensidspezifische Flächen berechnet (*A_surf*) und mit anderen spezifischen Oberflächen verglichen. Die theoretische, äußere Oberfläche eines Partikels, welcher als ideale, nicht-poröse Kugel angenommen wird, hat keinen Einfluß auf *A_surf*, d.h. daß die Korngröße keinen Einfluß auf die Tensidsorption bis zur Korngrößen kleiner ca. 0.003 mm (Schluff) hat. Der Vergleich von *A_surf* mit der der kumulativen Grenzfläche die aus der Stick-stoff-Adsorption (BET) und Quecksilber-Intrusion bestimmt wurde deutet darauf hin, daß das untersuchte Tensid Flächen in Makroporen (> 50 nm), nicht aber in Meso- (2 nm - 50 nm) und Mikroporen (< 2 nm) erreichen kann. Im Mittel werden ca. 2 % der BET-Grenzfläche von den Tensiden "gesehen". Die Säulenversuche zeigten, daß der

Tensidtransport nahezu unter Gleichgewichtsbedingungen stattfindet und damit aus der Gleichgewichts-Adsorptionsisotherme vorhergesagt werden kann. Die Tensidsorption ist vollständig reversibel. Der Transport von Phenanthren in Anwesenheit von Tensiden wird neben der Sorption am Aquifermaterial durch die Affinität zu den adsorbierten, immobilien Tensiden (Monolagen, Admizellen) und den Tensiden in der mobilen Wasserphase (Monomere, Mizellen) bestimmt. Diese Affinität wurde in Batchexperimenten durch Verteilungskoeffizienten quantifiziert. Der Verteilungskoeffizient zu den sorbierten Tensiddoppellagen (K_{bl}) ist ungefähr einen Faktor 3 größer als zu den Tensidmonolagen (K_{ml}). Die Verteilungskoeffizienten zu den entsprechenden Tensidpseudophasen im mobilen Wasser (Monomere und Mizellen) sind etwas niedriger. Die verschiedenden untersuchten Tenside sind unterschiedlich effizient, um Phenanthren zu solubilisieren bzw. adsolubilisieren. Generell liegen die Veteilungskoeffizienten (Literaturdaten eingeschlossen) jedoch in einem ähnlichen Bereich. Der Transport von Phenanthren hängt deshalb sehr stark vom Adsorptionsverhalten des Tensids im Aquifer ab. In Säulenversuchen wurde gezeigt, daß die Retardation von Phenanthren unterhalb der *CMC* mit steigender Tensidkonzentration und damit steigender Tensidbelegung des Aquifermaterials linear zunimmt (erhöhte Retardation). Die höchste Retardation wird im Bereich der *CMC* beobachtet. Eine Erhöhung der Tensidkonzentration über die *CMC* bewirkt die Abnahme der Retardation infolge der Erhöhung der Mizellenkonzentration in der mobilen Phase. Eine höhere Transportgeschwindigkeit von Phenanthren verglichen mit dem tensidfreien System wird erst bei Konzentrationen deutlich über der *CMC* erreicht. Der Transport von Phenanthren in Säulenexperimenten mit natürlichem Aquifermaterial läßt sich mit einem Massenbilanzmodell, in das die Parameter aus den Batchversuchen eingehen, hinreichend gut vorhersagen.

Table of Contents

Abbreviations

Å	Angstroem = 10^{-10} m
AlOx	Aluminum oxide
AOT	Aerosol OT (bis-2-ethylhexyl sodium sulfosuccinate)
BTC	Breaktrough curve
CMC	Critical micelle concentration
CRA	Canadian River Alluvium, Norman, Oklahoma, USA
DF 8390	Dowfax 8390 (di-anionic surfactant)
DPDS	Di-phenyl oxide disulfonates
EC	Effect concentration
ECEC	Effective cation exchange capacity
EEC	European Economic Community
EINECS	European inventory of existing chemical substances
EO	Ethoxy groups
HDTMA	Hexadecyl-trimethyl ammonium (cationic surfactant)
HH	River Neckar Alluvium (Horckheim)
HOCs	Hydrophobic organic contaminants
HW	Hüntwangen aquifer materials (Switzerland)
IC	Growth inhibition concentration
IUPAC	International Union of Pure and Applied Chemistry
JL	Jurassic limestones
LC	Lethal concentration
mM	Millimolar 10^{-3} M = 10^{-3} mol L^{-1}
MS	Marine seasand (Seesand MERCK)
NAPLs	Nonaqueous phase liquids
OECD	Organization for economic cooperation and development
OPA	Opalinuston (bav = Braunjura, alpha, verwittert Stufe V)
p,p'-DDT	1,1-bis(p-chlorophenyl)-2,2,2-trichloroethane
PAHs	Polycyclic aromatic hydrocarbons
PCB	Polychlorinated biphenyl
Qtz	Industrial artifically broken and sieved quartzes
Qz	Quartz, natural aquifer material
Rh-SS	Rhät sandstones, rock fragments from the source area, artifically broken and sieved
Rh-WT	Rhodamin WT (water tracer), fluorescence dye
RNA	River Neckar Alluvium (Hirschau)
RRA	River rhein aquifer material (Kehl)
SDBS	Sodium dodecyl benzene sulfonate
SDS	Sodium dodecyl sulfate
SESR	Surfactant enhanced subsurface remediation
SMDNS	Sodium mono- and dimethyl naphthalene sulfonate
SS	Sandstones (triassic light sandstones)
TCB	Trichlorobenzene
TL	Triassic limestones (Muschelkalk)
TL$_{br}$	TL (Muschelkalk), rock fragments from the source area, artifically broken and sieved
T-MAZ	Polyethoxylated (POE) sorbitan monolaurate (Tween)
TOC	Total organc carbon
TS G50	Terrasurf G50 (nonionic surfactant)
TS G80	Terrasurf G80 (nonionic surfactant)
TX-100	Triton X-100 (nonionic surfactant)

Notation

A	Cross-sectional area of a column $[L^2]$
A_{ext}	Specific external surface area of an ideal sphere $[L^2\,M^{-1}]$
A_o	Surface area of an ideal sphere (non-porous) $[L^2]$
a_{surf}	Surface area covered by a single surfactant molucule $[L^2]$
A_{surf}	Surfactant specific surface area $[L^2\,M^{-1}]$
a_{surf}	a_{surf} calculated from BET (assumption: surfactants can access the same pores as N_2) $[L^2]$
BET	Specific surface area determined by N_2 adsorption (BET method) $[L^2\,M^{-1}]$
C	Concentration $[M\,L^{-3}]$
C/C_0	Column effluent concentration normalized to the influent concentration C_0 [-]
C_0	Concentration at the beginning of an experiment or column influent concentration $[M\,L^{-3}]$
C_{aq}	Molar concentration of water $[mol\,L^{-3}]$
C_{dot}	Concentration added to a sediment/aqueous batch system $[M\,L^{-3}]$
C_{eq}	Aqueous equilibrium concentration $[M\,L^{-3}]$
C_{eq}	Aqueous equilibrium concentration in the presence of surfactant $[M\,L^{-3}]$
$c_{i,\,aq}$	Molar aqueous concentration of a compound i $[mol\,L^{-3}]$
$C_L,\,C_U$	Lower and upper concentration limit of transition zone of micellation $[M\,L^{-3}]$
C_m	Monitored or measured column effluent concentration $[M\,L^{-3}]$
C_{max}	Monitored maximum signal (fluorescence on-line detection) [-]
CMC	Critical micelle concentration $[M\,L^{-3}]$
CMC_e	Critical micelle concentration in the presence of electrolyte $[M\,L^{-3}]$
CMC_{ec}	Critical micelle concentration determined by electric conductiv $[M\,L^{-3}]$ity
CMC_{st}	Critical micelle concentration determined by a surface tension method $[M\,L^{-3}]$
C_{mic}	Surfactant micelle concentration $[M\,L^{-3}]$
C_{min}	Monitored background signal (fluorescence on-line detection) [-]
C_{mn}	Surfactant monomer concentration $[M\,L^{-3}]$
$C_{phe,\,0}$	Initial phenanthrene concentrations in batch systems without surfactant $[M\,L^{-3}]$
$C_{phe,\,0}$	Initial phenanthrene concentrations in batch systems containing surfactant $[M\,L^{-3}]$
$C_{phe,\,eq}$	Equilibrium phenanthrene concentrations in batch systems without surfactant $[M\,L^{-3}]$
$C_{phe,\,eq}$	Equilibrium phenanthrene concentrations in batch systems containing surfactant $[M\,L^{-3}]$
C_{surf}	Surfactant concentration $[M\,L^{-3}]$
ct	Index for "conservativ tracer"
D_L	Longitudinal hydrodynamic dispersion $[L^2\,T^{-1}]$
erf	Error function
$erfc$	Complementary error function
f_{carbon}	Carbon mass fraction of the surfactant $[M\,M^{-1}]$
f_{oc}	Organic carbon content $[M\,M^{-1}]$
f_{oc}	Organic carbon content increased by surfactant adsorption $[M\,M^{-1}]$
f_w	Fraction in the aqueous phase [-]
k	First order rate constant $[T^{-1}]$
$K_{0.5}$	Distribution coefficient determined from $R_{0.5}$ in a column system $[L^{-3}\,M^{-1}]$
$K_{0.5}(t)$	Nonequilibrium distribution coefficient determined from $R_{0.5}$ in a column system $[L^{-3}\,M^{-1}]$
$K_{aq,\,i}$	Partitioning coefficient between an aqueous surfactant phase i and water [-]
$K_{aq,\,i}$	Partitioning coefficients between water adsorbed surfactant pseudophase [-]
K_{bl}	Water/bilayer partitioning coefficient [-]
K_d	Solid/water partitioning coefficient $[L^3\,M^{-1}]$
K_d	Solid/water partitioning coefficient in the presence of surfactants $[L^3\,M^{-1}]$
$K_d(t)$	Nonequilibrium distribution coefficient $[L^3\,M^{-1}]$
$K_{d,\,mn}$	Surfactant monomer distribution coefficient $[L^3\,M^{-1}]$
$K_{d,surf}$	Distribution coefficient of surfactant $[L^3\,M^{-1}]$
$K_{d,surf}(t)$	Nonequilibrium distribution coefficient of surfactant $[L^3\,M^{-1}]$
K_f	Hydraulic conductivity $[L\,T^{-1}]$
K_{Fr}	Freundlich coefficient $[L^3\,M^{-1}]$
K_L	Langmuir coefficient $[L^3\,M^{-1}]$
$K_{m/m}$	Partitioning coefficient based on mass fractions (mass based partitioning coefficient) $[M\,M^{-1}]$
K_{mic}	Water/micelle partitioning coefficient [-]
K_{mic}	Micelle/Water partitioning coefficient [-]
K_{ml}	Water/monolayer partitioning coefficient [-]

K_{mn}	Water/monomer partitioning coefficient [-]
$K_{n/n}$	Partitioning coefficient based on mole fractions (molar partitioning coefficient) [mol mol^{-1}]
K_{oc}	Distribution coefficient normalized to the organic carbon content [L^3 M^{-1}]
K_{oc}^*	K_{oc} in the presence of surfactants [L^3 M^{-1}]
K_{ow}	Octanol/water partitioning coefficient [-]
$K_{s,}$	Partitioning coefficients between water adsorbed surfactant pseudophase [-]
$K_{s, i}$	Partitioning coefficient between an adsorbed surfactant phase i and the aqueous [-]
K_{surf}	Partitioning coefficients between water and the surfactant pseudophase [-]
K_{tr}	Partitioning coefficient for a transitional region of micellation [-]
$K_{V/m}$	Partitioning coefficient: moles of a compound i per surfactant mass normalized to $c_{i, aq}$ [L^3 M^{-1}]
$K_{V/n}$	Partitioning coefficient: moles of a compound i per surfactant moles normalized to $c_{i, aq}$ [M^{-1}]
K_{vol}	Volumetric distribution coefficient [L^3 L^{-3}]
L	Column length [L]
M_{aq}	Mass of water [M]
$M_{aq, i}$	Mass of the surfactant phase i in water [M]
$M_{HOC, aq}$	HOC mass in the water [M]
$m_{i, aq}$	Mass of a compound i in the aqueous phase [M]
$m_{i, surf}$	Mass of a compound i in a surfactant pseudophase [M]
M_m	HOC mass in the immobile phase [M]
$M_{s, i}$	Mass of the adsorbed surfactant [M]
M_{solid}	Mass of solid [M]
m_{surf}	Mass of surfactant [M]
M_{tot}	Total mass of HOC in a porous medium [M]
MW_{aq}	Molecular weight of water [M mol^{-1}]
MW_{surf}	Molecular weight of surfactants [M mol^{-1}]
MW_{surf}	Molecular weight of the surfactant [M mol^{-1}]
n	Porosity [-]
N_A	Avogadro number [mol^{-1}]
n_{aq}	Number of moles water [-]
n_{Fr}	Freundlich exponent [-]
n_{grav}	Gravimetric determined porosity [-]
$n_{i, aq}$	Number of moles of a compound i in the aqueous phase [-]
$n_{i, surf}$	Number of moles of a compound i in a surfactant pseudophase [-]
n_{surf}	Number of moles surfactant [-]
Pe	Peclet number [-]
PV	Pore volume, number of pore volumes displaced [-]
q	Adsorbed concentration [M M^{-1}]
Q	Flow Rate [L^3 T^{-1}]
q_{bl}	Adsorbed bilayer concentration [M M^{-1}]
q_{max}	Surfactant adsorption maximum [M M^{-1}]
q_{ml}	Adsorbed monolayer concentration [M M^{-1}]
$q_{ml, max}$	Surfactant monolayer adsorption maximum [M M^{-1}]
R	Gas constant [M L^2 T^{-2} mol^{-1} K^{-1}]
r	Radius [L]
$R_{0.5}$	Retardation factor determined from the $t_{0.5}$ ratios of the conservative and reactive tracer [-]
R_d	Retardation factor determined by first moment analysis [-]
rs	Index for "reactive solute"
r_{sw}	Solid/water ratio [-]
T	Temperature [K, °C]
t	Time [T]
$t_{0.5}$	Time when the normalized effluent concentration to reach $C/C_0 = 0.5$ [T]
t_d	Time for the displacement of the system dead volume V_d [T]
t_m	Measured or monitored time [T]
t_{mr}	Mean residence time of a solute within a column system [T]
t_{net}	Netto time corrected with respect to t_m [T]
TOC_{de}	Dissolved organic carbon desorbed from aquifer material [M L^{-3}]
V_{aq}	Volume of water [L^3]
V_d	System dead volume (Volume within fittings, tubing etc. not filled by the porous medium [L^3]
V_o	Volume of an ideal sphere (non-porous) [L^3]
V_{tot}	Total volume of a column system [L^3]

v_x Average linear velocity $[LT^{-1}]$ x Distance [L]

X_{aq} Fraction of phenanthrene in the aqueous phase [-]

$X_{aq,\,i}$ Fractional concentration of the related surfactant phase i in the aqueous phase [-]

$X_{s,\,i}$ Fractional concentration of the related surfactant phase i [-]

X_{surf} Fraction of phenanthrene in the adsorbed surfactant phase [-]

X_{aq}^{HOC} Fractional HOC concentration in water [-]

X_{surf}^{HOC} Fractional concentration of HOC in the surfactant phase [-]

Greek Symbols

α Dispersivity [L]

Γ Surfactant excess concentration at the water/air interface $[mol\ L^{-2}]$

χ Mass fraction of a lithocomponent [-]

σ Standard deviation

γ Surface tension $[M\ T^{-2}]$

ρ_{aq} Density of water $[M\ L^{-3}]$

ρ_b Bulk density $[M\ L^{-3}]$

μ_{ct} First moment of the conservative tracer [T]

μ_{rs} First moment of a reactive solute [T]

ρ_s Solid density of aquifer grains $[M\ L^{-3}]$

ρ_{surf} Density of surfactant $[M\ L^{-3}]$

1 Introduction

Hydrophobic organic contaminants (HOCs) in the subsurface environment pose a serious threat to groundwater resources. Drinking water standards are very low for many HOCs, e.g. polycyclic aromatic hydrocarbons (PAHs) due to their toxic, carcinogenic and mutagenic potential. These compounds, even at minor concentrations, impose a serious risk on groundwater quality (Menzie et al., 1992).

The sources of HOCs in many cases are nonaqueous phase liquids (NAPLs) present as pools or residual phase in the aquifer (e.g. tar-oil at former manufactured gas plant sites, chlorinated solvents). Since the release of HOCs from NAPLs and the desorption of HOCs from the aquifer material is limited by slow aqueous diffusion (Grathwohl and Reinhard, 1993; Grathwohl, 1998; Merkel, 1996; Loyek, 1998a; Eberhard, 1997), existing subsurface remediation techniques, e.g "pump and treat", require very long time periods and high operating costs. Recently, surfactant enhanced in-situ subsurface remediation technologies (SESR), based on specific interactions between surfactants and NAPL, have been evaluated (West and Harwell, 1992). A general scheme of an aquifer contaminated by NAPLs and possible SESR applications are shown in Fig. 1-1.

These interactions include (i) surfactant-induced reduction of interfacial tension in order to mobilize the nonaqueous phase ("mobilization", Abriola et al., 1995; Pennell et al., 1994 and 1997; Okuda et al., 1996; Crawford et al., 1997; Bai et al., 1997), (ii) bulk extraction of nonaqueous phase liquids by ultra-low interfacial tension associated with the in-situ formation of microemulsions (Clemens et al., 1993; Shiau et al., 1996 and 1994; Klier et al., 1997), (iii) micellar "solubilization" to enhance desorption and transport of HOCs during soil flushing (Kile and Chiou, 1989, 1990; Edwards et al. 1991) and (iv) sorption of surfactants onto solids for enhancing HOC sorption and immobilization to establish in-situ treatment zones using cationic surfactants (Burris and Antworth, 1992; Hayworth and Burris, 1997; Wagner et al., 1994; Li and Bowman, 1997) or using surfactants below their Krafft temperature (Nayyar et al., 1994).

The general behavior of surfactants in the aquatic environment is described by Aboul-Kassim et al. (1993). The influence of surfactants on the microbial degradation of hydrophobic organic compounds in described by Rouse et al. (1994), Aronstein et al. (1994), Di Corcia et al. (1994) and Thiem et al. (1997).
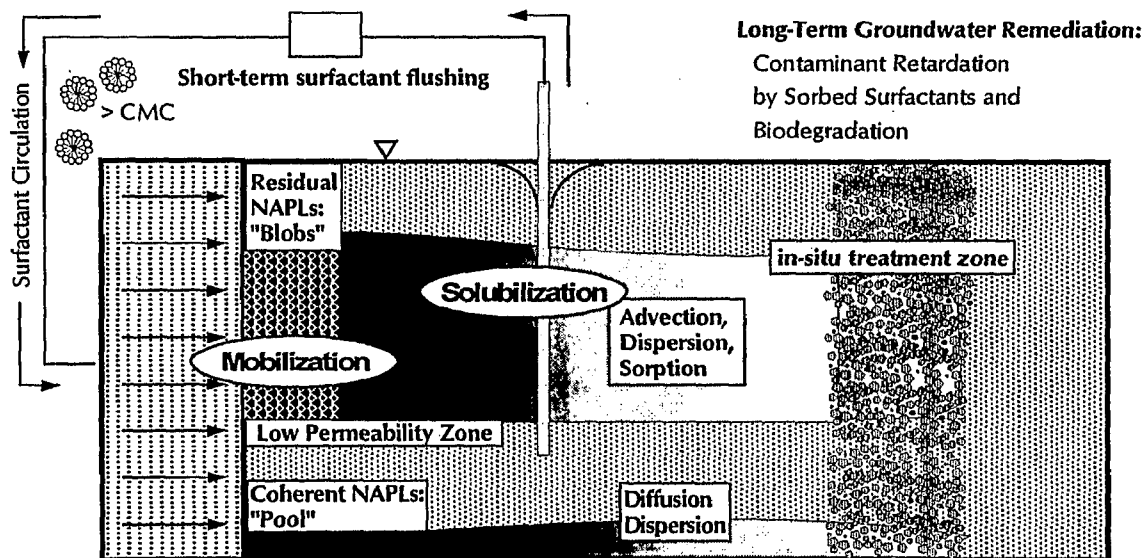

Fig. 1-1: Aquifer contaminated with non-aqueous phase liquids (NAPL) in a coherent pool or in residual phase and possible surfactant enhanced subsurface remediation (SESR) techniques

Objectives

This study focuses on the adsorption behavior of surfactants onto natural aquifer material and the coupled transport of PAHs and surfactants. Laboratory batch and column experiments were conducted to study both the micellar facilitated transport and the enhanced retardation of HOCs due to surfactant coated mineral surfaces. This study is related to the work of two coworkers at the Applied Geology Chair at the University of Tuebingen: Diana Loyek (1998b) identified the processes of PAH dissolution out of coal tar and the influence of surfactants on this dissolution. Michael Finkel (1998) developed the numerical model SMART (stream tube model of advective and reactive transport) to simulate the coupled transport of PAHs and surfactants in porous media. The processes identified within this study were incorporated in that model and the identified parameters were used as input parameters. The understanding and the quantification of the fundamental processes controling the coupled transport of PAHs and surfactants is essential for an appropriate design of SESR technologies or interfacial tracer tests.

In detail the following questions should be answered:

- How can the surfactants used be characterized?

- How adsorb different ionic and non-ionic surfactants onto natural aquifer material?

- Which surfaces within the intraparticle porosity can be reached by surfactants?

- Which influence has the organic matter and organic carbon content?

- Which influence has the grain size and surface properties of the natural aquifer material and its lithocomponents?

- How are surfactants transported under non-equilibrium conditions (column experiments)?

- Which processes control the coupled transport of PAHs and surfactants and how can they be quantified?

2 Theoretical Background

Figure 2-1 summarizes the most relevant processes for the transport of HOC and surfactant in natural aquifer material. The surfactant can exist in the aqueous phase as dissolved monomers and above a surfactant specific concentration, called the critical micelle concentration (*CMC*), as aggregated groups of molecules ("micelles"). Surfactant monomers also agglomerate at the solid/water interface and form monolayers ("hemimicelles") and bilayers ("admicelles") depending on the surfactant concentration. HOCs in such a system are dissolved in the water, associated with monomers or solubilized in the micelles as well as adsorbed directly onto the aquifer material and associated to admicelles. Solubilization is due to the partitioning of HOCs between micelles and aqueous phase and can be quantified by a partitioning coefficient K_{mic}. Similarly, the partitioning of HOC between adsorbed surfactants (monomers, hemimicelles and admicelles) and aqueous phase is called adsolubilization. The sorption of HOCs to the aquifer material is generally controlled by the

organic matter content and exhibits slow kinetics due to intraparticle and intra-organic matter diffusion. Under non-equilibrium conditions it can be quantified by an apparent, time dependent distribution coefficient $K_d(t)$.

Surfactant Adsorption

The behavior of the surfactant adsorption onto hydrophilic surfaces such as silica or clean aquifer sands as used in this study can be explained by a conceptual model based on numerous experimental observations (Clunie and Ingram, 1983; Somasundaran in Edwards et al., 1994a):

A typical adsorption isotherm is shown in Fig. 2-2 (West and Harwell, 1992). The adsorption of surfactant molecules onto the surface initially (zone 1) occurs when the hydrophilic moieties undergo relatively strong interactions with the silica surface, most likely through hydrogen bonding, i.e. the hydrophilic ethoxylated head groups (ethoxylated or negatively charged) are saturated with hydrated protons and therefore
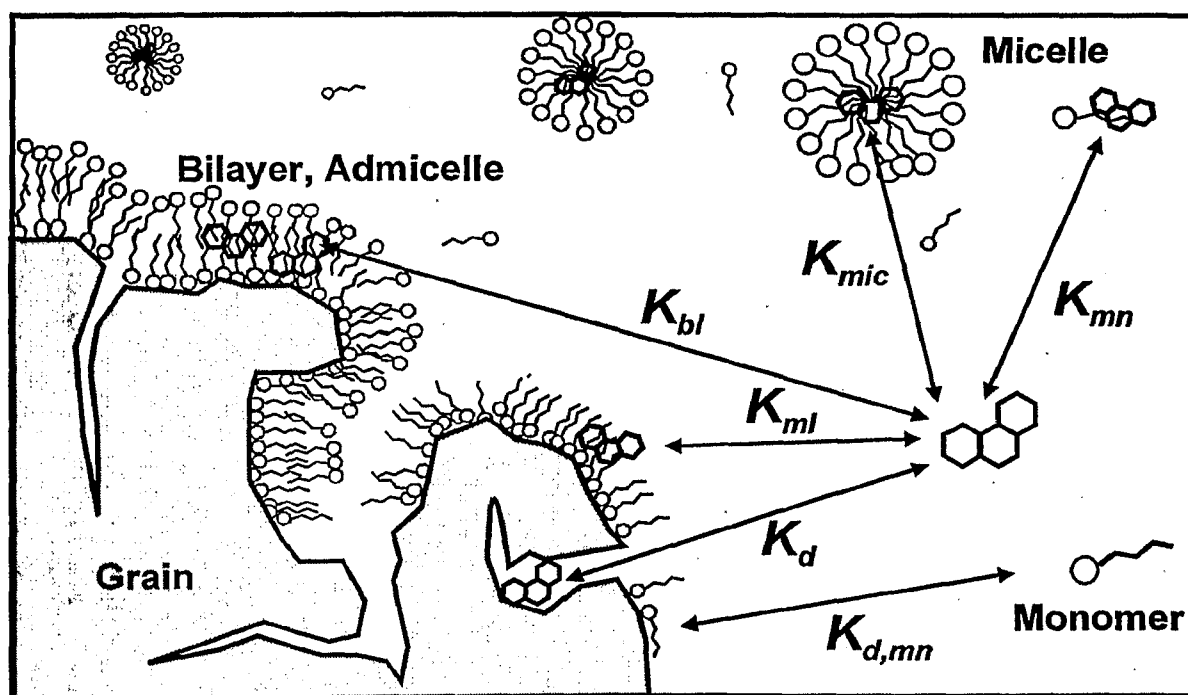

Fig. 2-1: Coupled transport of PAHs and surfactants in natural aquifer material - conceptual model: the transport of PAHs in the presence of surfactant is controlled by the transport (adsorption) behavior of the surfactant and the PAHs partitioning between the aqueous and the immobile surfactant bilayers and monolayers as well as the mobile surfactant monomers and micelles.

positively charged and attracted by the net negatively charged mineral surfaces (isomorphic substitution of Si^{4+} by Al^{3+} within the silicates). At higher concentrations the surfactant molecules begin to reorient such that their hydrophobic alkyl-moieties face outward into the aqueous phase. This realignment is attributed to strong mutual attraction between the hydrophobic moieties of adjacent surfactant molecules. This process continues with increasing surfactant concentration until monolayers of fairly perpendicular oriented surfactant molecules (hemimicelles) are created (zone 2). In that way the hydrophilic surface becomes more and more hydrophobic. With further increasing surfactant concentration, the surfactant molecules adsorb onto the existing monolayer due to the mutual attraction of the hydrophobic moieties of the molecules (zone 3). As a consequence, surface micelles, so called admicelles are formed and a complete bilayer is established at and above the CMC (zone 4).
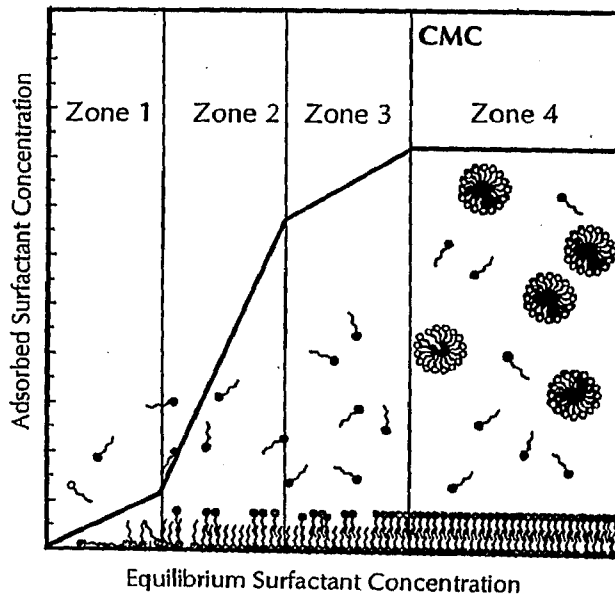

Fig. 2-2: Typical adsorption isotherm of an anionic surfactant onto mineral surfaces according to West and Harwell (1992).

HOC Transport

The behavior of a HOC in a solid/aqueous system is controlled by the distribution of the HOC between the immobile solid phase and the mobile aqueous phase. In the absence of surfactant the distribution coefficient K_d [$L^3 M^{-1}$] can be quantified according to:

$$K_d = \frac{q}{C_{eq}} \qquad (2\text{-}1)$$

where q [M M^{-1}] and C_{eq} [M L^{-3}] denote the HOC concentration in the solid phase and the concentration in the aqueous phase, respectively. The plot of the solid concentration q as a function of C_{eq} is know as adsorption isotherm and can be described by deterministic or empirical adsorption models. If the adsorption is independent of the concentration, the slope of the adsorption isotherm yields the distribution coefficient K_d. However, the adsorption of HOCs onto natural materials mostly depends on the HOC concentration in the aqueous phase which results in nonlinear adsorption isotherms. Then the K_d is not a constant, but a function of the concentration in the aqueous phase. These sorption isotherms may be described e.g. by the Freundlich (1909) adsorption model:

$$q = K_{Fr}\, C_{eq}^{n_{Fr}} \qquad (2\text{-}2)$$

where K_{Fr} [$L^3 M^{-1}$] and $n_{Fr} \neq 1$ [-] denote the Freundlich coefficients. The linear isotherm is a special case of the Freundlich isotherm characterized by $n_{Fr} = 1$.

The Langmuir isotherm accounts for an adsorption maximum:

$$q = \frac{K_L\, q_{max}\, C_{eq}}{1 + K_L\, C_{eq}} \qquad (2\text{-}3)$$

where K_L [$L^3 M^{-1}$] and q_{max} [M M^{-1}] denote the Langmuir coefficient and the adsorption maximum, respectively.

The presence of a surfactant in the solid/aqueous system results in the distribution of the HOC between different mobile and immobile surfactants, that are commonly referred to as surfactant pseudophases. The equilibrium distribution coefficient K_d has to be modified in the presence of a surfactant to a K_d^* according to:

$$K_d^* = \frac{q^*}{C_{eq}^*} \qquad (2\text{-}4)$$

where q^* and C_{eq}^* denote the total equilibrium HOC concentration in all immobile phases associated with the solid and the equilibrium HOC concentration in all pseudophases remaining in the aqueous solution, respectively.

The immobile HOC concentration with respect to the surfactant pseudophases can be expressed as (Sun and Jaffé, 1996):

$$q^* = q \left(1 + \sum_i K_{s,i} X_{s,i}\right) \qquad (2\text{-}5)$$

where $K_{s,i}$ and $X_{s,i}$ denote the HOC partitioning coefficient between an adsorbed surfactant phase i and the aqueous phase and the fractional concentration of the related surfactant phase i in the solid phase, respectively. The fractional concentration $X_{s,i}$ is the mass of the adsorbed surfactant phase i ($M_{s,i}$) divided by the sum of the mass of solid (M_{solid}) and the mass of every adsorbed surfactant phase ($M_{s,n}$):

$$X_{s,i} = \frac{M_{s,i}}{M_{solid} + \sum M_{s,n}} \qquad (2\text{-}6)$$

As an analogue to the immobile phase, the influence of the adsorbent in the aqueous phase (e.g. a surfactant micelle) can be expressed as (Kile and Chiou, 1989):

$$C_{eq}^* = C_{eq} \left(1 + \sum_i K_{aq,i} X_{aq,i}\right) \qquad (2\text{-}7)$$

where $K_{aq,i}$ and $X_{aq,i}$ denote the HOC partitioning coefficient between an aqueous surfactant phase i and water at equilibrium and the fractional concentration of the related surfactant phase i in the aqueous phase, respectively. This is e.g. the mass of the surfactant phase i ($M_{aq,i}$) divided by the mass of water (M_{water}) and the mass of every surfactant phase within the water ($M_{aq,n}$):

$$X_{aq,i} = \frac{M_{aq,i}}{M_{water} + \sum M_{aq,n}} \qquad (2\text{-}8)$$

Placing equations (2-5) and (2-7) in equation (2-4) yields:

$$K_d^* = \frac{q\left(1 + \sum_i K_{s,i} X_{s,i}\right)}{C_{eq}\left(1 + \sum_i K_{aq,i} X_{aq,i}\right)}$$

$$= K_d \frac{1 + \sum_i K_{s,i} X_{s,i}}{1 + \sum_i K_{aq,i} X_{aq,i}} \qquad (2\text{-}9)$$

The HOC partitioning coefficients between water and the surfactant pseudophase K_{surf}, e.g. adsorbed ($K_{s,i}$) or mobile in the aqueous phase ($K_{aq,i}$) can be obtained by the ratio of the fractional concentration of HOC in the surfactant phase (X_{surf}^{HOC}) to the fractional HOC concentration in water (X_{aq}^{HOC})

$$K_{surf} = \frac{X_{surf}^{HOC}}{X_{aq}^{HOC}} \qquad (2\text{-}10)$$

where X_{surf}^{HOC} is given by:

$$X_{surf}^{HOC} = \frac{M_{HOC,s}}{M_{HOC,s} + M_{surf}} \qquad (2\text{-}11)$$

The mass of the HOC within the water (X_{aq}^{HOC}) can be obtained similarly, according to:

$$X_{aq}^{HOC} = \frac{M_{HOC,aq}}{M_{HOC,aq} + M_{aq}} \qquad (2\text{-}12)$$

where $M_{HOC,aq}$ and M_{aq} denote the HOC mass in the water and the mass of water, respectively. It should be noted that the HOC partitioning between water and surfactant phases could be also determined using mole fractions, if the molecular weight of the surfactant is known. In opposite to that, mass fractions have to be used (as shown above) if the solid (aquifer material) is involved in partitioning processes since the molecular weight of the solid is generally not known. A conversion table of the partitioning coefficients obtained by the ratios mol and mass is given in Tab. 2-1.

In a solid/aqueous system the surfactant generally forms four pseudophases which alter the behavior of HOCs. In the immobile phase the surfactant can be adsorbed as monolayers or bilayers depending on the concentration. As an analogue it is present in the mobile aqueous phase as surfactant monomers or micelles. Thus, the general model (eq. 2-9) can be written in a more specific

form to describe the system considered within this study:

$$K_d^* = K_d \frac{1 + K_{ml}\, q_{ml} + K_{bl}\, q_{bl}}{1 + K_{mn}\, C_{mn} + K_{mic}\, C_{mic}} \quad (2\text{-}13)$$

The concentrations in the solid phase are replaced by the adsorbed monolayer concentration (q_{ml}) and bilayer concentration (q_{bl}), respectively. The concentration in the aqueous phase are replaced by the surfactant monomer (C_{mn}) and micelle concentration (C_{mic}). Then, the mass of HOC associated to these pseudophases can be calculated by multiplying the surfactant concentration with the respective HOC partitioning coefficient between water and monolayers (K_{ml}), bilayers (K_{bl}), monomers (K_{mn}) and micelles (K_{mic}). The term in the nominator accounts for the increase of the adsorbed phenanthrene concentration due to the presence of an adsorbed surfactant monolayer and bilayer. The term in the denominator represents the increase of the phenanthrene aqueous concentration due to the presence of surfactant monomers (C_{mn}) and micelles (C_{mic}).

Partitioning Coefficients

The partitioning coefficients of a hydrophobic compound i can be obtained by the ratio of the fraction of i in the surfactant pseudophase and fraction of i in the aqueous phase. These fractions can be given on different bases resulting in different values of the partitioning coefficients. The different possibilities to define the partitioning coefficients are mentioned below for comparison with literature data.

The dimensionless coefficient $K_{n/n}$ based on mol-fractions is:

$$K_{n/n} = \frac{\dfrac{n_{i,\,surf}}{n_{i,\,surf} + n_{surf}}}{\dfrac{n_{i,\,aq}}{n_{i,\,aq} + n_{aq}}} \quad [\text{-}] \quad (2\text{-}14)$$

where $n_{i,\,surf}$, n_{surf}, $n_{i,\,aq}$ and n_{aq} denote the number of moles of the compound i in the surfactant pseudophase, the number of moles of surfactant, the number of moles of the compound i in the

aqueous phase and the number of moles water, respectively.

The dimensionless coefficient $K_{m/m}$ based on mass fractions is:

$$K_{m,\,m} = \frac{\dfrac{m_{i,\,surf}}{m_{i,\,surf} + m_{surf}}}{\dfrac{m_{i,\,aq}}{m_{i,\,aq} + M_{aq}}} \quad [\text{-}] \quad (2\text{-}15)$$

where $m_{i,\,surf}$, m_{surf}, $m_{i,\,aq}$ and M_{aq} denote the mass of the compound i in the surfactant pseudophase, the mass of surfactant, the mass of the compound i in the aqueous phase and the mass of water, respectively. The fraction of the compound i in the aqueous phase is often characterized by the molar concentration $c_{i,\,aq}$ instead of the mole fraction or the mass fraction. This results in two different coefficients depending on the number of moles of the compound i is normalized to the surfactant number of moles and the surfactant mass:

$$K_{V/n} = \frac{\dfrac{n_{i,\,surf}}{n_{surf}}}{c_{i,\,aq}} \quad [\text{L kg}^{-1}] \quad (2\text{-}16)$$

$$K_{V/m} = \frac{\dfrac{n_{i,\,surf}}{m_{surf}}}{c_{i,\,aq}} \quad [\text{L mol}^{-1}] \quad (2\text{-}17)$$

The following ratio, where the number of moles of the compound i is related the volume of the surfactant and the volume of water, yields the volumetric partitioning coefficient K_{vol}:

$$K_{vol} = \frac{\dfrac{n_{i,\,surf}}{V_{surf}}}{\dfrac{n_{i,\,aq}}{V_{aq}}} \quad [\text{-}] \quad (2\text{-}18)$$

The octanol/water partitioning coefficient K_{ow} is also given as a volumetrical partitioning coefficient (based on the volume of octanol and water). The conversion of the different partitioning coefficients is given in Tab. 2-1. It should be noted, that the coefficients K_{vol}, $K_{V/m}$ and $K_{m/m}$ have the same values if the density of the surfactant or the organic solvent equals the density of water.

Tab. 2-1: Conversion of partitioning coefficients which describe the partitioning of a compound i between a surfactant or organic phase and an aqueous phase.

	Factor to convert in:				
calculatd from:	$K_{n/n}$ [mol mol⁻¹] $\frac{(n_i)}{n_{surf}} \frac{n_{aq}}{(n_i)}$	$K_{m/m}$ [kg kg⁻¹] $\frac{(m_i)}{m_{surf}} \frac{m_{aq}}{(m_i)}$	$K_{V/n}$ [kg⁻¹] $\frac{(n_i)}{n_{surf}} \frac{V_{aq}}{(n_i)}$	$K_{V/m}$ [L kg⁻¹] $\frac{(n_i)}{m_{surf}} \frac{V_{aq}}{(n_i)}$	K_{vol} [L L⁻¹] $\frac{(n_i)}{V_{surf}} \frac{V_{aq}}{(n_i)}$
$K_{n/n}$ [mol mol⁻¹]	1	$\frac{MW_{aq}}{MW_{surf}}$ [-]	0.01805^a [M⁻¹]	$\frac{18.05^{ab}}{MW_{surf}}$ [L kg⁻¹]	$\frac{\rho_{surf}}{MW_{surf}} \frac{MW_{aq}}{\rho_{aq}}$ [-]
$K_{m/m}$ [kg kg⁻¹]	$\frac{MW_{surf}}{MW_{aq}}$ [-]	1	$\frac{MW_{surf}}{1000^b \rho_{aq}}$ [M⁻¹]	$\frac{1}{\rho_{aq}}$ [L kg⁻¹]	$\frac{\rho_{surf}}{\rho_{aq}}$ [-]
$K_{V/n}$ [kg⁻¹]	$\frac{1}{0.01805^a}$ [M]	$\frac{1000^b \rho_{aq}}{MW_{surf}}$ [M]	1	$\frac{1000^b}{MW_{surf}}$ [mol kg⁻¹]	$\frac{1000^b \rho_{surf}}{MW_{surf}}$ [M]
$K_{V/m}$ [L kg⁻¹]	$\frac{MW_{surf}}{18.05^{ab}}$ [kg L⁻¹]	ρ_{aq} [kg L⁻¹]	$\frac{MW_{surf}}{1000^b}$ [kg mol⁻¹]	1	ρ_{surf} [kg L⁻¹]
K_{vol} [L L⁻¹]	$\frac{\rho_{aq}}{MW_{aq}} \frac{MW_{surf}}{\rho_{surf}}$ [-]	$\frac{\rho_{aq}}{\rho_{surf}}$ [-]	$\frac{MW_{surf}}{1000^b \rho_{surf}}$ [M⁻¹]	$\frac{1}{\rho_{surf}}$ [L kg⁻¹]	1

ª Molar volume of water at 25°C. ᵇ Factor 1000 to convert MW_{surf} from g mol⁻¹ into kg mol⁻¹.

The transport velocity of HOC relative to the groundwater velocity (conservative tracer) is referred to as retardation and is given by a dimensionless retardation factor R_d. It can be expressed as the ratio of the total mass of HOC in the porous medium (M_{tot}) to the mass in the mobile phase (M_m).

$$R_d = \frac{M_{tot}}{M_m} = \frac{M_m + M_{im}}{M_m} = 1 + \frac{M_{im}}{M_m} \quad (2\text{-}19)$$

A porous medium of a total volume V_{tot} [L³] consisting of a volume of mobile water V_{aq} [L³] and a mass of immobile solids M_{solid} [M] is characterized by the bulk density $\rho_b = M_{solid} V_{tot}^{-1}$ [M L⁻³] and the porosity $n = V_{aq} V_{tot}^{-1}$ [-].

In the absence of surfactants the retardation factor of a HOC in equilibrium can be calculated according to:

$$R_d = 1 + \frac{q\, M_{solid}}{C_{eq} V_{aq}} = 1 + \frac{C_{eq} K_d M_{solid}}{C_{eq} V_{aq}}$$

$$= 1 + K_d \frac{\rho_b}{n} \quad (2\text{-}20)$$

In the presence of surfactants the distribution coefficient K_d has to be replaced by K_d^* or $K_d^*(t)$ in the non-equilibrium case:

$$R_d = 1 + \frac{\rho_b}{n} \frac{K_d^* + K_{ml}\, q_{ml} + K_{bl}\, q_{bl}}{1 + K_{mn}\, C_{mn} + K_{mic}\, C_{mic}} \quad (2\text{-}21)$$

The retardation of the HOC depends on the distribution coefficient K_d^* and the partitioning coefficients K_{ml}, K_{bl}, K_{mn} and K_{mic}. The behavior of the surfactant is described by the adsorbed surfactant concentrations q_{ml} and q_{bl} as well as the concentration of the monomers C_{mn} and micelles C_{mic}. Micelles are not present at surfactant concentrations below the CMC and the retardation factor increases with increasing adsorbed surfactant concentration q. Above the CMC a maximum adsorbed surfactant concentration q_{max} is reached, micelles are formed, and the retardation factor decreases proportional to the increasing micelle concentration.

3 Data Analysis - Parameter Identification

3.1 Adsorption

The adsorbed surfactant concentration q [mmol kg^{-1}] based on mass balance considerations was calculated according to:

$$q = \frac{\left(C_{dot} - \left(C_{eq} - TOC_{de}\right)\right)}{f_{carbon} \, MW_{surf}} \frac{V_{aq}}{M_{solid}} \qquad (3\text{-}1)$$

where C_{dot} [mg L^{-1}], C_{eq} [mg L^{-1}], TOC_{de} [mg L^{-1}], V_{aq} [L], f_{carbon} [g g^{-1}], MW_{surf} [mg mmol^{-1}] and M_{solid} [kg] denote the surfactant concentration added to the sediment/aqueous system, the surfactant concentration in the aqueous phase after equilibration, the dissolved organic carbon that is generally desorbed or dissolved in small amounts from the aquifer material, the volume of water in the system, the carbon mass fraction of the surfactant, the molecular weight of the surfactant and the mass of the aquifer material, respectively. The equilibrium concentration C_{eq} is equal to the sum of the surfactant monomer concentration C_{mn} and the micelles concentration C_{mic}. For low, sub-CMC values the monomer concentration C_{mn} increases linearly and the micelles concentration C_{mic} is zero. For supra-CMC values the micelles concentration is a variable and C_{mn} has a constant value equal to the CMC.

Adsorption isotherms were obtained by plotting the surfactant adsorbed concentration q versus the surfactant equilibrium concentration C_{eq} in the bulk solution. The adsorption of the surfactant monomers can be described by the linear relationship:

$$q = K_{d, \, mn} \, C_{eq} \qquad (3\text{-}2)$$

where $K_{d, \, mn}$ is the distribution coefficient of surfactant monomers between solid and aqueous phase. It was obtained by the slope of the linear isotherm segment through the origin using a linear regression. The quality of the regression is given by R^2.

The maximum sorption q_{max} is characterized by a second linear segment of the isotherm parallel to

the x-axis. The value of q_{max} was calculated as the mean of the values of that isotherm segment and their standard deviation ($q_{max} \pm 1 \, \sigma$).

The adsorption maximum of a aquifer material bulk sample can be calculated from the measured adsorption maxima of the lithocomponent isotherms with respect to their mass fractions (e.g. Fig. 4-7) according to:

$$q_{max}(bulk) = \sum_{i=1}^{n} \chi_i \, q_{max, \, i} \qquad (3\text{-}3)$$

where $q_{max}(bulk)$, n, χ and $q_{max, \, i}$ denote the adsorption maximum of the bulk sample, the number of different lithocomponents identified, the mass fraction of lithocomponent i and the adsorption maximum associated with the lithocomponent i, respectively.

3.2 Surfactant Specific Interfacial Area

Adsorption of surfactants from dilute aqueous solution (activity coefficient close to unity) at a air-water interface, in the absence of excess electrolyte, can be described by the Gibbs adsorption isotherm (Rosen, 1989, Hunter, 1989, Saripalli et al., 1997):

$$\begin{aligned} d\gamma &= -R \, T \, \Gamma \, d\ln C \\ &= -2.303 \, R \, T \, \Gamma \, \log C \end{aligned} \qquad (3\text{-}4)$$

where $d\gamma$, R [J mol^{-1} K^{-1}], T [K], Γ [mol m^{-2}] and C denote the change of the surface or interfacial tension of the solvent (water), the gas constant, the absolute temperature (294 K), the surfactant excess concentration at the interface and the concentration of surfactant in solution, respectively. The concentration of surfactant at the interface can be calculated from surface tension data by use of the appropriate Gibbs equation for a dilute solution of a nonionic surfactant:

$$\Gamma = -\frac{1}{2.303\, R\, T}\left[\frac{\partial \gamma}{\partial \log C}\right]_T \qquad (3\text{-}5)$$

and for solutions of ionic surfactants in the absence of any other solutes (anionic surfactants)

$$\Gamma = -\frac{1}{4.606\, R\, T}\left[\frac{\partial \gamma}{\partial \log C}\right]_T \qquad (3\text{-}6)$$

The surface area occupied per molecule a_{surf} [Å^2] at the interface can be calculated from Γ using following equation (Rosen, 1989):

$$a_{surf} = \frac{10^{20}}{N_A\, \Gamma} \qquad (3\text{-}7)$$

where N_A denotes the Avogardo number ($6.022 \cdot 10^{23}\ mol^{-1}$).

Assuming that a surfactant molecule could reach the same surfaces located in the intraparticle porosity like the nitrogen molecule which is used to determine the BET surface area, the area covered by one surfactant molecule could be calculated by the following equation:

$$a_{surf}{}^* = \frac{BET}{\frac{q_{max}}{2}\, N_A} \qquad (3\text{-}8)$$

where BET [m^2 kg^{-1}], q_{max} [mol kg^{-1}] and N_A denote the specific surface area determined by nitrogen adsorption/desorption isotherms, the maximum surfactant adsorption and the Avogadro number. Again it is assumed that a complete bilayer is established and therefore only 50 % of the molecules "see" the surface.

The specific surface area A_{surf} [cm^2 g^{-1}] which is covered by surfactant was calculated according to:

$$A_{surf} = \frac{q_{max}\, N_A\, a_{surf}}{2} \qquad (3\text{-}9)$$

where q_{max} [mmol kg^{-1}], N_A [mmol^{-1}] and a_{surf} [cm^2] denote the maximum surfactant adsorption, the Avogadro number and the area covered by one surfactant molecule, respectively. It was assumed that the surfactant molecules cover the same area as at the liquid/air interface but form a complete bilayer. If no complete bilayer is formed the denominator in equation (3-9) is less than 2. It is larger than 2, if adsorption occurs in multilayers

or multi-bilayers. Values of A_{surf} determined according to equation (3-9) were compared to the N$_2$-BET surface area and the external surface area of the grains assuming them as ideal spheres. The surface area to volume ratio of an ideal sphere is given by:

$$\frac{A_o}{V_o} = \frac{4\pi r^2}{\frac{4}{3}\pi r^3} = \frac{r}{3} \qquad (3\text{-}10)$$

where A_o, V_o and r denote the surface area, the volume and the radius of the sphere. The surface area to volume ratio of equation (3-10) can be given as specific external surface area A_{ext} [cm^2 g^{-1}] per mass of aquifer material:

$$A_{ext} = \frac{3}{r\, \rho_s} \qquad (3\text{-}11)$$

where ρ_s denotes the solid density of the grains.

The area covered by the surfactant A_{surf} compared to the area that is given by the external surface area of ideal spheres A_{ext} is given by following ratio:

$$\frac{A_{surf}}{A_{ext}} = \frac{q_{max}\, N_A\, a_{surf}}{2}\frac{r\, \rho_s}{3} \qquad (3\text{-}12)$$

3.3 Adsolubilization

Kinetics

A first order reaction can be described by:

$$C(t) = C_0\, e^{-kt} \qquad (3\text{-}13)$$

where $C(t)$, C_0 and k denote the concentration at time t, the initial concentration and the first order rate constant, respectively. The first order rate constant can be identified from the slope of ln $(C\, C_0^{-1})$ versus time. Then the kinetics of phenanthrene adsolubilization can be presented according to:

$$\frac{K_d{}^*(t)}{K_d{}^*} = 1 - e^{-kt} \qquad (3\text{-}14)$$

where $K_d{}^*(t)$ and $K_d{}^*$ denote the apparent distribution coefficient of phenanthrene in the presence

of surfactant at time t and the distribution coefficient at equilibrium, respectively.

Partitioning

The fraction of phenanthrene in the adsorbed surfactant phase X_{surf} is calculated according to:

$$X_{surf} = \frac{(C_{phe, 0}^* - C_{phe, eq}^*) - (C_{phe, 0} - C_{phe, eq})}{(C_{phe, 0}^* - C_{phe, eq}^*) + q}$$

(3-15)

where $C_{phe, 0}^*$, $C_{phe, eq}^*$, $C_{phe, 0}$, $C_{phe, eq}$, and q denote the initial and equilibrium phenanthrene concentrations in the presence of surfactant, the initial and equilibrium phenanthrene concentrations without surfactant and the adsorbed surfactant concentration, respectively. q was calculated from the surfactant fraction in the aqueous phase f_w knowing the surfactant distribution coefficient $K_{d, surf}$ from the adsorption isotherm and the solid to water ratio r_{sw} of the batch systems:

$$f_w = \frac{1}{1 + r_{sw} K_{d, surf}}$$

(3-16)

and $q = 1 - (f_w C_{dot})$ (3-17)

The phenanthrene fraction in the aqueous phase X_{aq} is given by:

$$X_{aq} = \frac{C_{phe, eq}^*}{C_{phe, eq}^* + C_{aq}}$$

(3-18)

where C_{aq} denotes the molar concentration of water (55.55 mol L^{-1}). The partitioning coefficient on a mol/mol-basis $K_{n/n}$ is defined analogous to the micellar partitioning coefficient K_{mic} as:

$$K_{n/n} = \frac{X_{surf}}{X_{aq}}$$

(3-19)

This definition a priori does not distinguish between partitioning into surfactant monolayers or bilayers (admicelles). Thus, the value of $K_{n/n}$ may be different for different adsorbed surfactant concentrations.

The phenanthrene distribution coefficient normalized to the organic carbon content f_{oc} was determined according to:

$$K_{oc} = \frac{K_d}{f_{oc}}$$

(3-20)

and in the presence of surfactant indicated by the asterisks:

$$K_{oc}^* = \frac{K_d^*}{f_{oc}^*}$$

(3-21)

where f_{oc}^* denotes the increased organic carbon content due to the adsorbed surfactant expressed as adsorbed carbon:

$$f_{oc}^* = f_{oc} + f_{carbon} \, q \, MW_{surf}$$

(3-22)

where f_{carbon}, q and MW_{surf} denote the organic carbon fraction of the surfactant molecule, the adsorbed surfactant concentration and the molecular weight of the surfactant, respectively.

3.4 Column Experiments

The monitored time t_m [s] of the breakthrough experiments was converted into real time t [s] with respect to the system dead volume V_d [cm^3] as follows:

$t = t_m - t_d$ for $(t_m - t_d) > 0$

$t = 0$ for $(t_m - t_d) < 0$

where t_d [s] denotes the time to displace V_d at a certain volumetric flow rate Q [cm^{-3} s^{-1}]:

$$t_d = \frac{V_d}{Q}$$

(3-23)

The fluorescence signal which represents the measured effluent concentration C_m was corrected according to:

$$C/C_0 = \frac{C_t - C_{min}}{C_{max} - C_{min}}$$

(3-24)

where C/C_0, C_{min} and C_{max} denote the effluent concentration normalized to the influent concentration [-], the background concentration (fluorescence signal or surfactant concentration) and the maximum measured influent signal, respectively.

The pore volume was determined from the first moment of the breakthrough curve of the conservative tracer:

$$\mu_{ct} = \int_0^\infty (1 - C/C_0)\, dt \qquad (3\text{-}25)$$

where μ_{ct} [t] denotes the first moment of the conservative tracer. It was calculated by numerical integration of the on-line breakthrough curve according to:

$$\mu_{ct} = \sum_{i=1}^{z-1} \left[\left(1 - \frac{(C/C_0)_{i+1} + (C/C_0)_i}{2} \right)(t_{i+1} - t_i) \right] \quad (3\text{-}26)$$

where z denotes the total number of observed data points. Then, the porosity n was calculated according to:

$$n = \frac{\mu_{ct}\, Q_{ct}}{V_{tot}} \qquad (3\text{-}27)$$

where V_{tot} [cm^3] denotes the total volume of the column without porous medium.

The gravimetric porosity n_{grav} was calculated according to:

$$n_{grav} = 1 - \frac{M_{solid}}{\rho_s\, V_{tot}} \qquad (3\text{-}28)$$

where M_{solid} and ρ_s denote the mass and the density of the solids in the column.

The dimensionless time (=number of pore volumes displaced: PV) was calculated from the dead volume corrected time t_{net} and the first moment of the conservative tracer:

$$PV = \frac{t_{net}}{\mu_{ct}} \qquad (3\text{-}29)$$

Slightly different flow rates between the breakthrough experiment of the reactive solute and the corresponding conservative tracer experiment were respected according to:

$$\mu_{rs} = \frac{\mu_{ct}\, Q_{ct}}{Q_{rs}} \qquad (3\text{-}30)$$

were μ_{rs}, Q_{ct} and Q_{rs} denote the first moment of the reactive solute, the volumetric flow rate of the conservative tracer and the flow rate of the reactive solute, respectively.

The average linear velocity v_x [cm s^{-1}] of a non-retarded particle was calculated according to:

$$v_x = \frac{Q}{n\,A} \qquad (3\text{-}31)$$

where A [cm^2] denotes the cross sectional area of the column. The mean residence time t_{mr} of a non-retarded particle was calculated according to:

$$t_{mr} = \frac{L}{v_x\, n} \qquad (3\text{-}32)$$

where L denotes the column length [cm].

The coefficient of longitudinal hydrodynamic dispersion D_L [cm^2 s^{-1}] was determined by fitting the following solution of the advection dispersion equation (Ogata and Banks, 1961) to the measured breakthrough curve:

$$C/C_0 = \frac{1}{2}\left[erfc\left(\frac{L - v_x t}{2\sqrt{D_L t}} \right) + exp\left(\frac{v_x L}{D_L} \right) erfc\left(\frac{L + v_x t}{2\sqrt{D_L t}} \right) \right]$$

$$(3\text{-}33)$$

where $erfc$ denotes the complementary error function. The equation (3-33) is valid for a homogenous one-dimensional column system under steady state flow conditions with a continuous feed of a constant concentration of the tracer. The initial and boundary condition are given by:

$$C(x, 0) = 0 \qquad 0 \le x \le L$$

$$C(0, t) = C_0 \qquad t \ge 0$$

The initial condition denotes the zero concentration within the column at time t = 0 and the boundary condition at the column inlet (x = 0) is a fixed concentration boundary.

The dispersivity α [mm] was calculated according to:

$$\alpha = \frac{D_L}{v_x} \qquad (3\text{-}34)$$

Assuming that αv_x is much larger than the pore diffusion coefficient (D_p) the dimensionless Peclet number Pe relates the velocities of mass transport by advection to the mass transport by either dis-

persion or diffusion (Fetter, 1992). It was calculated according to:

$$Pe = \frac{v_x L}{D_L} = \frac{v_x L}{v_x \alpha + D_p} \qquad (3-35)$$

For Peclet numbers smaller than about 0.4 diffusion/dispersion predominantes the mass transfer. For Pe values larger than 10 the advection controls the mass transport (Fetter, 1992).

Two methods were used to quantify the retardation factor of the reactive solute (Nkedi-Kizza et al., 1987). In method 1 the R_d was obtained from moment analysis according to:

$$R_d = \frac{\mu_{rs}}{\mu_{ct}} \qquad (3-36)$$

where μ_{rs} and μ_{ct} denote the first moment of the reactive solute and the conservative tracer, respectively.

Based on the principle of mass conservation the retardation factor can be visualized as the total mass of reactive solute in the system compared to the mass in the mobile phase. They equal for a nonsorbing conservative tracer resulting in $R_d = 1$.

The retardation factor $R_{0.5}$ was determined in method 2 according to:

$$R_{0.5} = \frac{t_{0.5\ (rs)}}{t_{0.5\ (ct)}} \qquad (3-37)$$

where $t_{0.5\ (rs)}$ and $t_{0.5\ (ct)}$ denote the time required for the effluent concentration to reach $C/C_0 = 0.5$ for the reactive solute and the conservative tracer, respectively. This method is based on the assumption of sigmoidal breakthrough curves and involves the implicit assumption that the transport of the reactive solute through the column occurs under equilibrium conditions. The time $t_{0.5}$ was determined according to the following linear interpolation:

$$t_{0.5} = \frac{0.5 - C/C_{0_{i-1}}}{\dfrac{C/C_{0_i} - C/C_{0_{i-1}}}{t_{net_i} - t_{net_{i-1}}}} + t_{net_{i-1}} \qquad (3-38)$$

where t_{net_i} is the corresponding time to the first measured data point of $C/C_0 > 0.5$.

For practical purposes the first arrival of a contaminant, e.g. given by $R_{0.5}$, may be more important. For theoretical considerations the R_d derived from the mass balance is more important for the comparison of non-equilibrium column results to equilibrium batch systems. Both retardation factors are afflicted with a uncertainty due to the experimental and parameter identification methods. R_d is very sensitive to uncertainties in the influent concentration and may be generally overestimated by numerical integration of the area left of the breakthrough curve since it is difficult to distinguish between a 99 % and 100 % breakthrough. $R_{0.5}$ is more reliable to determine but it is more sensitive to the flow velocity and generally it underestimates the mass of phenanthrene adsorbed in the column. Due to this, both retardation factors are given in the result tables. The indices "d" and "0.5" in the following calculations of the distribution coefficients indicate that they relate to R_d and $R_{0.5}$, respectively. The equilibrium transport of a sorbing compound through a column yields a fairly symmetrical breakthrough curve. A high degree of asymmetry or skewness of the breakthrough curve may indicate adsorption non-equilibrium (Nkedi-Kizza, 1987). A measure for the skewness can be obtained by the ratio $R_{0.5} R_d^{-1}$, which compares the retardation factor based on the first moment analysis R_d and the retardation factor at 50 % breakthrough $R_{0.5}$. For ideal equilibrium breakthrough curves this ratio equals one indicating adsorption equilibrium within the column transport experiment. Values smaller than one indicate an increasing asymmetry of the breakthrough curves and thus non-equilibrium. The retardation factors of the elution curves, i.e. the retardations of water in a solute equilibrated column, were determined by converting the elution curves into "breakthrough curves" by using $1 - C/C_0$.

The apparent (non-equilibrium) distribution coefficients $K_d(t)^*$ and $K_{0.5}(t)^*$ in the column systems were calculated from the retardation factors according to:

$$K_d(t)^* = \frac{(R_d - 1)\ n}{\rho_b} \qquad (3-39)$$

$$K_{0.5}(t)^* = \frac{(R_{0.5}-1)\,n}{\rho_b} \qquad (3\text{-}40)$$

To compare these non-equilibrium distribution coefficients with the equilibrium distribution coefficient K_d^* obtained from adsorption isotherms they were converted into "equilibrium" distribution coefficients with respect to the kinetics of phenanthrene adsolubilization equation (3-14) and the mean residence time t_{mr} within a column system:

$$K_d^* = \frac{K_d^*(t)}{1 - e^{-k\,t_{mr}}} \qquad (3\text{-}41)$$

$$K_{0.5}^* = \frac{K_{0.5}^*(t)}{1 - e^{-k\,t_{mr}}} \qquad (3\text{-}42)$$

where k is the first order rate constant of the phenanthrene adsolubilization.

The adsorbed surfactant mass q of the surfactant column experiments was calculated according to:

$$q = K_{d,\,surf}(t) \cdot C_0 \qquad (3\text{-}43)$$

where $K_{d,\,surf}(t)$ is obtained analogous to equation (3-39) and C_0 denotes the surfactant influent concentration.

The data analysis was carried out by using the mathematical software tool MathCAD Plus 6.0 (MathSoft, 1995).

4 Materials and Methods

4.1 Phenanthrene

Phenanthrene was selected from the group of the PAHs as a relatively safe to handle, non-volatile and fairly hydrophobic chemical probe, which is representative other HOCs. Phenanthrene was obtained from Aldrich Chemical Co. with a purity greater 98 % and was used without further treatment. The properties of phenanthrene are listed in Tab. 4-1.
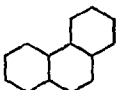
4.2 Surfactants

4.2.1 Selection

The surfactants, that are probably suitable for SESR from an ecotoxicological and economic point of view were selected in cooperation with D. Sabatini (Institute for Applied Surfactant Research, University of Oklahoma, U.S). The non-ionic surfactants Terrasurf G50 (TS G50) and Terrasurf G80 (TS G80) are fatty alcohol ethoxylates, which were designed for environmental purposes by Dow Chemicals. In the production process an initial fatty alcohol is modified into a surfactant by introducing a different number of ethoxy groups (C_2H_4O-). The hydrophobic moiety of the surfactant molecule is the $C_{12}C_{14}$-alkyl chain while the hydrophilic head is characterized by the ethoxylated moiety with an alcohol group in terminal position. The exact structures of the molecules have been not provided by the supplier. The Terrasurf surfactants are commonly used in commercial cleaner formulations and are classified according to the European Economic Com-

munity (EEC) as polymers (Kleiner, 1996). All polymers are listed according the 7th amendment to directive 67/548/EEC (dangerous substances directive) in the list of European inventory of existing chemical substances (EINECS). No bioaccumulation is expected because of the high water solubility. The acute aquatic toxicity is 3 mg L^{-1} lethal concentration (LC50: 50 % of the organisms are killed) for rainbow trout (Onchorynchus mykiss), an effect concentration (EC50) of 1.6 mg^{-1} for water flea (Daphnia magna) and the growth inhibition (IC50) for green algae (Scenedesmus subspicatus) is 2.3 mg L^{-1}. This leads to a general toxicity to aquatic organisms (LC50, EC50, IC50) between 1 mg L^{-1} - 10 mg L^{-1} (Dow, 1994). The Terrasurf surfactants are biodegraded to 90 % within 28 days using the modified screening test of the organization for economic cooperation and development (OECD). Thus, the surfactants are considered as readily biodegradable (DOC loss after 28 days greater than 70 %). Because of the "ready" biodegradability and the aquatic toxicity better than 1 mg L^{-1} the Terrasurf surfactants need not to be labeled as dangerous substances in the environment, which is characterized by the risk label of the leafless tree and the dead fish symbol (Kleiner, 1996).

The Dowfax 8390 (DF 8390) surfactant belongs to the Dowfax high performance surfactant series which are also used in commercial cleaner and degreasing products. The di-phenyl oxide disulfonates (DPDS) consist of two aromatic rings which are linked by an oxygen. An anionic sulfate group is attached to each ring resulting in a di-anionic hydrophilic head. The hydrophobic

Tab. 4-1: Structure and physico-chemical properties of phenanthrene.

Compound (Formula)	Structure	Molecular Weight [g mol^{-1}]	Vapor Pressure [Pa] (20°C)	Water Solubility [mg L^{-1}] (25°C)	log K_{ow} [-]
Phenanthrene ($C_{14}H_{10}$)		178	0.091	1.29 [a] 1.18 [b]	4.63 [b] 4.57 [c] 4.46 [d]

[a] Mackay and Shiu, (1977). [b] Yalkowsky and Valvani, (1979). [c] Miller et al., (1985). [d] Sims and Overcash, (1983).

moiety of the Dowfax surfactants consists of alkyl chains of different lengths. This hydrophobic alkyl can be attached either to one (mono-alkylation) or to both (di-alkylation) of the aromatic rings. The DF 8390 used in this study has an alkyl chain length of 16 carbon atoms (hexadecyl), which is present in 80 % as mono-alkylation and 20 % as di-alkylation (Kleiner, 1994). The DPDS were developed to substitute nonylphenol ethoxylate surfactants, which were transformed into alkylphenol monoethoxylates and diethoxylates as well as alkylphenols during anaerobic degradation (Brunner, 1988). These degradation products show an estrogen mimikry, i.e. they show the same effect as the female hormone estrogen if they are incorporated by mammals or humans. DF 8390 has an acute aquatic toxicity of 0.42 mg L^{-1} LC50 for rainbow trout (Onchorynchus mykiss), LC50 of 13.9 mg L^{-1} for water flea (Daphnia magna) and the growth inhibition (IC50) for green algae (Selenastrum capricornutum) is 42 mg L^{-1}. DF 8390 is very toxic to aquatic organisms since the general toxicity to aquatic organisms (LC50, EC50, IC50) is smaller than 1 mg L^{-1} and it also may cause adverse long-term effects (Dow, 1996). The biodegradation of DF 8390 after 28 days using the modified OECD screening test was 0 % - 6 %. Thus, it is not easily biodegradable according to OECD/EEC regulations. Finally, DF 8390 has to be labeled with the leafless tree/dead fish symbol in the EU.

The nonionic nonylphenol surfactant Triton X-100 (TX-100), which shows estrogen mimikry in the environment as described above, was mainly used in the surfactant enhanced tertiary oil recovery (EOR). In this study it was used since TX-100 is well described in the literature and it was used in preceding experiments at the Applied Geology Institute of the University of Tübingen (Schüth, 1994; Pyka, 1994).
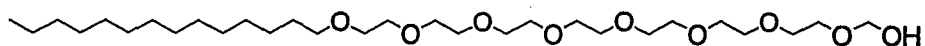
The anionic surfactant sodium dodecyl sulfate (SDS) was selected, since it is also well described in the literature. Furthermore, it is used for surfactant based admicellar chromatography which

has been suggested as a viable alternative for stationary phases in separation processes (Nayyar et al., 1994). In these systems the surfactant admicelles are favored sorption sites for HOCs. The surfactant bleeding can be minimized by using a surfactant below its Krafft temperature (also known as Krafft point). Below this Krafft temperature the solubility of the surfactant, which depends on the temperature, does not reach the CMC, i.e. the surfactant precipitates if a micellar surfactant solution is cooled below its Krafft temperature. Only that fraction which can be dissolved at this temperature remains in solution. The adsolubilization of HOCs has been demonstrated by Nayyar et al. (1994) using SDS below the Krafft temperature (14°C) and aluminum oxides as carrier medium.

The anionic surfactant Marlinat was selected for comparison and since it is possibly suitable for the application as interfacial tracer (Sabatini, 1997). It belongs to the series of lauryl ether sulfates, which are linear fatty alcohol ether sulfates with a different grade of ethoxylation. They are typically used in shampoos and body care products and are considered to be biodegradable (Rouse et al., 1996).

The cationic surfactant hexadecyl-trimethyl ammonium (HDTMA) with bromide as counterion was also used to evaluate the stability of a reactive sorption zone for HOCs. Since the net charge of aquifer material is mostly negative due to isomorphic substitution of Silicium by Aluminum, the sorption of a cationic surfactant is very strong because of electrostatic attraction.

All these commercial surfactants were purchased as pure compounds (TS G50, TX-100, SDS, HDTMA) with a purity greater 98 % or as concentrated aqueous solutions (TS G80: 95%, DF 8390: 45%, Marlinat: 70%). All surfactants were used without further purification. The structures of the surfactants used are shown in Fig. 4-1 and the physico-chemical properties are summarized in Tab. 4-2.
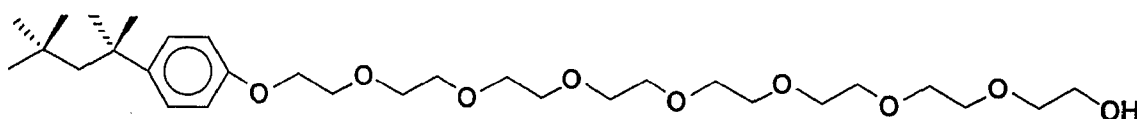
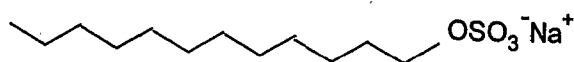Terrasurf G50 (TS G50), nonionic, exact structure not known
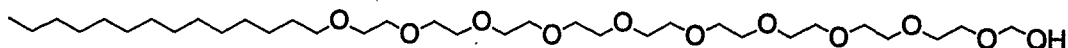
Terrasurf G80 (TS G80), nonionic, exact structure not known

$SO_3^-Na^+$ $SO_3^-Na^+$
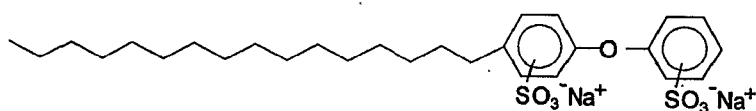
Dowfax 8390 (DF 8390), di-anionic

Triton X-100 (TX-100), nonionic

$OSO_3^-Na^+$

Sodium dodecyl sulfate (SDS), anionic

$OSO_3^-Na^+$
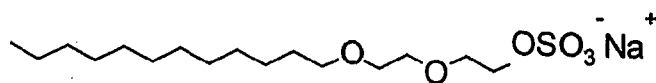
Sodium lauryl ether sulfate (Marlinat), anionic

Br^- CH_3
$^+N-CH_3$
CH_3
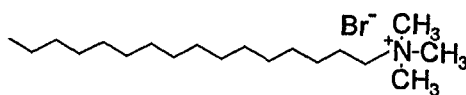
Hexadecyl-trimethyl ammonium bromide (HDTMA), cationic

Fig. 4-1: Structure of the surfactants used within this study.

Tab. 4-2: Characteristics of surfactants used within this study: CMC_{st}^*, surface tension data and interfacial area covered by one molecule.

Surfactant Abbreviation (Supplier)	Type Formula[a]	Mw_{surf}[b]	HLB[c]	CMC_{st}[d]	Micellar Surface Tension	Area per Molecule a_{surf}
		[g mol⁻¹]	[-]	this study [mM (mg L⁻¹)]	this study [mN m⁻¹]	this study [Å²]
				other sources [mM]	other sources [mN m⁻¹]	other sources [Å²]
Terrasurf G50 TS G50 (Dow Europe)	ethoxylated fatty alcohol (nonionic) C_{12}-C_{14} [e]- EO [f] 8	567	12.9	0.88 (500) -	35.2 27.4[g]	44 -
Terrasurf G80 TSG80 (Dow Europe)	ethoxylated fatty alcohol (nonionic) C_{12}-C_{14} [e] - EO [f] 10.5	677	14	1.11 (750) -	35.2 29.6[g]	47 -
Triton X 100 TX-100 (Aldrich)	octylphenol-ethoxylate (nonionic) $C_8H_{17}C_6H_4O(C_2H_4O)_{9.5}H$	625	13.5	0.24 (150) 0.21 [h] 0.18 [i]	40.5 -	66 66[j]
Dowfax 8390 DF 8390 (Dow Europe)	C_{16}- diphenyl oxide disulfonate (di-anionic) $C_{16}H_{33}C_{12}H_7O(SO_3Na)_2$	642	> 40 [n]	2.49 (1600) 6.2 [k] 3.1 [l]	51.0 49.2[g]	117 -
SDS (Aldrich)	sodium dodecyl sulfate (anionic) $C_{12}H_{25}OSO_3Na$	265	40	7.55 (2000) 9.1 [m]	37.0 39.0[m]	49 53 [j m]
Marlinat (Hüls)	lauryl ether sulfate sodium salt (anionic) C_{12}-C_{14}[a] $(C_2H_4O)_2SO_3Na$	385	-	3.05 (1011) 3.2 [m]	37.0 35.0	59 64 [m]
Lutensol A8 (BASF)	ethoxylated fatty alcohol (nonionic) C_{12}-C_{14}[e] - EO [f] 8	551	16.7	(109) -	- -	- -
Lutensol TO 389 (BASF)	C_{13}- oxo-alcohol (anionic)	-	-	(152) -	- -	- -
Lutensol GD 70 (BASF)	alcyl poly glucoside (nonionic)	-	-	(1348) -	- -	- -
Lutensit A-BO (BASF)	dioctylsulfosuccinat, sodium salt (anionic)	-	-	(262) -	- -	- -
HDTMA (Merck)	hexadecyltrimethyl-ammonium chloride (cationic) $C_{16}H_{33}N(CH_3)_3Br$	288	-	1.18 (340) -	- -	- -

* Critical micelle concentration determined by a surface tension method (see next chapter). [a] Average value. [b] Molecular weight (average value). [c] Hydrophilic lypophilic balance provided by the supplier. [d] Critical micelle concentration (average value) determined by surface tension method (capillary rise). [e] Initial fatty alcohol. [f] Grade of ethoxylation. [g] Dow Chemicals. [h] Kile & Chiou (1989). [i] Edwards et al. (1994a). [j] Rosen (1989). [k] Intersection of straight lines, capillary rise (Rouse et al. 1996). [l] Surface tension data (maximum bubble pressure method provided by Dow Chemicals Co.) cited in Rouse et al. (1996). [m] Rouse et al. (1996). [f] Sabatini, 1997, personal communication. "-" = Not reported or not determined.

4.2.2 Characterization - Critical Micelle Concentration and Surfactant Molecular Surface Area

The critical micelle concentration obtained by surface tension measurements (CMC_{st}) was determined by the capillary rise method (Adamson, 1990) in a small-volume pipette (blaubrand; 0.1 mL capacity with ticks at 0.001 mL). The capillary rise was measured for a serial dilution of surfactant in deionized water. For each concentration tested the pipette was wetted with the surfactant solution and the meniscus was allowed to come to a steady level (requiring approximately 5 minutes) above a reference mark at the solution surface. Before use the pipette was cleaned with concentrated hydrochloric acid, rinsed with deionized water and oven dried. The CMC_{st} measurements of the nonionic and anionic surfactant using the capillary rise method are shown in Fig. 4-2 and Fig. 4-3. The height of the capillary rise decreases with increasing surfactant concentration and thus decreasing surface tension until the CMC_{st} is reached. The determination of the CMC_{st} is based on the intersections of straight-line extensions in the declining surface tension region and the constant level of a micellar surface tension region. The CMC_{ec} of the cationic HDTMA was determined by the change of the electric conductivity at the CMC_{ec} (Fig. 4-4). The CMC_{st} values and micellar surface tensions are summarized in Tab. 4-2. The capillary rise was converted into surface tension data by using an empirical factor (3.52) reported by Rouse et al. (1996), who used a pipette system with the same dimensions parallel to direct surface tension measurements.

The surface tensions of the micellar solutions investigated are in a range between 23 mN m^{-1} and 44 mN m^{-1}. The lower micellar surface tension indicates a greater surface activity of the surfactant, i.e. more surfactant molecules are present at the air/water interface (Kosswig and Stache, 1993). Since the anionic surfactants are better soluble in water they show a higher micellar surface tension compared to the nonionic compounds.
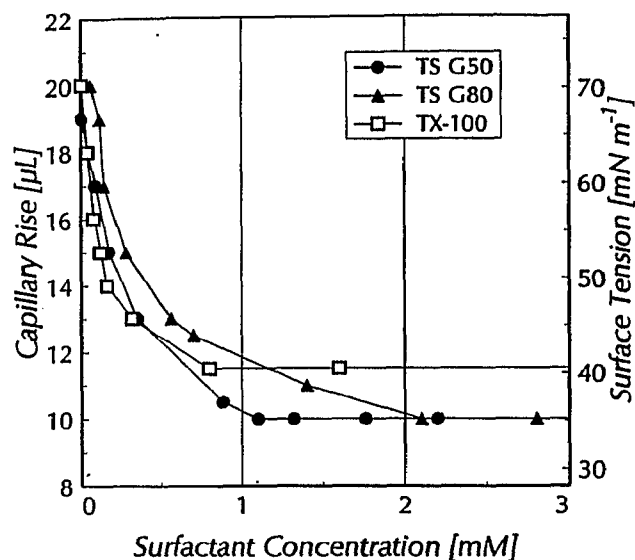

Fig. 4-2: Capillary rise in a small volume pipette (read from the pipette calibration and therefore given in volume units on the left y-axis) versus surfactant concentration for the nonionic surfactants used to determine the CMC_{st}. The respective surface tension is given on the right y-axis.
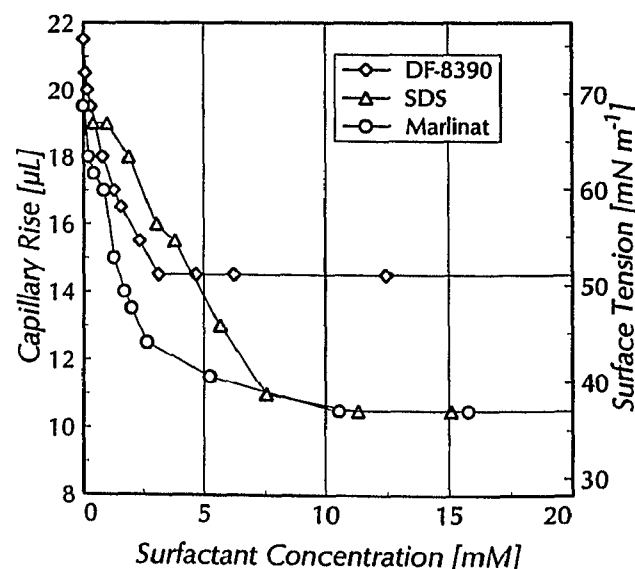

Fig. 4-3: Capillary rise in a small volume pipette (read from the pipette calibration and therefore given in volume units on the left y-axis) versus surfactant concentration for the anionic surfactants to determine the CMC_{st}. The respective surface tension is given on the right y-axis.
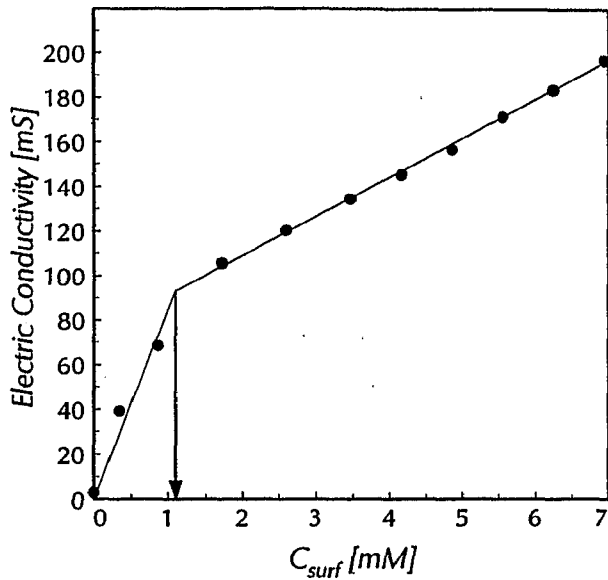
Fig. 4-4: CMC_{ec} of the cationic surfactant HDTMA determined by the change of the electric conductivity at the CMC_{ec} (1.18 mmol L^{-1} , 340 mg L^{-1}).
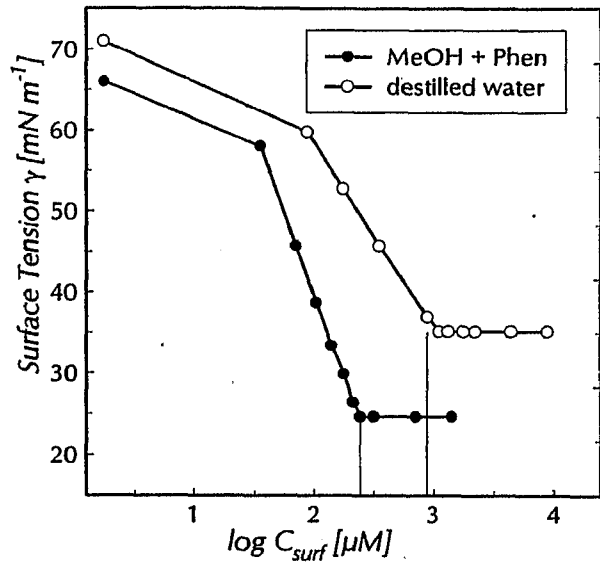

Fig. 4-6: Decrease of the CMC_{st} of TS G50 from 0.88 mM (without electrolyte and hydrocarbons) to 0.24 mM in the presence of phenanthrene spiked in methanol to the surfactant solution.
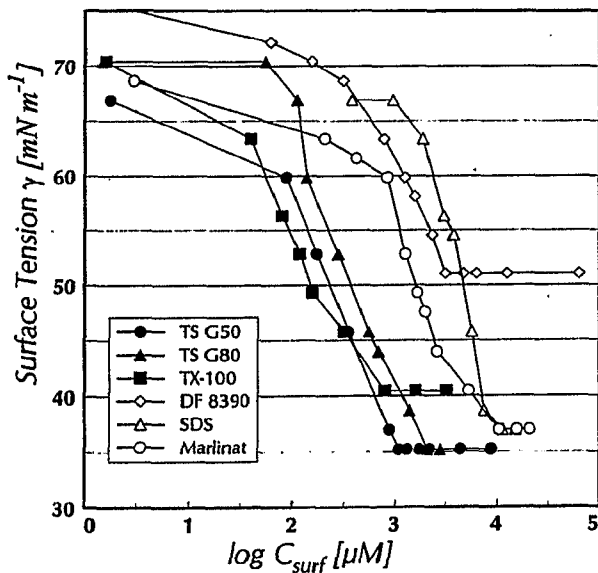

Fig. 4-5: Surface tension versus logarithmic surfactant concentration of aqueous solution of the surfactants used for determination of the surface area covered by a surfactant molecule at the air/water interface.

The nonionic TX-100 has the lowest CMC_{st} of about 0.24 mM, followed by the ethoxylated TS G50 (0.88 mM) and TS G80 (1.1 mM) with a higher grade of ethoxylation. Even higher CMC_{st} values were found for the di-anionic DF 8390 (2.49 mM), the anionic Marlinat (3.05 mM) and the anionic SDS (7.55 mM). These values agree well with CMC_{st} values reported in the literature (see Tab. 4-2).

The surface area that is covered by one surfactant molecule was determined by using the Gibbs adsorption isotherm according to equation (3-4) to (3-7). The values are also included in Tab. 4-2 and range from approximately 44 Å^2 to 60 Å^2 per molecule for the nonionic surfactants and between 49 Å^2 and 117 Å^2 per molecule for the anionic surfactants. These values are in between the range from 38 Å^2 to 100 Å^2 per molecule for comparable nonionic and anionic surfactants (Rosen, 1989, Rouse et al., 1996).

During the breakthrough experiments it turned out, that the CMC seems to be further decreased in the presence of phenanthrene which was spiked in small amounts of methanol to the influent solution. Thus the CMC_{st} in the presence of these hydrocarbons and the electrolyte was determined again using the capillary rise method. The results are shown in Fig. 4-6.

4.3 Solids

4.3.1 Selection

Several natural aquifer materials were selected in order to identify the influence of the surface properties and the grain size of petrographic and sedimentological different grains on the surfactant sorption. Following aquifer materials were used:

Natural Aquifer Materials

- River Neckar alluvium (RNA) is an mixed alluvial sediment deposited by the river Neckar. It was collected at Hirschau, near Tuebingen (southwest Germany). RNA is a heterogeneous aquifer material with low organic carbon content. It consists of Triassic limestones (TL), Jurassic limestones (JL), different sandstones (SS) and quartz (Qz) in different mass percentages depending on the grain size (Fig. 4-7). While the larger grain size fractions are dominated by the limestones the percentage of the most stable mineral quartz increases with decreasing grain size.

- Horkheim aquifer material (HH) was taken from the Horkheim aquifer test site, in the river Neckar valley close to Horkheim (southwest Germany). Deposits collected from a borehole (P11) depth of 5 m - 10 m (for details see Strobel, 1996; Teutsch and Kobus, 1990; Terton, 1994).

- Hüntwangen aquifer gravels (HW) were collected at an outcrop near Hüntwangen (Switzerland) by Huggenberger and Siegenthaler (1993), and represent lithofacies types of a braided river environment (for details see Siegenthaler and Huggenberger 1993, Kleineidam 1998).

- River Rhein alluvium (RRA) from the field test side in Kehl. RRA is a quartz dominated aquifer materials characterized by a very low organic carbon and clay content.

- Canadian river alluvium (CRA) from Norman, Oklahoma, USA (for details see Shiau et al. 1995).
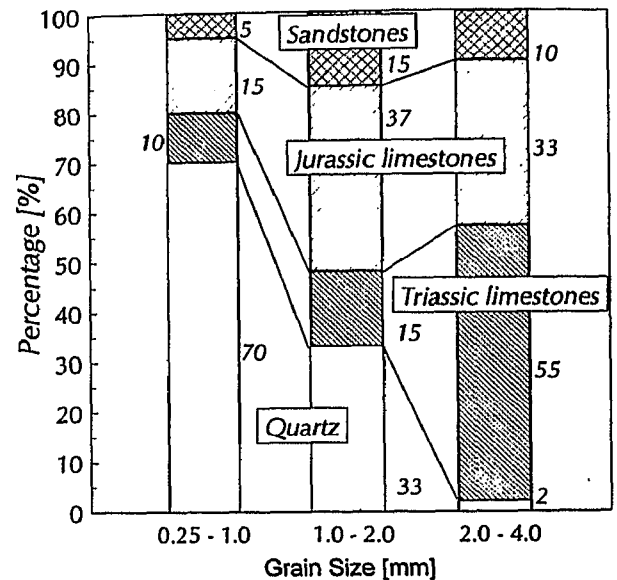
Fig. 4-7: Percentages (w/w) of the lithocomponents of RNA depending on the grain size, the smallest grain size was estimated.

- Jurrasic silty clay "Opalinuston" OPA (bav). For details see Grathwohl (1989).

Unweathered Rock Fragments

- Carbonate free quartzitic sandstone from triassic fluvial sand deposits: "Rhät-Sandstones" (Rh-SS).

- Dark colored micritic to sparitic marine limestones, triassic mud-flats (TL$_{br}$).

Artificial Aquifer Materials

- Kaolinitic marine sand (MS) obtained by MERCK.

- Industrial quartzes.

Prior to use the samples were wet sieved into different grain sizes, washed with deionized water to remove any silt and clay particles, air-dried and stored in the dark at room temperature. The materials consists of typical varieties of petrographic components, erosional products of either Triassic and Jurassic rocks (RNA, HH) or Alpine derived rocks (HW).

The fine gravel fraction (2 mm - 5 mm) of RNA, HH and HW was separated into its petrographical

different subcomponents based on visual appearance. Industrial quartz sands and gravels (Qtz) as well as sequentially broken and sieved dark Triassic limestone (TL$_{br}$) of different grain sizes were used to assess the influence of the grain size on the surfactant adsorption. The properties of all samples used are listed in Tab. 4-4.

4.3.2 Characterization of Solids

The carbonate content was determined by oxidation using hydrochloric acid (1n) and backtitration with N caustic soda (1n). The grain density was measured using a helium pycnometer (accu pyc, Micromeretics). For organic carbon measurements (f_{oc}) the samples were pretreated with hydrochloric acid to remove inorganic carbon and measured by dry combustion at 850° C under oxygen (boat sampler, Rosemount). The CO$_2$ produced was quantified by using an infrared detector (Horiba).

The intraparticle porosity, pore size distribution and interfacial areas of the mesopore range and of the macropore range were determined by BET N$_2$-adsorption/desorption isotherms (ASAP 2010 Micromeretics) and mercury intrusion (Autopore 9220, Micromeretics), respectively. The porosity determination methods are described in detail by Rügner (1998), who conducted all the porosity measurements. The definition of pore sizes used (Tab. 4-3) follows the intraparticle pore size classification according to IUPAC (International Union of Pure and Applied Chemistry). Figure 4-8 shows the cumulative surface area [m^2 g^{-1}] determined by combined mercury intrusion (macropores) and nitrogen adsorption/desorption (mesopores) depending on the pore diameter (Rügner, 1998) for the different lithocomponents of RNA.
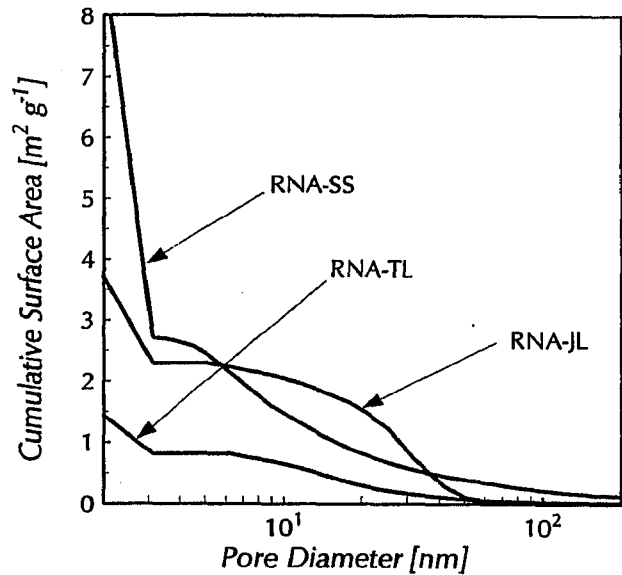
Fig. 4-8: Cumulative surface area determined by BET nitrogen adsorption/desorption (mesopores) and mercury intrusion (macropores) data versus pore diameter for lithocomponents of RNA. SS = sandstones, JL = Jurassic limestones, TL = Triassic limestones (see Table 4-4).

Tab. 4-3: Classification of intraparticle pores according to IUPAC.

	Pore Diameter	
	[nm]	[Å]
Micropores	<2	< 20
Mesopores	2-50	20 - 500
Macropores	>50	> 500

Effective Cation Exchange Capacity

The effective cation exchange capacity ($ECEC$) of the aquifer materials was determined by a method that is generally used for soil material containing carbonates (Drechsel, 1992). All exchangeable inorganic cations were displaced by Mg^{2+} in three successive displacement steps using 1 N MgCl$_2$. After three washing steps using ethanol Mg^{2+} was replaced with Ca^{2+} using 1 N CaCl$_2$. The Mg^{2+} ions were analyzed by atomic absorption spectrophotometry (AAS, Perkin and Elmer).

Tab. 4-4: Characteristics of the solids ("natural and artificial aquifer materials") used.

Solid Abbreviation	Component	Grain Size [mm]	f_{OC} [%][a]	$CaCO_3$ [b] [%]	BET [m² g⁻¹][c]	Density ρ_s [g cm⁻³]	ECEC [meq[f] kg⁻¹]
RNA	bulk sample	0.25 - 1.0	0.05	25.0	8.7	2.73	12.8
RNA	bulk sample	2.0 - 4.0	0.07	84.0	-	2.73	-
RNA - JL	Jurassic limestones	2.0 - 4.0	0.07	88.9	3.5	2.67	-
RNA - TL	Triassic limestones	2.0 - 4.0	0.13	87.7	1.3	2.48	-
RNA - SS	sandstones	2.0 - 4.0	0.01	10	4.2	2.29	-
RNA -Qz	quartz	2.0 - 4.0	0.01	<0.2	0.2	2.63	-
HH - JL	Jurassic limestones	2.0 - 4.0	0.07	95.4	1.9	2.67	-
HH - TL	Triassic limestones	2.0 - 4.0	0.05	91.8	1.4	2.48	-
HH - SS	sandstones	2.0 - 4.0	0.01	0.6	4.7	2.29	-
HH - Qz	quartz	2.0 - 4.0	0.01	<0.2	0.4	2.63	-
HW - dHL [d]	Helvetic limestones	2.0 - 4.0	0.04	85.0	0.6	2.73	-
HW - lHL [d]	Helvetic limestones	2.0 - 4.0	0.02	81.0	1.8	2.73	-
HW - dTS [d]	sandstones	2.0 - 5.0	0.07	36.0	2.0	2.67	-
HW - lS [d]	sandstones	2.0 - 4.0	0.04	31.0	3.1	2.66	-
HW - Met [d]	metamorphic rocks	2.0 - 4.0	0.01	2.0	0.8	2.65	-
HW - Qz [d]	quartz	2.0 - 4.0	0.00	15.0	0.1	2.63	-
RRA	bulk sample	0.2 - 0.63	0.02	1.2	-	-	8.7
OPA (bav)	Opalinuston	<0.063	0.96 [g]	-	40.3 [g]	2.70 [g]	455 [g]
CRA	bulk sample	<0.5	1.19	4.8	36 [e]	-	-
Rh-SS *	Rhät sandstones	different	0.004	0	1.02	2.48	
TL$_{br}$ *	Triassic limestones	different	0.072	92	1.43	2.71	-
MS	marine sand	0.1 - 0.3	0.01	-	-	2.61	-
Quartz	industrial broken	different	0.01	<0.2	0.1	2.65	-

[a] Organic carbon content. [b] Calcium carbonate content. [c] Determined by N_2 adsorption/desorption isotherms. [d] Data from Kleineidam 1998. [e] Shiau et al., 1995. [f] Milli-equivalent charge ($mmol_{charge}$). [g] Grathwohl, 1989. * Rock fragments from the source areas.

4.4 Batch Methods

4.4.1 Surfactant Adsorption Kinetics

The adsorption kinetics were measured for TS G50 in a batch system using a surfactant concentration of 0.88 mM, which is just above the CMC_{st}. The data are shown in Fig. 4-9 where the apparent distribution coefficient $K_{d, surf}(t)$ normalized to the distribution coefficient in equilibrium $K_{d, surf}$ is plotted versus time. The adsorption equilibrium seems to be reached within 150 min. However, since the sampling intervals were kept very short, the batch system was probably not mixed thoroughly between taking two successive samples. Thus, the measured adsorption kinetics seem to be to slow compared to a completely mixed batch or column system, which exhibit shorter distances to potential sorption sites.
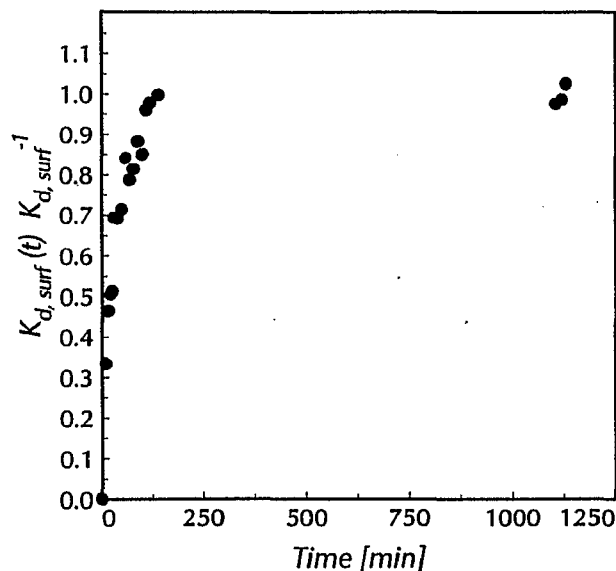

Fig. 4-9: Adsorption kinetics of TS G50 onto RNA; equilibrium seems to be reached within about 150 minutes. This time seems to be overestimated due to the experimental setup.

4.4.2 Surfactant Isotherms

The adsorption of the surfactants onto the aquifer material was determined in batch experiments at different aqueous surfactant concentrations in the solution. For each concentration (from zero up to 10 times the CMC_{st}) an equal ratio of aquifer material to solution was placed in 5 mL to 20 mL crimp top reaction glass vials (chrompac) sealed with teflon lined butyl rubber septas (Alltech). The different concentrations of the isotherms were obtained by diluting a surfactant stock solu tion with degassed and deionized water, that was filtrated through activated carbon and a C18 cartridge-filter (SEP-PAK Cartridges, Alltech) in order to remove organic compounds. To all samples (except SDS) an aliquot of $CaCl_2$ stock solution was added resulting in a final $CaCl_2$ concentration of 0.01 M in the batch systems to gain a constant ionic strength and facilitate the liquid/solid separation. The optimum solid to water phase ratio was determined in preliminary batch tests which aimed at a decrease of the surfactant concentration in the aqueous phase of about 50 %. The samples were shaken overnight on a horizontal shaker and left for equilibration at

room temperature, temporarily shaken by hand. Before measurement the vials were centrifuged with about 2500 rpm for 20 minutes. The surfactant concentration in the supernatant water was measured as total organic carbon (TOC) using a TOC-Analyzer (highTOC, elementar, Hanau, Germany), that combusts the organic carbon at 950°C detecting the CO_2 by non-disperse infrared detection (NDIR). The calibration curve for TOC (Fig. 4-10) shows a highly linear relationship between the TOC concentration and the peak area obtained from the NDIR detection. The conventional detection limit was taken three times the value of the background organic carbon concentration (noise). It depends on the water quality which was available to run the TOC analyzer. In these experiments the detection limits were 10 mg C L^{-1} (tapwater without purification), 2 mg C L^{-1} (deionized water purified with activated carbon filter, C18-cartridge, 0.2 μm membrane filter) and 1 mg L^{-1} (millipore water).

The TOC concentrations were converted into surfactant concentrations. The adsorbed mass of surfactant was determined based on mass balance consideration in order to construct an adsorption isotherm (Fig. 4-11). All samples were investigated in triplicate. Surfactant and media blanks were conducted as appropriate.
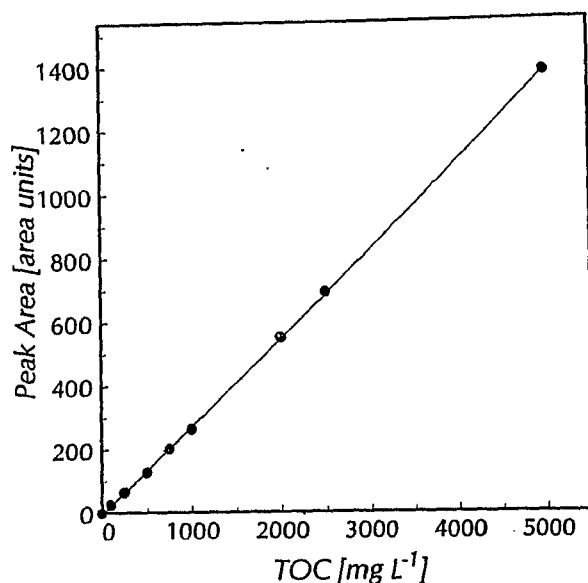
Fig. 4-10: Calibration curve for total organic carbon (TOC); $R^2 > 0.999$.

Fig. 4-11: Sketchmap of a batch system in order to obtain adsorption data resulting in an adsorption isotherm

4.4.3 Phenanthrene Adsolubilization

Adsolubilization studies were conducted using a titration method described by Nayyar et al. (1994). In a single 1 L batch reactor (Schott) containing aquifer material and surfactant solution (0.01 M $CaCl_2$) in a constant ratio of 1 : 10 the phenanthrene concentration was stepwise increased by maintaining a constant surfactant adsorbed concentration. Phenanthrene was added in small volumes of a concentrated methanol stock solution (500 µg mL^{-1}). The volume of the added stock solution did not exceed 0.2 % of the total volume in the reactor at the end of the experiment and should not have any influence on the behavior of phenanthrene (Nkedi-Kizza et al., 1987). Preliminary tests showed, that equilibrium of phenanthrene partitioning between adsorbed surfactants and aqueous phase is reached within half an hour (Fig. 4-9). Thus 1 h of horizontal shaking was allowed between two successive titrations to ensure equilibration. For analysis about 3 mL of the supernatant solution were transferred into a quartz glass cuvette and the phenanthrene concentration was measured using a fluorescence detector (Perkin & Elmer LS 3B, excitation 260 nm, emission 345 nm). After measurement the sample was poured back into the batch reactor.
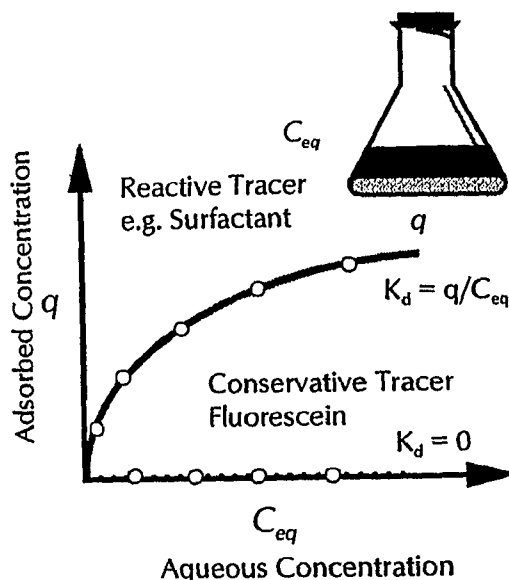
Controls which contained only the the aquifer material and the 0.01 M $CaCl_2$ solution (no surfactant) were included in order to measure the phenanthrene adsorption onto the natural solids. Similar controls without aquifer material and without surfactants were conducted in order to quantify phenanthrene losses due to sorption onto system components.

4.5 Column Methods

4.5.1 Packing of Columns

One dimensional column experiments under water saturated conditions were performed using stainless steel columns with a transport length of 70 mm, 90 mm and 123.5 mm, respectively. The inner diameter of the columns was 10 mm and 25 mm, respectively, with female type stainless steel end fittings (Alltech). RNA grain size fractions of 0.25 mm - 1.0 mm and 1.0 mm - 2.0 mm were used for the column experiments. Stainless steel capillaries were used with an inner diameter of 0.5 mm (Alltech). Stainless steel frits of 0.125 mm pore size were used to prevent migration of fine particles of the aquifer material. Changes in the flow rate were minimized by using a peristaltic pump (Ismatec). Each column was

packed as uniformly as possible by flooding from below and filling in the aquifer material from above at the same time. During the procedure the column was slightly shaken. In that way the column could be homogeneously packed which minimized entrapped air bubbles and grain size separation due to gravity in the supernatant aqueous phase. The columns were cleaned and repacked for each separate experiment. A newly filled column was conditioned by pumping 250 mL or more of 0.01 M CaCl$_2$ solution in order to obtain steady state conditions and to remove any suspended colloids. All influent solutions of the column experiments were degassed prior to use and contained 0.01 M CaCl$_2$ in order to prevent migration of fines by providing uniform ionic strength.

4.5.2 Transport of the Conservative Tracer

The hydrodynamic parameters (porosity, longitudinal dispersion coefficient and dispersivity) which characterize each column system were obtained from breakthrough curves of a conservative tracer (Fluorescein). These tracer tests were conducted as front type experiments where the tracer was fed continuously to the column. The breakthrough of the conservative tracer Fluorescein was measured using a fluorescence on-line detection setup (Fig. 4-12, excitation: 487 nm, emission: 512 nm), which consists of the influent solution reservoir, the stainless steel column containing the aquifer material, a fluorescence detector (Merck-Hitachi, F-1080), the peristaltic pump and the effluent reservoir in that order. The fluorescence detector was coupled to a personal computer with a chromatographic software (Waters Maxima 820) to record breakthrough curves in real time. The system dead volume V_d of the connection tubings, fittings etc. between the influent solution bottle and the detector which was not filled by the porous medium was below 0.2 cm^3 for the phenanthrene breakthrough experiments using on-line
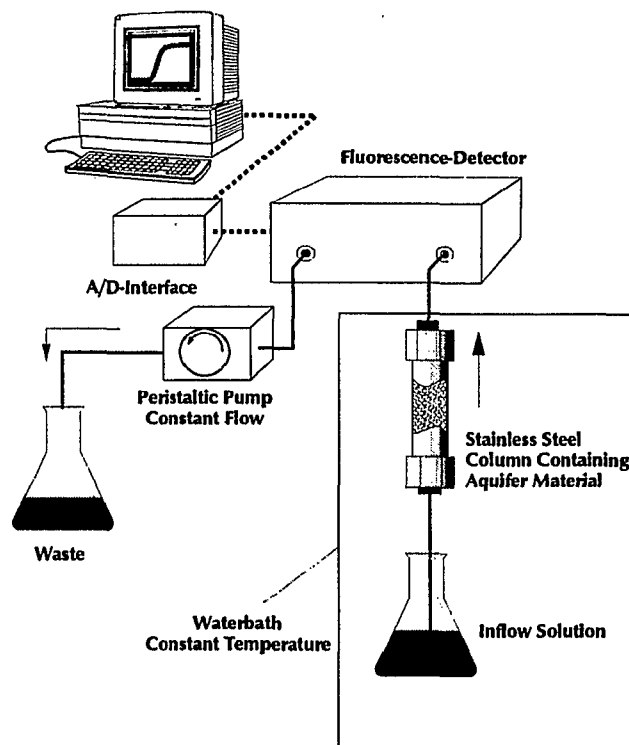
Fig. 4-12. Experimental setup for the on-line detection of breakthrough curves of the conservative tracer (Fluorescein) and the reactive tracer phenanthrene in the presence and absence of surfactant (from Schüth, 1994, modified).

detection and below 0.5 cm^3 for the surfactant breakthrough experiments using a fraction collector. The influent concentration C_0 was measured before and after each experiment using the same setup bypassing the column.

In order to compare the column experiments the monitored data were transformed into breakthrough curves (BTCs) where the effluent concentration relative to the influent concentration (C/C_0) is plotted versus dimensionless time expressed as number of pore volumes displaced. An example of a typical breakthrough curve of the conservative tracer is shown in Fig. 4-13. The sigmoidal breakthrough curve is almost symmetrical and is perfectly fitted by the solution of the one-dimensional advection-dispersion equation (3-33), Ogata and Banks, 1961).

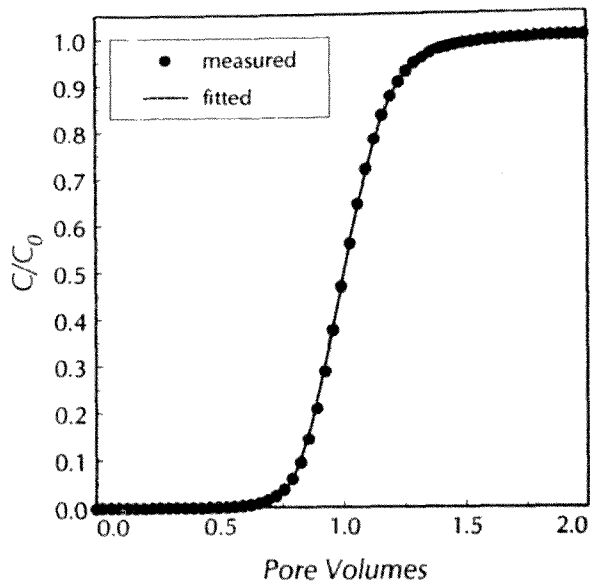Fig. 4-13: Breakthrough curve of the conservative tracer (Fluorescein) and fitted analytical solution of the advection dispersion equation (Ogata and Banks, 1961).

Fig. 4-14: Scheme of the experimental setup for the surfactant column experiments and the transformation of the measured data into a breakthrough curve (BTC).

4.5.3 Surfactant Transport

To study the transport of surfactants in the absence of phenanthrene several independent column experiments were conducted at room temperature using the nonionic surfactant TS G50 at concentrations below and above the CMC_{st}. The experimental setup consists of the influent solution reservoir, the peristaltic pump, the stainless steel column containing the aquifer material and a fraction collector in that order. After equilibrating the column the influent was switched to the surfactant solution and the experiment was started.

Samples were collected in 10 mL glass tubes at different time intervals depending on the flow rate to obtain highly resolved breakthrough curves. The samples were diluted for analysis to a volume of about 20 mL and measured as TOC. The influent concentration C_0 of the sampled surfactant breakthrough experiments was determined by taking samples of the influent solution throughout the experiment.

4.5.4 Coupled Transport of PAHs and Surfactants

The surfactant facilitated transport was studied using phenanthrene concentrations of 50 µg L^{-1} and 100 µg L^{-1} (about 5 % and 10 % of the water solubility, respectively) and different surfactant concentrations. The phenanthrene was added in a small amount of methanol in which the phenanthrene was dissolved in the standard stock solution (1000 ng µL^{-1}). Phenanthrene standard was added to 1 L of surfactant solution resulting in a final concentration of 50 µg L^{-1} and 100 µg L^{-1}, respectively. An influence on the transport behavior of phenanthrene is not to be expected for such small amounts of methanol according to Nkedi-Kizza et al. (1987). They observed the transport of pesticides within column systems and reported an influence of methanol on the transport of the pesticides only for methanol concentration above several percent. However, methanol influences the CMC. Column experiments of phenanthrene without surfactant were performed for comparison.

Fig. 4-15: Phenanthrene concentration (left y-axis) and resulting fluorescence signal (right y-axis) versus surfactant concentration for the TS G50 using the PERKIN & ELMER Fluorescence detector; excitation: 260 nm, emission 345 nm.
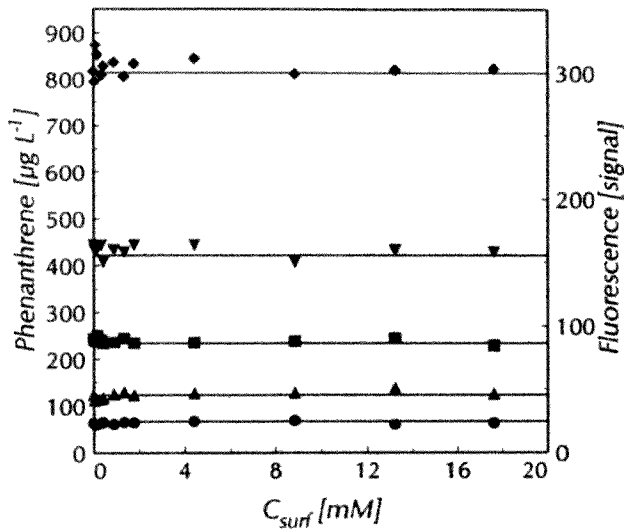
Fig. 4-16: Phenanthrene calibration curves using fluorescence detection; plotted is the relative fluorescence signal normalized to the maximum signal versus phenanthrene concentration for the PERKIN & ELMER detector (adsolubilization experiments) and the MERCK-Hitachi F-1080 detector (transport experiments with on-line detection); excitation: 260 nm, emission: 345 nm.

The setup of the column experiments as described in chapter 4.5.2 ensures that the surfaces contacted by the aqueous solution were either stainless steel or glass. Thus, the loss of phenanthrene e.g. due to sorption onto hydrophobic tubing etc. (e.g. fluoro-elastomers of the peristaltic pump) could be minimized. The influent solution reservoir and the column were temperated in a waterbath to obtain a constant temperature, which has a significant influence on the fluorescence signal. In preliminary tests it turned out that phenanthrene showed a linear relationship between concentration and fluorescence signal at wavelengths of 260 nm for excitation and 345 nm for emission. A crucial point of this method could be the suppression of the fluorescence signal by surfactants present in solution. This phenomena is commonly called "quenching" and was also used to determine partitioning coefficients between the aqueous phase and dissolved organic

matter (Gauthier et al., 1986 and 1987). In this study no quenching was observed for phenanthrene and the surfactants used (Fig. 4-15), i.e. phenanthrene can be detected regardless whether it is free in the aqueous solution, associated to a surfactant monomer or dissolved within the pseudophase of a micelle. The calibration curves (Fig. 4-16) show a highly linear relationship between phenanthrene concentration and fluorescence signal for both used detectors($R^2 > 0.999$). The detection limit is conventionally given by the value of three times the average (self-) fluorescence of water or surfactant solution without phenanthrene (PERKIN & ELMER: 5 µg L^{-1}]. This value was even smaller for the on-line detection where relative concentrations were measured (MERCK-Hitachi: 1 µg L^{-1}].

4.5.5 Hydraulic Conductivity

A simple permeameter setup was used to monitor the variation of the hydraulic conductivity during a surfactant breakthrough experiment. The hydraulic head was measured in polyethylene tubings at the column inlet and column outlet to obtain the headloss along the column. For details of the permeameter setup see Kleineidam (1998) and Lösch (1997; master thesis).

Additional large scale experiments using aquifer material of a smaller grain size were conducted by Lemp (1996; master thesis) to examine the influence of surfactants on the hydraulic conductivity She used columns of 1 m length containing homogenized industrial quartz sand and alluvial loam after the application of a soil mixing procedure (Klein, 1998). The percentage of loam ranged between 14 % and 20 %. Breakthrough curves of TS G50 (10.86 mM) were measured and the variation of the hydraulic conductivity K_f during the surfactant breakthrough was monitored using a similar permeameter (Lemp, 1996; master thesis).

5 Results

5.1 Surfactant Adsorption

All surfactant adsorption isotherms presented in this chapter are inverse L-shaped plotting in two different pseudo-linear segments linked by a more or less established intermediate region. They can be described by two linear relationships: $q = K_{d,\,mn} C_{eq}$ followed by the adsorption maximum where q equals q_{max}. The critical micelle concentration in the presence of electrolytes (CMC_e) was obtained by the intersection of these two straight lines ($CMC_e = q_{max} K_{d,\,mn}^{-1}$). Regarding all surfactant adsorption isotherms the CMC_e ranges between 0.31 mM and 0.98 mM with a mean value ($\pm$ standard deviation 1σ) of (0.55 $\pm$ 0.09) mM. This value is significantly smaller than CMC_{st} (0.88 mM) obtained by surface tension measurements (capillary rise).

The surfactant specific interfacial area A_{surf} which is covered by the surfactants is given in the tables in order to compare different surfactants. In addition the ratios $A_{surf} BET^{-1}$ and $A_{ext} A_{surf}^{-1}$ are included in order to show which interfacial area is covered by the surfactants compared to the BET surface area and the external surface area of the grains, respectively.

It should be noted that all isotherms have an identification number, e.g. i12, in order to facilitate the finding of the respective data in figures or tables.

5.1.1 Adsorption of TS G50

The non-ionic surfactant TS G50 was used as a chemical probe for the surfactants to characterize different aquifer materials including lithological subcomponents and different grain sizes.

River Neckar Alluvium (RNA)

Typical adsorption isotherms of TS G50 onto the different grain sizes of the natural aquifer material
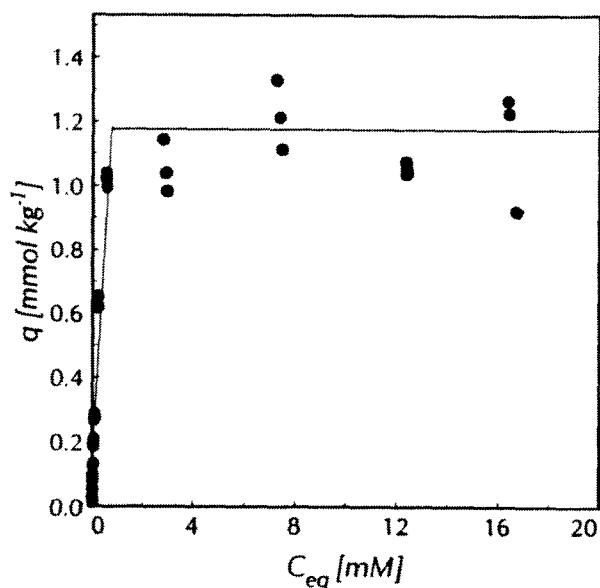
Fig. 5-1: Adsorption of the nonionic TS G50 onto RNA, grain size 0.25 mm - 1.0 mm, (i12).

RNA are shown in Fig. 5-1 and Fig. 5-2. The identified parameters are summarized in Tab. 5-1.

The geometric mean diameters of the grain size fractions used range from 0.35 mm to 2.83 mm. $K_{d,\,mn}$ and q_{max} range from 1.87 L kg^{-1} to 3.05 L kg^{-1} and 0.94 mmol kg^{-1} to 1.94 mmol kg^{-1}, respectively. Low values of $K_{d,\,mn}$ correspond to low values of of q_{max} with the lowest values for the isotherm of the largest grain size (i51). The surfactant covered interface A_{surf} ranges between 1245 cm^2 g^{-1} and 2566 cm^2 g^{-1}. The external surface of the aquifer grains (A_{ext}) is between 0.62 % and 3 % of A_{surf}, while the latter (A_{surf}) is between 1.6 % and 3.2 % of BET.

All isotherms where measured at room temperature (20 °C) except the isotherm i8. However, the isotherm parameters determined for i8 do not differ significantly from the corresponding isotherm i9: $K_{d,\,mn}$: 2.83 L kg^{-1} versus 3.05 L kg^{-1} and q_{max}: 1.94 mmol kg^{-1} versus 1.81 mmol kg^{-1}, respectively (see Tab. 5-1).

Fig. 5-2: Adsorption isotherms of TS G50 onto different grain size fractions of RNA. The small and large grain size fractions are dominated by Quartz (i12) and by Triassic limestones, respectively (see Fig 4-7).

Fig. 5-3: Adsorption isotherms of TS G50 onto the bulk sample and lithocomponents of RNA (grain size 2 mm - 4 mm).

RNA, Horkheim and Hüntwangen Lithocomponents

The adsorption isotherms of TS G50 onto RNA are shown in Fig. 5-3. The low concentrations are zoomed out in Fig. 5-4 for closer inspection. The isotherms of the bulk sample and lithocomponents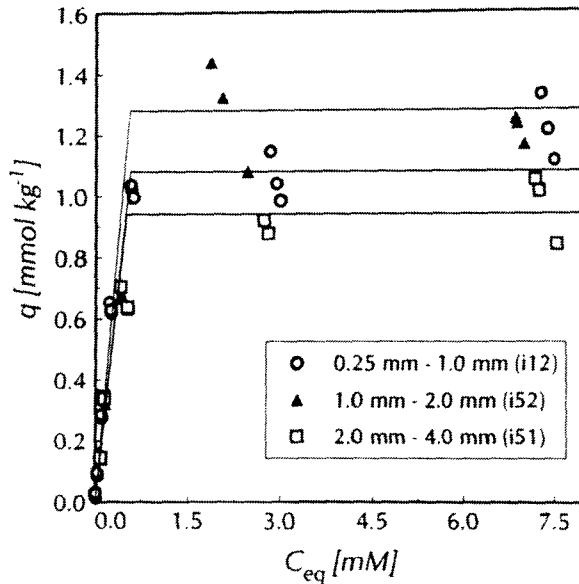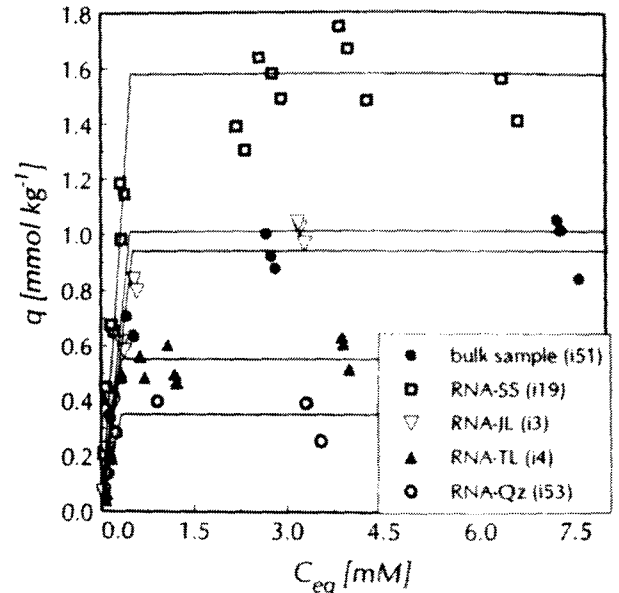 of Horkheim (HH) and Hüntwangen (HW) are shown in Fig. 5-5 and Fig. 5-6, respectively. The identified parameters of these isotherms are summarized in Tab. 5-1.

All isotherms show the same nonlinear shape. The values of $K_{d\ min}$, q_{max} and A_{surf} range from 0.18 L kg^{-1} to 3.32 L kg^{-1}, 0.10 mmol kg^{-1} to 1.58 mmol kg^{-1} and 135 cm^2 g^{-1} to 2094 cm^2 g^{-1}, respectively. The A_{surf} values were highest for the sandstones, followed by Triassic limestones, Jurassic limestones and finally quartz. The measured adsorption maximum of the bulk sample of 2 mm - 4 mm RNA (i51) was compared to the $q_{max}(bulk)$, which was calculated according to equation (3-3) from the individual adsorption maxima of the measured lithocomponent

isothermtherms. The calculated value of (0.80 ± 0.06) mmol kg^{-1} was somewhat smaller than the measured q_{max} of (0.94 ± 0.09) mmol kg^{-1}, but it is still in reasonably good agreement considering the measurement errors.

The values for RNA-Qz (i53) and RNA-SS (i19) fit reasonably good to HH-Qz (i45) and HH-SS (i48), respectively. The values of the Horkheim limestones (i46, i47) are smaller than the RNA limestones (i3, i4). A possible reason for that observation could be a slightly different source area of the lithocomponents of these River Neckar valley sediments.

The Hüntwangen aquifer material in general shows lower surfactant adsorption than the Neckar sediments and the differences between the individual lithocomponents are less significant. The $A_{ext} A_{surf}^{-1}$ and $A_{surf} BET^{-1}$ ratios range frome 0.4 % to 6.0 % and from 1.1 % to 15.0 %, respectively.. The highest values of the $A_{ext} A_{surf}^{-1}$ and $A_{surf} BET^{-1}$ ratios where found for the quartz-minerals (i53, i45, i40) and the lowest values for the sandstones (i19, i48, i43).
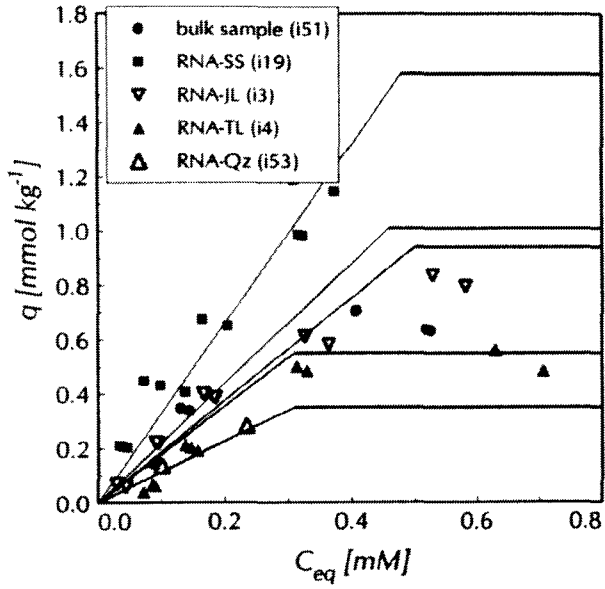
Fig. 5-4: Adsorption isotherm of TS G50 onto the bulk sample of RNA of the grain size 2 mm - 4 mm.
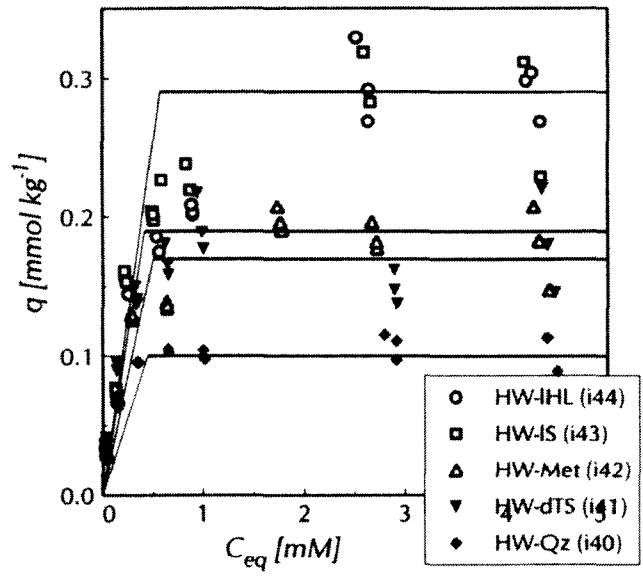

Fig. 5-6: Adsorption isotherms of TS G50 onto lithocomponents of Hüntwangen aquifer material; grain size 2 mm - 4 mm.
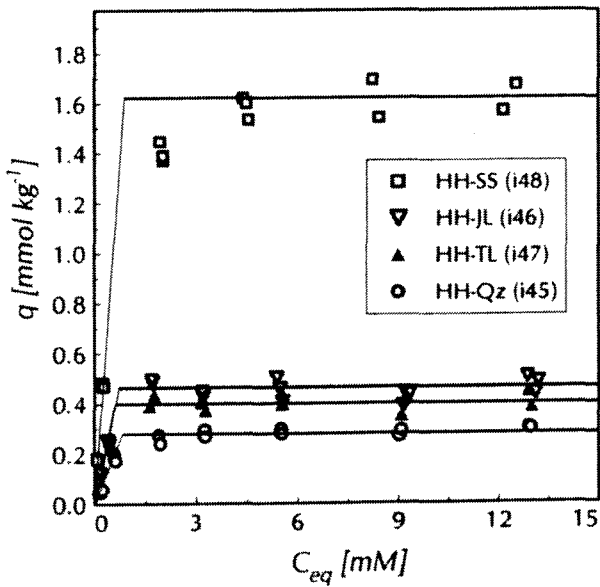
Fig. 5-5: Adsorption isotherms of TS G50 onto lithocomponents of Horkheim aquifer material; grain size 2 mm - 4 mm.

Tab. 5-1: Results from the adsorption experiments of TS G50 for bulk samples and lithological subcomponents of River Neckar Alluvium (RNA) and Horkheim (HH) as well as onto lithological subcomponents of Hüntwangen (HW).

Solid (Exp. #)	Grain Size[a]	T	$K_{d, mn}$	R^2	q_{max}	CMC_c^c	A_{ext}	A_{surf}	$\frac{A_{ext}}{A_{surf}}^{-1}$	$\frac{A_{surf}}{BET}^f$
	[mm]	[°C]	[L kg⁻¹]	[-]	[mmol kg⁻¹]	[mM]	[cm² g⁻¹]	[cm² g⁻¹]	[%]	[%]
RNA-bulk (i51)	2.83	20	1.87	0.90	0.94 ± 0.09	0.5	7.8	1245	0.6	1.6
RNA-bulk (i9)	0.35	20	3.05	0.924	1.94 ± 0.19	0.64	62.2	2566	2.4	3.2
RNA-bulk (i8)	0.35	10	2.83	0.984	1.81 ± 0.09	0.64	62.2	2403	2.6	3.0
RNA-bulk (i12)	0.50	20	2.57	0.991	1.10 ± 0.12	0.43	44.1	1461	3.0	1.8
RNA-bulk (i52)	1.41	20	2.60	0.891	1.28 ± 0.10	0.49	15.5	1699	0.9	2.1
RNA Qz (i53)	2.83	20	1.11	0.955	0.35 ± 0.08	0.31	8.1	460	1.8	11.5
RNA-TL (i4)	2.83	20	1.78	0.982	0.55 ± 0.06	0.31	8.55	734	1.2	5.3
RNA-JL (i3)	2.83	20	2.22	0.968	1.01 ± 0.11	0.46	7.95	1337	0.6	3.6
RNA-SS (i19)	2.83	20	3.32	0.901	1.58 ± 0.15	0.50	9.26	2094	0.4	2.4
HH-Qz (i45)	2.83	20	0.33	0.972	0.28 ± 0.02	0.85	8.07	372	2.2	9.7
HH-TL (i47)	2.83	20	0.49	0.955	0.38 ± 0.05	0.77	8.55	500	1.3	3.1
HH-JL (i46)	2.83	20	0.56	0.970	0.46 ± 0.04	0.81	7.95	603	1.7	3.5
HH-SS (i48)	2.83	20	1.88	0.973	1.57 ± 0.13	0.84	9.26	2080	0.5	4.5
HW-Qz (i40)	2.83	20	0.18	0.949	0.10 ± 0.03	0.57	8.07	135	6.0	15.0
HW-LhL (i44)	2.83	20	0.60	0.921	0.29 ± 0.02	0.49	7.77	389	2.0	1.9
HW-lS (i43)	2.83	20	0.46	0.743	0.26 ± 0.04	0.57	7.97	346	2.3	1.1
HW-dTS (i41)	3.16	20	0.47	0.716	0.18 ± 0.03	0.38	5.02	232	3.1	1.5
HW-Met (i42)	2.83	20	0.45	0.949	0.19 ± 0.02	0.42	8.00	249	3.2	3.1

[a] Geometric mean of the respective grain size fraction sieved.

Marine Sand, Opalinuston (OPA) and Canadian River Alluvium (CRA)

The adsorption isotherms of TS G50 onto marine seasand, OPA and CRA are shown in Fig. 5-7 and Fig. 5-8. The data are summarized in Tab. 5-2. Values of $K_{d, mn}$, q_{max} and A_{surf} range from 3.63 L kg^{-1} to 117.9 L kg^{-1}, 1.08 mmol kg^{-1} to 65.86 mmol kg^{-1} and 1435 cm^2 g^{-1} to 87254 cm^2 g^{-1}, respectively.

While the adsorption of TS G50 onto the kaolinitic, marine sand is very similar to that onto RNA (describing parameters in the same range), the adsorption onto CRA and OPA is significantly higher. The $A_{ext} A_{surf}^{-1}$ ratios range between 3 % and 9 % while the $A_{surf} BET^{-1}$ ratios range between 2 % for CRA and 22 % for OPA. The high value for OPA may be due to the small grain size and the surface properties of this silty, clayey material.

Industrial Quartzes, Artificially Broken Triassic Limestones and Rhät Sandstones

The adsorption isotherms of TS G50 onto different grain sizes of industrial quartzes, Triassic limestones (TL$_{br}$) and Rhät sandstones are shown in Fig. 5-9, Fig. 5-10 and Fig. 5-11, respectively. The data are summarized with the data of additional isotherms in Tab. 5-2. It should be noted that for these experiments the solids were sequentially broken and sieved to obtain the different grain size fractions. Thus, artificial surfaces where created which are not weathered compared to natural aquifer materials.

The isotherms of TS G50 onto different grain sizes of the Rh-SS almost coincide, while the isotherms onto different grain sizes of TL$_{br}$ show a significantly increasing adsorption maximum with decreasing grain size. The $K_{d, mn}$ q_{max} and A_{surf} values range from 0.12 L kg^{-1} to 2.50 L kg^{-1}, 0.06 mmol kg^{-1} to 1.58 mmol kg^{-1} and 78 cm^2 g^{-1} to 2098 cm^2 g^{-1}, respectively. The $A_{ext} A_{surf}^{-1}$ ratio range between 13 % and about 100 % for the quartzes and the TL$_{br}$, i.e. a significant amount of the surfactant is adsorbed at the external surface of the grains. The $A_{ext} A_{surf}^{-1}$ ratio decreases with increasing size of the grains, i.e. less surfactants
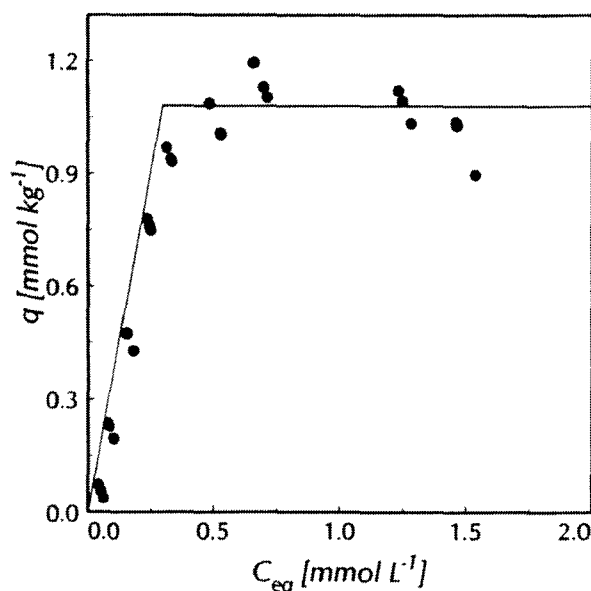
Fig. 5-7: Adsorption isotherm of TS G50 onto marine sand MS (i20).
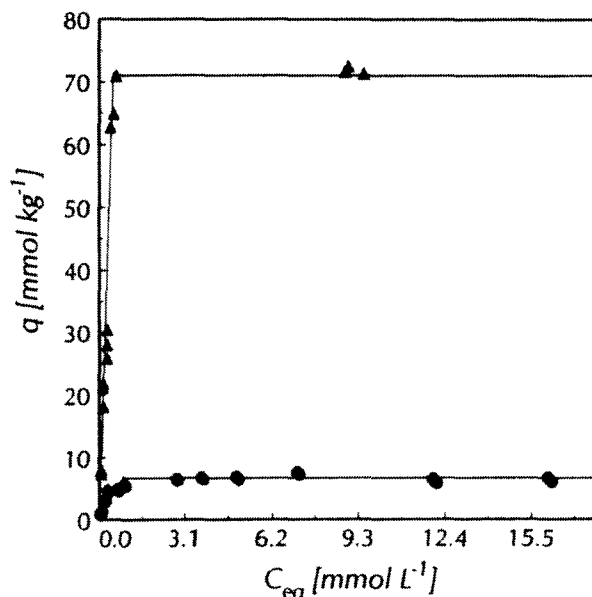
Fig. 5-8: Adsorption isotherms of TS G50 onto CRA and OPA.

are adsorbed at the external surface. This may be due to rougher surfaces or fissures/pores in the larger grain sizes. The $A_{surf} BET^{-1}$ ratios for the quartzes range between 8 % and 15 %, i.e. over 80 % of the BET surface area is not accessible to the surfactant.

It should be noted that all isotherms where measured at a temperature of 20 °C except the isotherm i18 which was measured at 10 °C. However, the isotherm parameters identified do not significantly differ from the parameters of the corresponding isotherm which was measured at 20° C (i14).
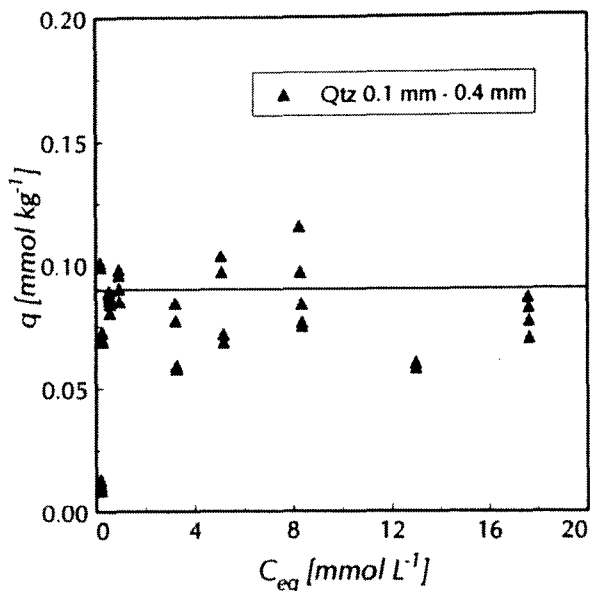
Fig. 5-9: Adsorption isotherm of TS G50 onto industrial quartz sand (i14).
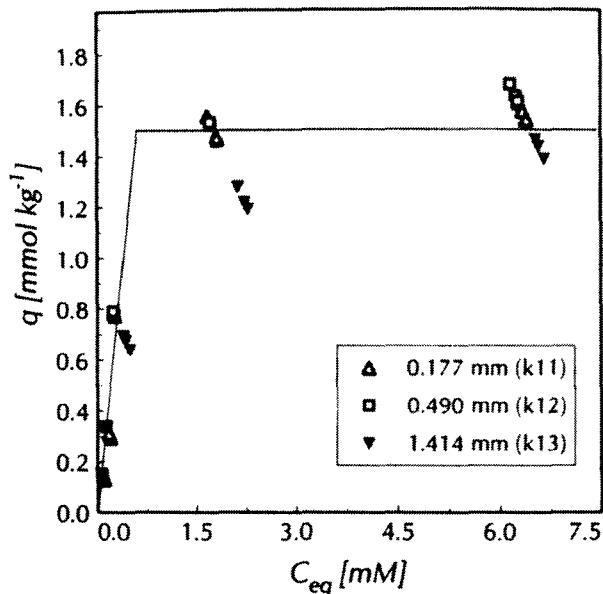
Fig. 5-11: Adsorption isotherms of TS G50 onto different grain sizes of Rhät sandstones (Rh-SS). The grain size has almost no influence on q_{max}.
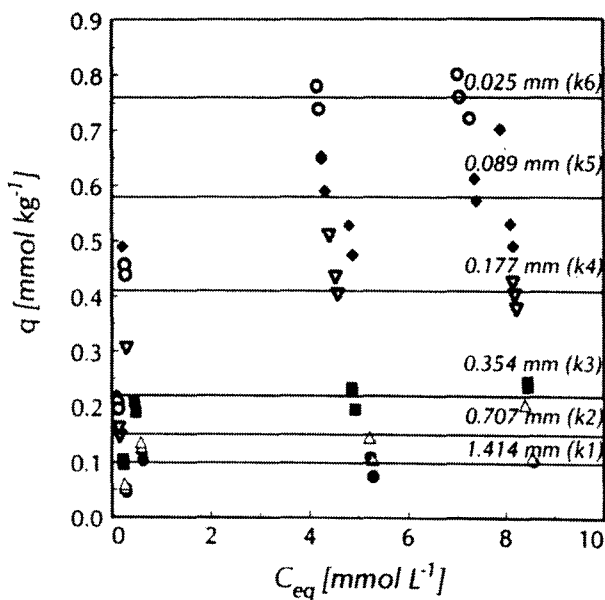
Fig. 5-10: Adsorption isotherms of TS G50 onto different grain sizes of artificially broken and sieved Triassic limestones (TL$_{br}$). The adsorption maximum increases significantly with decreasing grain size.

Tab. 5-2: Results from the adsorption experiments of TS G50 for marine sand (MS), Opalinuston (OPA), Canadian River Alluvium (CRA) and different grain sizes of industrial quartzes (Qtz), Triassic limestones (TL_{br}) and Rhät sandstones (Rh-SS). TL_{br} and Rh-SS are rock fragments from the respective source area of RNA (artificially broken rocks, sieved to the grain sizes).

Solid (Exp. #)	Grain Size [a]	T	$K_{d, mn}$	R^2	q_{max}	CMC_s	A_{ext}	A_{surf}	$A_{ext} A_{surf}^{-1}$	$A_{surf} BET^{-1}$
	[mm]	[°C]	[L kg^{-1}]	[-]	[mmol kg^{-1}]	[mM]	[cm^2 g^{-1}]	[cm^2 g^{-1}]	[%]	[%]
MS (i20)	0.20	20	3.63	0.955	1.08 ± 0.08	0.30	111	1435	8	-
OPA (i13)	0.003	20	117.9	0.940	65.86 ± 5.85	0.56	7407	87254	9	22
CRA (i1)	0.10	20	14.3	0.979	6.62 ± 0.44	0.46	222	8772	3	2
Qtz (i14)	0.20	20	0.12	0.927	0.09 ± 0.02	0.80	114	125	91	13
Qtz (i18)	0.20	10	0.16	0.820	0.11 ± 0.02	0.69	114	147	78	15
Qtz (i15)	0.20	20	-	-	0.09 ± 0.01	-	114	113	101	11
Qtz (i16)	0.85	20	-	-	0.06 ± 0.03	-	27	78	34	8
Qtz (i17)	2.65	20	0.15	0.923	0.07 ± 0.02	0.45	9	92	9	9
TL_{br} (k6)	0.03	20	1.65	0.972	0.76 ± 0.03	0.46	964	1002	96	-
TL_{br} (k5)	0.09	20	1.84	0.976	0.58 ± 0.07	0.32	273	769	36	-
TL_{br} (k4)	0.18	20	1.03	0.946	0.41 ± 0.06	0.40	137	541	25	-
TL_{br} (k3)	0.35	20	0.42	0.948	0.22 ± 0.02	0.52	68	290	23	-
TL_{br} (k2)	0.71	20	0.22	0.979	0.15 ± 0.04	0.68	34	199	17	-
TL_{br} (k1)	1.41	20	0.16	0.984	0.10 ± 0.02	0.65	17	136	13	-
Rh-SS (k11)	0.18	20	1.57	0.907	1.53 ± 0.05	0.98	137	2033	7	-
Rh-SS (k12)	0.49	20	2.50	0.980	1.58 ± 0.06	0.73	49	2098	2	-
Rh-SS (k13)	1.41	20	2.28	0.962	1.33 ± 0.12	0.58	17	1760	1	-

[a] Geometric mean of the respective grain size fraction sieved. "-" Not determined.

5.1.2 Adsorption of Non-ionic, Anionic and Cationic Surfactants

TS G80, TX-100, DF 8390, SDS and HDTMA onto RNA

The adsorption isotherms of the non-ionic TS G80 and TX-100 as well as the di-anionic DF 8390 onto RNA are shown in Fig. 5-12. The isotherm of the anionic SDS onto RNA is shown in Fig. 5-13. The isotherms of the cationic HDTMA onto RNA and RRA, respectively, are shown in Fig. 5-14. The results of all these isotherms are summarized in Tab. 5-3. It should be noted, that all adsorption isotherms were measured in the presence of 0.01 M CaCl$_2$ except the SDS isotherms, since the presence of Ca^{2+} in that system caused precipitation of SDS. The isotherms of the di-anionic DF-8390 and the anionic Marlinat were measured like the nonionic surfactants in the presence of CaCl$_2$ since they are less susceptible to precipitation in the presence of Ca^{2+}.

Considering the surfactant adsorption onto the bulk sample of RNA (grain sizes 0.35 mm and 0.5 mm) the $K_{d, mn}$ and q_{max} values range from 0.61 L kg^{-1} to 77.1 L kg^{-1} and 0.63 mmol kg^{-1} to 28.9 mmol kg^{-1}, respectively. No adsorption could be measured for Marlinat in the millimolar concentration range (mM).

Fig. 5-13: Adsorption of anionic SDS onto RNA, 0.25 mm - 1.0 mm, i33, Martin (1997).
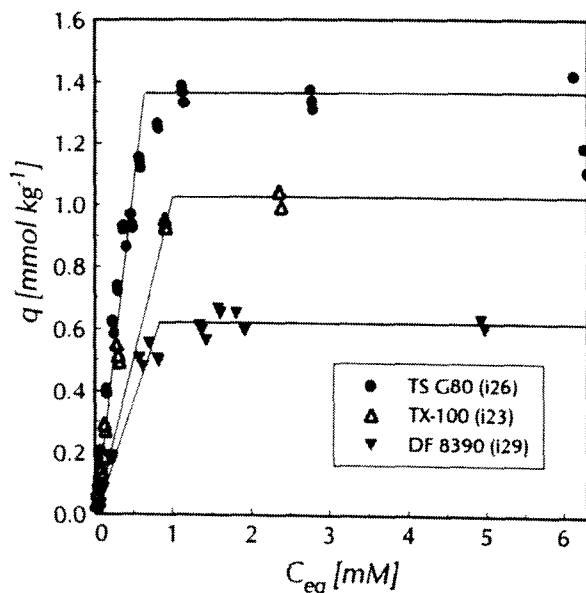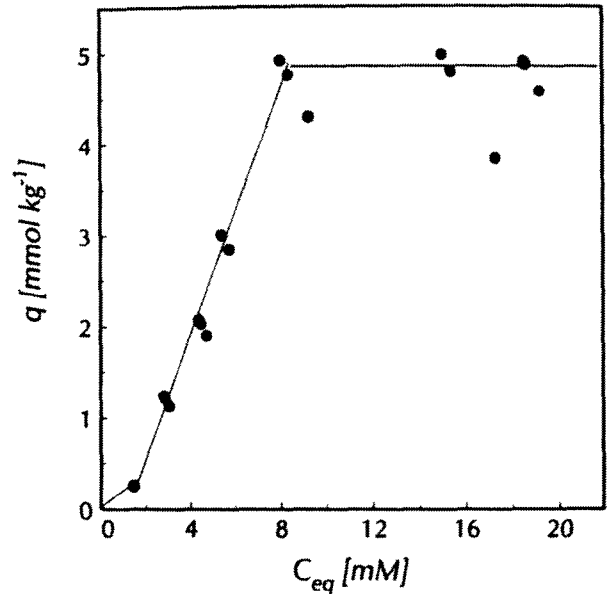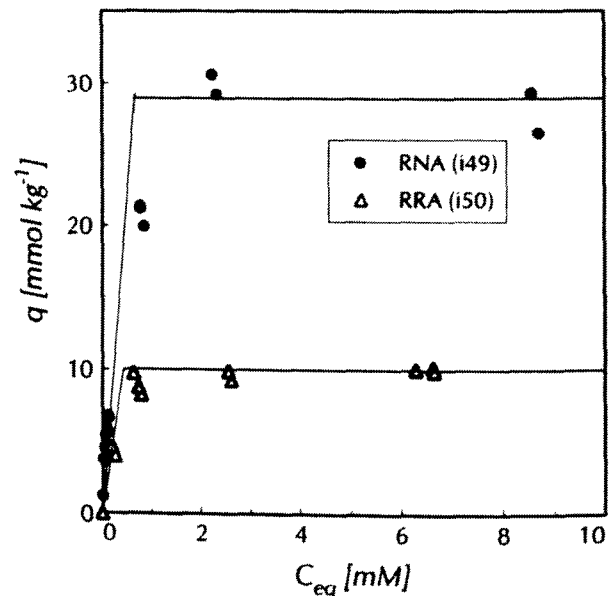

Fig. 5-14: Adsorption of the cationic HDTMA onto RNA and RRA.

Fig. 5-12: Adsorption isotherms of the nonionic surfactants TS G80 and TX-100 as well the di-anionic DF 8390 onto RNA.

The cationic surfactant HDTMA shows the highest values of $K_{d, mn}$, followed by the non-ionic TS G50 (Tab. 5-1, i9, i8, i12), TS G80, TX-100, the di-anionic DF 8390 and the anionic SDS. This order may be reasonably due to repulsion of the negatively charged anionic surfactants by the also net negatively charged surface of the natural aquifer material. The order for the q_{max} values is almost the same except SDS exhibits the second highest value. The A_{surf} values which should be very similar if the different surfactants have access to the same surfaces range from 1838 cm^2 g^{-1} to 7171 cm^2 g^{-1}. Considering the 0.35 mm grain size the non-ionic surfactants show a relatively small value of A_{surf} between 1775 cm^2 g^{-1} (TX-100) and 2566 cm^2 g^{-1} (Tab. 5-1, TS G50, i9) with a resulting mean value of (2096 ± 362) cm^2 g^{-1} compared to the mean A_{surf} value for DF 8390 (3018 cm^2 g^{-1}) and SDS (7171 cm^2 g^{-1}) which are a factor of about 1.5 and 3.4 higher. The $A_{ext} A_{surf}^{-1}$ and $A_{surf} BET^{-1}$ ratios range from 0.6 % to 3.4 % and from 2.2 % to 9 %, respectively.

The temperature has no significant influence on the adsorption of TX-100 and DF 8390 according to the corresponding isotherms i22, i23 and i29, i30, which were measured at different temperatures.

For comparison Tab. 5-3 shows the CMC_{st} obtained by the surface tension method (capillary rise) and CMC_e. The CMC_e of TS G80, DF 8390 and HDTMA is smaller than CMC_{st} by a factor of about 2, 2.5 and 3, respectively. The CMC_e of TX-100 seems to be increased by a factor of about 3. The differences between CMC_e and CMC_{st} may be due to the CaCl$_2$ present in these batch systems. The CMC_e of SDS equals almost the CMC_{et} due to the absence of CaCl$_2$.

SDS Adsorption onto Lithocomponents of RNA

The adsorption isotherms of SDS onto the bulk sample and lithocomponents of RNA (grain size 2.0 mm - 4.0 mm) are shown in Fig. 5-15 and the results are summarized in Tab. 5-3.
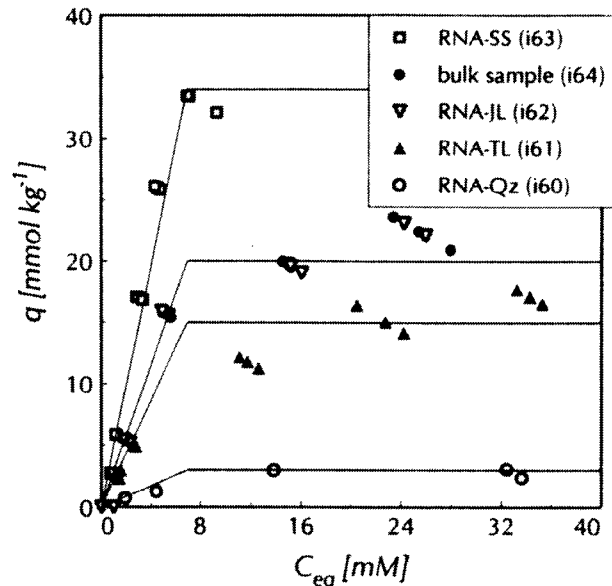
Fig. 5-15: Adsorption isotherms of SDS onto the bulk sample and lithocomponents of RNA (grain size 2 mm - 4 mm).

All isotherms show the same nonlinear shape. The values of $K_{d, mn}$, q_{max} and A_{surf} range from 0.30 L kg^{-1} to 5.11 L kg^{-1}, 2.9 mmol kg^{-1} to 33.0 mmol kg^{-1} and 4242 cm^2 g^{-1} to 48682 cm^2 g^{-1}, respectively. The A_{surf} values were highest for the sandstones, followed by Triassic limestones, Jurassic limestones and the finally quartz. The $A_{ext} A_{surf}^{-1}$ ratios range between 0.02 % and 0.19 % with the highest value for the quartzes RNA-Qz. These values are about two orders of magnitude smaller than the respective values obtained for the surfactants mentioned above. The $A_{surf} BET^{-1}$ ratios range between 39 % and 171 %. SDS seems to cover a significant amount of the BET surface area. In the case of RNA-Qz (i60) and RNA-TL (i61) even more than 100 % of the BET surface area is covered by SDS. This may be due to precipitation of SDS in these systems.

The measured adsorption maximum of the bulk sample of 2 mm - 4 mm RNA (i64) was compared to the $q_{max}(bulk)$, which was calculated according to equation (3-3) from the individual adsorption maxima of the measured lithocomponent isotherms. The calculated value of (19.8 ± 1.3) mmol kg^{-1} was smaller than the measured q_{max} of (21.0 ± 1.7) mmol kg^{-1}, but it is still in reasonably good agreement considering the measurement errors.

Tab. 5-3: Results from the adsorption experiments of the surfactants TS G80 and TX-100 (non-ionic), HDTMA (cationic), DF 8390 (di-anionic), Marlinat and SDS (anionic) for RNA, RRA, OPA as well as SDS onto RNA lithocomponents.

Surfactant (Exp. #)	Solid	Grain Size[a]	T^b	$K_{d,mn}$	R^2	q_{max}	CMC_e^c	CMC_{st}^d	A_{ext}	A_{surf}^e	$\frac{A_{ext}}{A_{surf}}^{-1}$	$\frac{A_{surf}}{BET}^f$
		[mm]	[°C]	[L kg^{-1}]	[-]	[mmol kg^{-1}]	[mM]	[mM]	[cm^2 g^{-1}]	[cm^2 g^{-1}]	[%]	[%]
TS G80 (i26)	RNA	0.35	20	2.41	0.967	1.30 ±0.09	0.54	1.11	62	1838	3.4	2.3
TX-100 (i23)	RNA	0.35	20	1.74	0.952	0.98 ± 0.05	0.56	0.24	62	1775	3.5	2.2
TX-100 (i22)	RNA	0.35	10	1.59	0.948	1.05 ± 0.07	0.72	0.24	62	1897	3.0	2.6
TX-100 (i25)	OPA	0.003	20	133.02	0.956	71.4 ± 12.3	0.54	0.24	7407	129040	5.7	32.3
DF 8390 (i29)	RNA	0.35	20	0.90	0.988	0.86 ± 0.08	0.95	2.49	62	3018	2.1	3.8
DF 8390 (i30)	RNA	0.35	6	0.69	0.979	0.89 ± 0.04	1.29	2.49	62	3131	2.0	3.9
DF 8390 (i31)	RNA	0.50	20	0.71	0.952	0.63 ± 0.00	0.89	2.49	44	2221	2.0	2.8
DF 8390 (i31b)	OPA	0.003	20	25.0	0.823	13.43 ± 1.36	0.54	2.49	7407	47306	15.7	11.8
Marlinat (i34a)	RNA	0.50	20	-[h]	-	-	-	3.05	44	-	-	-
HDTMA (i49)	RNA	0.50	20	77.1	0.940	28.9 ± 1.7	0.38	1.19	44	-	-	-
HDTMA (i50)	RRA	0.50	20	21.9	0.901	9.6 ± 0.67	0.43	1.19	44	-	-	-
SDS[g] (i33)	RNA	0.50	20	0.61	0.959	4.61 ± 0.37	7.52	7.55	44	7171	0.6	9
SDS (i64)	RNA	2.83	20	2.94	0.939	21.0 ± 1.7	7.2	7.55	8	31028	0.03	39
SDS (i65)	RNA	1.41	20	3.26	0.922	23.2 ± 2.3	7.1	7.55	16	34157	0.05	43
SDS (i60)	RNA-Qz	2.83	20	0.30	0.759	2.9 ± 0.3	9.6	7.55	8	4242	0.19	111
SDS (i61)	RNA-TL	2.83	20	1.64	0.844	16.2 ± 1.3	9.8	7.55	9	23851	0.04	171
SDS (i62)	RNA-JL	2.83	20	3.01	0.975	21.0 ± 1.7	7.0	7.55	8	30966	0.03	83
SDS (i63)	RNA-SS	2.83	20	5.11	0.970	33.0 ± 0.8	6.5	7.55	9	48682	0.02	57

[a] Geometric mean of the respective grain size fraction. [b] Temperature. [c] Critical micelle concentration obtained by the intersection of the two isotherm segments. [d] critical micelle concentration determined by the capillary rise method. [e] Surfactant specific interfacial area according to equation (3-9). [f] According to equation (3-12). [g] Martin (1997). [h] No adsorption of Marlinat could be measured in the mM-range examined. "-" Not determined.

5.2 Surfactant Column Experiments

5.2.1 Surfactant Transport Experiments

Column experiments were conducted to examine the surfactant transport through RNA. The experiments were performed at different surfactant influent concentrations and different flow velocities to obtain information about the different adsorption behavior and adsorption kinetics of surfactant monomers and surfactant micelles, respectively. The composition of the aqueous influent solution containing 0.01 M $CaCl_2$ beside the respective surfactant concentration was the same as in the batch systems from which the isotherms where obtained as described above. Thus, the CMC_e (0.55 ± 0.09) mM derived from the adsorption isotherms was assumed to be the same in these column systems. The surfactant influent concentrations C_0 ranged from about 0.1 mM up to 11 mM, i.e. from $0.2\ CMC_e$ to $20\ CMC_e$. The surfactant breakthrough curves are shown in Fig. 5-16 (supra-CMC_e) and Fig. 5-17 (sub-CMC_e), respectively. The breakthrough curves of the conservative tracer Fluorescein are included in the figures for comparison. The desorption of the surfactant after a complete breakthrough was studied by switching the influent surfactant concentration C_0 to surfactant free $CaCl_2$ solution and measuring the elution curves which are shown in Fig. 5-18.

In one set of experiments using the same column system (a5 to a8) the influent concentration C_0 was successively changed from 2.29 mM $(4\ CMC_e)$ to 8.65 mM $(15\ CMC_e)$ and then back to 2.29 mM and 0 mM, respectively. The complete breakthrough/ elution curves of these "stepwise" adsorption/ desorption experiment are shown in Fig. 5-19.

The properties of the column systems and the results of the surfactant transport experiments are summarized in Tab. 5-4. The bulk density ρ_b and the porosity n of the columns range from 1.687 g cm^{-1} to 1.764 g cm^{-1} and from 0.33 to 0.38, respectively, which are reasonable values for the aquifer material used. The values of n deter-

mined by the moment analysis of the conservative tracer yield relatively well the value of the total porosity n_{grav} according to equation (3-28). The values of v_x, D_L and Pe range from 11 m day^{-1} to about 30 m day^{-1}, from 0.002 cm^2 s^{-1} to 0.006 cm^2 s^{-1}, and from 26 to 113, respectively. The dispersivity ranges from 0.59 mm to 1.69 mm, which is in the order of magnitude of the grain size of the aquifer material used. This indicates a homogenous flow field within the column systems.

Surfactant Breakthrough Curves

The breakthrough curves of the surfactant at supra-CMC_e concentrations (Fig. 5-16) show a sigmoidal shape with extended tailing. The tailing increases with decreasing surfactant concentration. The breakthrough curves at sub-CMC_e concentrations (Fig. 5-17) show a convex shape with intensive tailing just from the beginning.

The retardation factors R_{05} and R_d increase with decreasing surfactant concentration and range from 1.2 to 6.6 and from 1.4 to 12.2, respectively. The $R_{05} R_d^{-1}$ ratio, which characterizes the skewness or the asymmetry of the breakthrough curves ranges from 0.51 to 0.99 with the lowest values for the supra-CMC_e surfactant concentrations. It should be noted that a value of one would indicate an ideal breakthrough curve at equilibrium conditions. The corresponding R_{eq} values obtained from the equilibrium adsorption isotherms are slightly higher than the measured retardation factors resulting in $R_d R_{eq}^{-1}$ ratios which range from 0.51 to 1 indicating equilibrium and non-equilibrium transport, respectively. Corresponding to that the adsorbed surfactant concentration in the column systems is slightly smaller than the corresponding concentration obtained from the adsorption isotherm (1.1 ± 0.12) mmol kg^{-1}.

Surfactant Elution Curves

The elution curves show a rapid drop of the reduced effluent concentrations C/C_0 within the first 2 to 4 pore volumes displaced followed by an
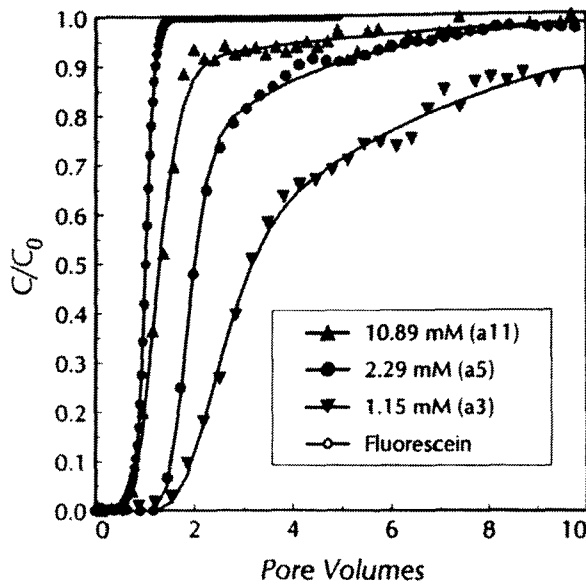
Fig. 5-16: Surfactant breakthrough curves of TS G50 through RNA for influent concentrations above the CMC_e.

Fig. 5-17: Surfactant breakthrough curves of TS G50 through RNA, influent concentrations C_0 below the CMC_e.

asymptotical approach to zero. The elution curves are less asymmetrical (less skewed) compared to the breakthrough curves which is indicated by slightly higher $R_{05} R_d^{-1}$ ratios. However, they show a tailing over a large number of pore volumes displaced. The ongoing slow desorption of the surfactant takes place according to the increasing $K_{d, surf}$ with decreasing surfactant concentration obtained from the isotherm. The desorbed surfactant concentration equals the adsorbed surfactant concentration which indicates that the surfactant adsorption is completely reversible.

Stepwise Adsorption/Desorption

The increase of the influent concentration C_0 from 2.29 mM to 8.65 mM and the decrease vice versa can be observed in the column effluent after one pore volume displaced (retardation factors equal one). This indicates that no further surfactant adsorption takes place if the solid/water interface is covered by surfactants already.

Fig. 5-18: Elution curves for different concentrations of TS G50 through RNA.
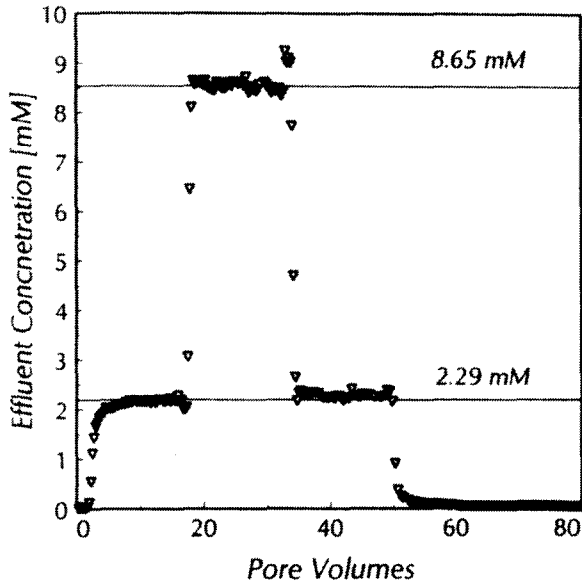
Fig. 5-19: Stepwise adsorption/desorption break-through/elution curves of TS G50 through RNA. For concentrations above the CMC_e no further retardation occurs (q reached q_{max}).

Fig. 5-20: Variation of the hydraulic conductivity K_f during a breakthrough of TS G50 (10.86 mM) through a column packed with industrial quartz sand and alluvial loam after soil mixing; Data from Lemp (1996; master thesis); $L = 1$ m; mean value of $K_f = 6.3 \cdot 10^{-5}$ m s^{-1}.

5.2.2 Influence on the Hydraulic Conductivity

The headloss of some of the column systems was monitored during surfactant breakthrough experiments, since the application of surfactants for in-situ remediation schemes could be limited by the surfactant induced reduction of the hydraulic conductivity resulting in increasing headloss. No reduction of the hydraulic conductivity was observed within the columns packed with RNA. This may be due to the low surfactant concentration used and the properties of the sandy aquifer material. RNA was washed prior to use to remove clay and silt particles. Thus, no fines which could be disperged by the surfactant were present in the system.

Fig. 5-20 shows the breakthrough curve of TS G50 (10.86 mM) and the monitored hydraulic conductivity for a large scale column (length 1 m) containing a homogenized mixture of quartz sand and alluvial loam (data from Lemp, 1996). The mean values of the hydraulic condictivity K_f ranged from $6.3 \cdot 10^{-5}$ m s^{-1} to $8.4 \cdot 10^{-4}$ m s^{-1} with a larger deviation between two experiments compared to the variations within an experiment. This indicates that TS G50 has no impact on the hydraulic conductivity for the surfactant concentrations and the aquifer material used within these experiments.

Tab. 5-4: Transport of the non-ionic surfactant TS G50 through RNA (grain size: 0.5 mm - 1.0 mm, adsorption maximum q_{max} from the isotherm i12: 1.1 ± 0.12 mmol kg^{-1}, unless noted): Column properties and results obtained from the breakthrough curves. The properties of a column which was used for more than one experiment (desorption, change of C_0) are given in the respective first row. The retardation factors of the desorption experiments represent the retardation of water or the lower surfactant concentration. They were obtained by converting the desorption curve into a breakthrough curve ($1 - C/C_0$ versus PV). The CMC_e in the surfactant influent solution containing 0.01 M CaCl$_2$ is (0.55 ± 0.09) mM.

C_0 [mM] (Exp. #)	L [cm]	ρ_b [g cm^{-3}]	n [-]	D_L [cm^2 s^{-1}]	α [mm]	v_x [m day^{-1}]	Pe [-]	$R_{0.5}$ [-]	R_d [-]	R_{eq} [-]	q_s [mmol kg^{-1}]	$R_{0.5}R_d^{-1}$ [-]	$R_dR_{eq}^{-1}$ [-]
0.10 (a10)	9	1.687	0.38	0.002	1.11	16.7	87	6.2	12.2	12.4	0.26	0.51	0.98
0.20 (a2)	7	1.764	0.33	0.004	0.96	13.7	28	6.6	9.1	14.7	0.27	0.73	0.62
1.15 (a3)	9	1.746	0.35	0.004	1.24	27.6	72	4.1	4.5	5.7	0.71	0.91	0.79
0 (a3de)	*Desorption of 1.15 mM*							4.2	4.6	5.7	0.74	0.91	0.81
1.51 (a4)	9	1.713	0.36	0.003	0.89	27.2	113	1.9	2.3	4.5	0.40	0.82	0.51
0 (a4de)	*Desorption of 1.51 mM*							2.2	2.3	4.5	0.42	0.95	0.51
2.29 (a5)	9	1.698	0.38	0.002	0.59	11.6	61	2.0	2.8	3.2	0.92	0.71	0.88
8.65 (a6)	*Increase of C_0 from 2.29 mM to 8.65 mM*							1.0	1.0	1.0	0.00	0.99	1.00
2.29 (a8)	*Decrease of C_0 from 8.65 mM to 2.29 mM*							1.0	1.0	1.0	0.10	0.97	1.00
0 (a7de)	*Desorption of 2.29 mM*							2.2	2.6	3.2	0.81	0.85	0.81
9.74 (a1)[a]	9	1.725	0.37	0.006	1.69	24.2	42	1.1	1.4	1.5	0.84	0.79	0.93
0 (a1de)[a]	*Desorption of 9.74 mM*							1.1	1.3	1.5	0.71	0.85	0.87
10.08 (a9)	7	1.764	0.35	0.004	1.02	12.9	26	1.4	1.5	1.5	1.01	0.93	1.00
10.89 (a11)[a]	9	1.698	0.38	0.005	1.53	24.7	51	1.2	1.4	1.9	0.75	0.86	0.93

[a] Grain size 0.25 mm - 0.5 mm; $q_{max} = 1.94$ mmol kg^{-1}.

5.3   Adsolubilization

Kinetics

The phenanthrene adsolubilization kinetics into TS G50 adsorbed to RNA are shown in Fig. 5-21 and Fig. 5-22. The adsorbed surfactant concentration in the batch systems used was about 1.1 mmol kg^{-1}, which is close the adsorption maximum q_{max} where a complete surfactant bilayer is established. The adsolubilization was found to be fast and reached equilibrium within about 30 minutes. The adsolubilization kinetics can be described by a first order process with a rate constant k of about 0.11 min^{-1}.

Equilibrium Partitioning

The adsorption isotherms of phenanthrene onto RNA in the presence of different TS G50 surfactant concentration are shown in Fig. 5-23. All of these isotherms are highly linear indicating the partitioning of phenanthrene between the aqueous phase and the adsorbed surfactant phase. The partitioning of phenanthrene into the adsorbed surfactant phase (adsolubilization) is in equilibrium (see Fig. 5-22). The adsorption of phenanthrene onto the natural aquifer solids is not in equilibrium due to the slow intra particle diffusion (Grathwohl and Reinhard, 1993). However, this very slow process can not be seen in the time scale of the experiments conducted here. The slope of the isotherms represent the distribution coefficient K_d^* of phenanthrene between the aqueous phase and the solid phase coated with different adsorbed surfactant concentrations. The partitioning coefficients of phenanthrene to the adsorbed surfactant phase were obtained by normalizing the adsorbed phenanthrene mass to the adsorbed surfactant mass instead of the solid mass present in the system. The partitioning coefficients were obtained by the slope of X_{surf} versus X_{aq} as shown in Fig. 5-24. The results of the adsolubilization experiments are summarized in Tab. 5-5. The adsorbed surfactant concentration (q) and the organic carbon content increased by the adsorbed surfactants (f_{oc}^*) range zero to about
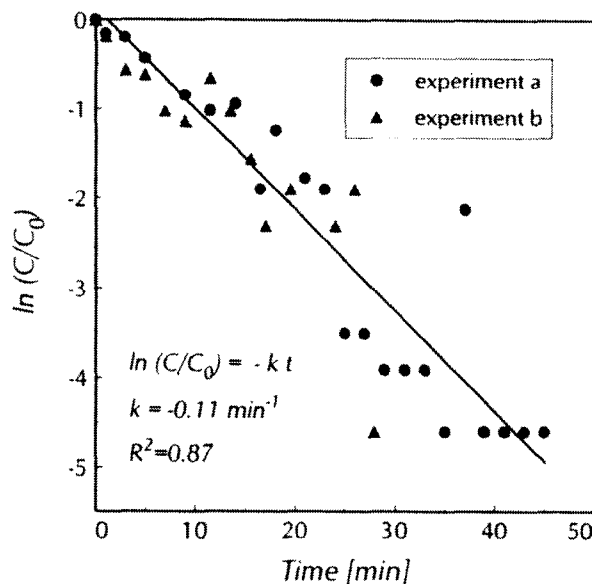
Fig. 5-21: Kinetics of phenanthrene adsolubilization onto RNA coated by TS G50 (1.1 mmol kg^{-1}). Determination of the first order rate constant.
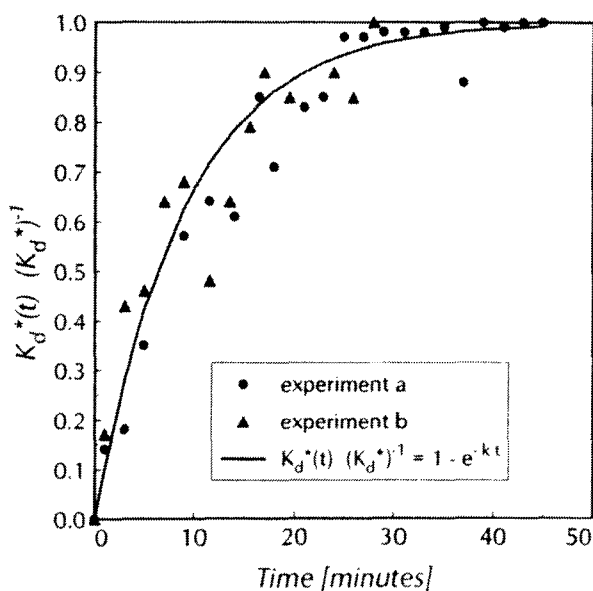
Fig. 5-22: Kinetics of phenanthrene adsolubilisation onto RNA in the presence of adsorbed TS G50 (1.1 mmol kg^{-1}).

17.5 mmol kg^{-1} and 0.52 % to 0.283 %, respectively. The values of K_d^* and K_{oc}^* range from 1.9 L kg^{-1} to 19.0 L kg^{-1} and 3602 L kg^{-1} to 13083 L kg^{-1}, respectively. This indicates that the aquifer material became up to a factor 4 more attractive for phenanthrene adsorption compared to the system without surfactants.
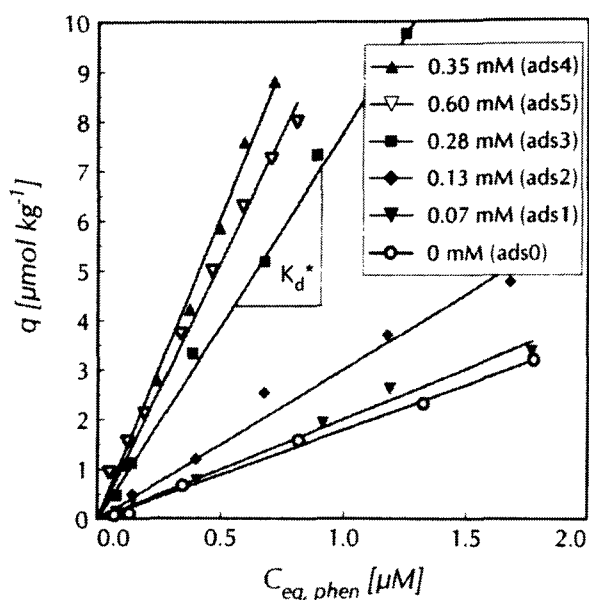
Fig. 5-23: Adsorption isotherms of phenanthrene in the presence of the nonionic surfactant TS G50 at different concentrations.
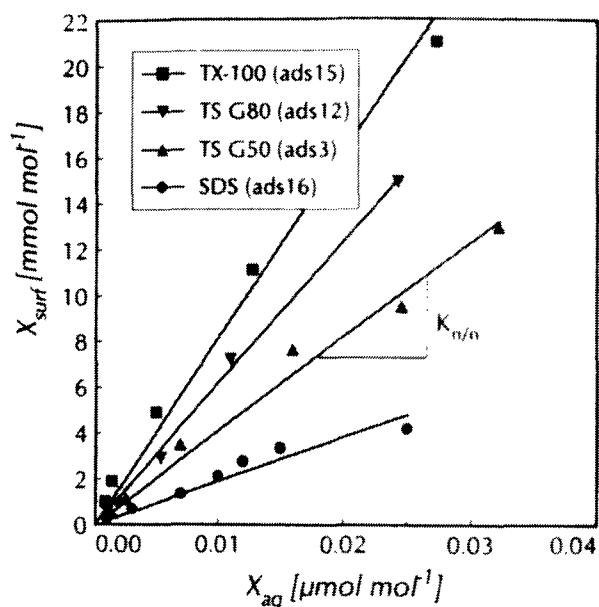
Fig. 5-24: Calculation of phenanthrene partitioning coefficients between aqueous phase and adsorbed surfactants.

The partitioning coefficients $logK_{n\,n}$, $logK_{vol}$ and $logK_{V\,n}$ range from 5.15 to 5.94, 3.65 to 4.37 and 3.41 to 4.19, respectively. The highest values of the partitioning coefficients were found for TX-100, followed by TS G80, TS G50 and SDS. The comparison of K_{vol} with the octanol/water partitioning coefficient K_{ow} indicated by the $K_{vol}K_{ow}^{-1}$ ratio yields values between 0.12 and 0.63.

Tab. 5-5: Phenanthrene partitioning coefficients between aqueous phase and adsorbed surfactants; octanol/water-partitioning coefficient of phenanthrene K_{ow}: 37154 [*] ($logK_{ow}$: 4.57). The partitioning coefficient are converted acoording to Tab. 2-1.

Surfactant (Exp. #)	$C_{surf, eq}$	q	f_{oc}[*]	K_d[*]	K_{oc}[*]	$logK_{n/n}$	R^2	K_{vol}	$logK_{vol}$	$K_{vol} K_{ow}^{-1}$	$logK_{V/n}$
	[mM]	[mmol kg^{-1}]	[%]	[L kg^{-1}]	[L kg^{-1}]	[-]	[-]	[-]	[-]	[-]	[M^{-1}]
TS G50 (ads0)	0.00	0.00	0.052	1.9	3602	-	-	-	-	-	-
TS G50 (ads1)	0.07	0.18	0.059	2.1	3494	5.15	0.960	4440	3.65	0.12	3.41
TS G50 (ads2)	0.13	0.33	0.065	3.0	4569	5.18	0.896	4741	3.68	0.13	3.43
TS G50 (ads3)	0.28	0.72	0.078	7.7	9831	5.61	0.984	12935	4.11	0.35	3.87
TS G50 (ads4)	0.35	0.90	0.085	11.1	13083	5.63	0.990	13516	4.13	0.36	3.89
TS G50 (ads5)	0.60	1.10	0.092	9.7	10480	5.65	0.985	14197	4.15	0.38	3.91
TS G80 (ads12)	0.15	0.28	0.065	5.6	8665	5.94	0.985	23370	4.37	0.63	4.19
TX-100 (ads15)	0.68	0.12	0.057	4.1	7227	5.91	0.987	23487	4.37	0.63	4.17
SDS (ads16)	5.81	17.42	0.283	19.0	6708	5.34	0.947	14813	4.17	0.40	3.59

[*] Miller et al. (1985).

5.4 Transport of PAHs and Surfactants

An important factor for planning surfactant enhanced subsurface remediation is the understanding of the HOC transport through porous media in the presence of surfactants. Especially non-equilibrium sorption processes associated with surfactant-influenced transport of HOCs may be very important during transport under rapid flow conditions that may occur during surfactant enhanced pump-and-treat operations. Thus, non-equilibrium column experiments were conducted to study the transport of phenanthrene in the presence of different surfactant concentrations (TS G50). Three sets of experiments were carried out using different aquifer materials and column dimensions:

Set A: Pulse type breakthrough experiments using industrial quartz sand (grain size: 0.1 mm - 0.4 mm, column length: 9 cm, column inner diameter: 1 cm).

Set B: Front type (continous feed) breakthrough experiments using RNA (grain size: 0.25 mm - 1.0 mm, column length: 7 cm and 9 cm, column inner diameter: 1 cm).

Set C: Front type (continous feed) breakthrough experiments using RNA (grain size: 1.0 mm - 2.0 mm, column length: 12.35 cm, column inner diameter: 2.1 cm).

Since the breakthrough curves were monitored on-line, only the 20th to 50th data points are presented in the figures in order to indicate that the breakthrough curves are measured but not modeled.

Industrial Quartz Sand (Set A)

Fig. 5-25 shows the pulse type breakthrough curve of phenanthrene through a column packed with industrial quartz sand of the grain size 0.1 mm - 0.4 mm in the absence of surfactant and in the presence of different concentrations of TS G50. The column properties and results of set A are summarized in Tab. 5-6. The pulses show a fairly symmetric shape indicating that the

retardation of phenanthrene is due to partitioning into the adsorbed surfactant phases and that it is reversible. Since the industrial quartz sand has no significant intraparticle porosity, where the phenanthrene can diffuse into, only one column was used for the experiments with different surfactant concentrations. The column was flushed in between two experiments with the surfactant concentration used in the next experiment.

The phenanthrene retardation factors $R_{0.5}$ and R_d range from 1.8 to 5.9 and decrease with increasing surfactant concentration. They do not differ significantly from each other indicated by $R_{0.5} R_d^{-1}$ ratios close to one. Since this was a very early experiment within this study, the CMC in this column system was believed to be the CMC_{st} of about 0.88 mM which was measured by the capillary rise method. Thus, it was very surprising that the retardation of phenanthrene decreases for concentrations even below the CMC_{st}. This indicates that the CMC in this column system must be smaller than CMC_{st}. Thus, further experiments were conducted with lower surfactant concentrations.

River Neckar Alluvium (Sets B and C)

The front type breakthrough curves of phenanthrene in the presence of different TS G50 surfactant concentrations through RNA are shown for the set B (grain size 0.25 mm - 1.0 mm) and set C (grain size 1.0 mm - 2.0 mm) in Fig. 5-26 and Fig. 5-27, respectively. The column properties as well as the identified parameters are summarized in Tab. 5-7 (set B) and Tab. 5-8 (set C). It should be noted that the columns were equilibrated with the surfactant solution of the respective concentration prior the influent solution was switched to surfactant solution spiked with phenanthrene at the beginning of the experiment ($t = 0$). The phenanthrene influent concentration was 50 µg L^{-1} (set B) and 100 µg L^{-1} (set C), respectively.
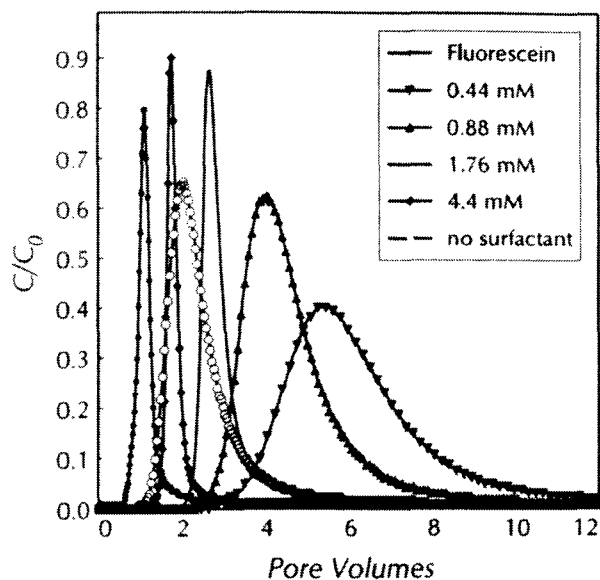
Fig. 5-25: Set A: Pulse type breakthrough curves of phenanthrene through industrial quartz sand (grain size 0.1 mm - 0.4 mm) sand in the presence of different concentrations of TS G50.

The bulk density ρ_b and the porosity n of both sets range from 1.664 g cm^{-1} to 1.766 g cm^{-1} and from 0.34 to 0.41, respectively, which are reasonable values for the aquifer materials used. The values of n determined by the moment analysis of the conservative tracer agree reasonably well with the value of the total porosity n_{grav} according to equation (3-28).

The v_x, D_L and Pe values of set B (Tab. 5-7) range from 6 m day^{-1} to 67.1 m day^{-1}, from 0.001 cm^2 s^{-1} to 0.004 cm^2 s^{-1}, and from 58 to 223, respectively.

The dispersivity values range from 0.63 mm to 1.64 mm, which are in the order of magnitude of the grain size of the aquifer material used indicating a homogenous flow field. The mean residence time ranges between 4.0 min and about 60 min depending on the flow velocity. The v_x, D_L and Pe values of set C (Tab. 5-8) are more uniform and range from 8.0 m day^{-1} to 8.8 m day^{-1}, from 0.002 cm^2 s^{-1} to 0.003 cm^2 s^{-1}, and from 40 to 64, respectively. The dispersivity values α range from 1.94 mm to 3.11 mm which are slightly larger due to the larger grain size fraction and the longer column used. The mean residence time ranges from 52.7 min to 56.7 min due to the lower flow velocity. Thus, in the column systems of set B the transport of phenanthrene should be closer to equilibrium compared to the systems described before.

The breakthrough curves of the experimental sets B and C show a sigmoidal shape with significant tailing especially in the presence of low surfactant concentrations. Phenanthrene does not show an early breakthrough in the presence of low surfactant concentrations. The phenanthrene retardation factors $R_{0.5}$ and R_d of set B and C range between 3.4 and 6.6 without surfactant. The values of $R_{0.5}$ and R_d increase with increasing surfactant concentration to a maximum retardation from which they decrease with further increasing surfactant concentration. The maximum $R_{0.5}$ and R_d values of

Tab. 5-6: Set A: Coupled transport of phenanthrene and TS G50 through industrial quartz sand (grain size: 0.1 mm - 0.4 mm): Column properties and results. Phenanthrene influent concentration in all experiments 50 µg L^{-1}.

C_{surf} [mM] (Exp. #)	L [cm]	ρ_b [g cm^{-3}]	n [-]	D_L [cm^2 s^{-1}]	α [mm]	v_x [m day^{-1}]	Pe [-]	t_{mr} [min]	$R_{0.5}$ [-]	R_d [-]	$R_{0.5} R_d^{-1}$ [-]	$K_{0.5}^*$ [L kg^{-1}]	K_d^* [L kg^{-1}]
0 (q1)	9	1.606	0.47	$1.4 \cdot 10^{-7}$	0.1	18	138	15.0	2.1	2.3	0.91	3.0	3.5
0.44 (q2)	9	1.606	0.47	$1.4 \cdot 10^{-7}$	0.1	18	138	15.0	5.7	5.9	0.97	12.7	13.3
0.88 (q3)	9	1.606	0.47	$1.4 \cdot 10^{-7}$	0.1	18	138	15.0	4.2	4.6	0.91	8.7	9.7
1.76 (q4)	9	1.606	0.47	$1.4 \cdot 10^{-7}$	0.1	18	138	15.0	2.8	3	0.93	4.9	5.4
4.41 (q5)	9	1.606	0.47	$1.4 \cdot 10^{-7}$	0.1	18	138	15.0	1.8	1.9	0.95	2.2	2.4
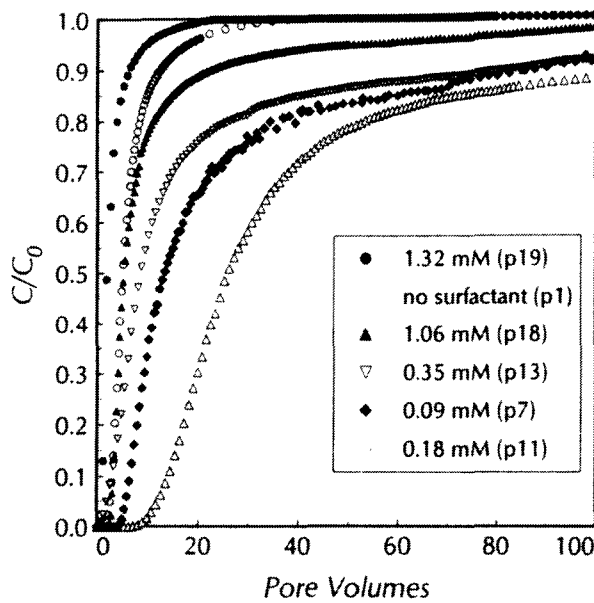
Fig. 5-26: Set B: Phenanthrene breakthrough curves through RNA (grain size: 0.25 mm - 1.0 mm) at different surfactant concentrations; column properties are given in Tab. 5-7.
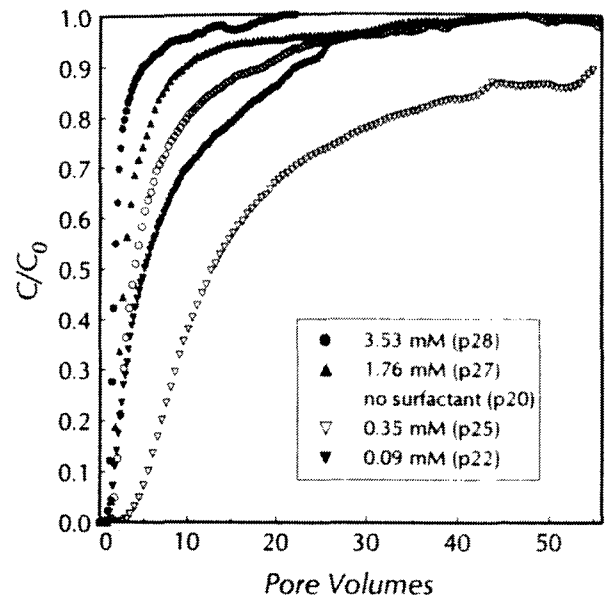
Fig. 5-27: Set C: Phenanthrene breakthrough curves through RNA (grain size: 1.0 mm - 2.0 mm) at different surfactant concentrations; column properties are given in Tab. 5-8.

set B range from 8.5 to 29.9 and from 14.4 to 41.6, respectively. The maximum $R_{0.5}$ and R_d values of set C range from 12.5 to 15.7 and from 19.0 to 19.5, respectively. The corresponding surfactant concentration range between 0.18 mM and 0.44 mM. The same retardation of phenanthrene without surfactant is reached for surfactant concentrations larger than 1.06 mM (B) and 1.76 mM (C). A surfactant facilitated transport of phenanthrene can be observed above that concentrations.

The $R_{0.5} R_d^{-1}$ ratios of C range independently from the surfactant concentration rather uniform between 0.5 and 0.8. In opposite, the $R_{0.5} R_d^{-1}$

ratios of B show a wide range between 0.19 and 1. The lowest values were found for surfactant concentration between 0.22 mM and 0.88 mM. The $K_{0.5}^{*}$ and K_d^{*} distribution coefficients of B range from 0.5 L kg^{-1} to 6.2 L kg^{-1} and from 0.9 L kg^{-1} to 14.7 L kg^{-1}, respectively. The corresponding surfactant concentration for the highest values range between 0.18 mM and 0.44 mM. The $K_{0.5}^{*}$ and K_d^{*} distribution coefficients of C range from 0.2 L kg^{-1} to 3.3 L kg^{-1} and from 0.3 L kg^{-1} to 4.5 L kg^{-1}, respectively. The corresponding surfactant concentration for the highest values range between 0.18 mM and 0.35 mM.

Tab. 5-7: Set B: Coupled transport of phenanthrene and TS G50 through RNA (grain size: 0.25 mm - 1.0 mm): Column properties and results. The phenanthrene influent concentration in all experiments was 50 µg L^{-1}.

C_{surf} [mM] (Exp. #)	L [cm]	ρ_b [g cm^{-3}]	n [-]	D_L [cm^2 s^{-1}]	α [mm]	v_x [m day^{-1}]	Pe [-]	t_{mr} [min]	$R_{0.5}$ [-]	R_d [-]	$R_{0.5} R_d^{-1}$ [-]	$K_{0.5}^{*}$ [L kg^{-1}]	K_d^{*} [L kg^{-1}]
0.00 (p1)	9	1.684	0.41	0.004	1.55	22.4	58	14.2	4.7	6.3	0.75	0.8	1.2
0.00 (p2)	9	1.736	0.36	0.003	0.82	53.5	223	6.8	6.6	6.4	1.04	1.1	1.1
0.09 (p7)	9	1.746	0.36	0.001	0.72	6.0	126	59.9	13.0	22.9	0.57	2.4	4.3
0.09 (p8)	9	1.687	0.38	0.002	0.90	16.9	100	20.4	12.8	14.4	0.88	2.9	3.3
0.18 (p11)	9	1.698	0.37	0.003	1.29	20.1	70	17.4	23.4	32.1	0.73	5.4	7.6
0.22 (p12)	7	1.682	0.38	0.002	0.63	38.6	174	6.9	12.3	27.6	0.45	4.7	11.1
0.35 (p13)	7	1.637	0.39	0.003	0.96	34.5	104	7.5	8.5	24.9	0.34	3.1	10.0
0.44 (p14)	7	1.733	0.36	0.003	0.87	54.9	178	5.1	6.5	34.1	0.19	2.5	14.9
0.44 (p15)	9	1.682	0.38	0.004	1.64	20.0	55	17.0	25.0	41.6	0.60	6.2	10.4
0.71 (p16)	9	1.722	0.36	0.003	0.97	53.7	187	6.8	4.6	10.5	0.44	1.5	3.9
0.88 (p17)	7	1.664	0.37	0.004	1.13	51.3	109	5.3	3.3	8.1	0.41	1.2	3.6
1.06 (p18)	9	1.726	0.37	0.004	1.32	27.4	71	12.9	5.1	11.3	0.46	1.1	2.8
1.32 (p19)	7	1.706	0.37	0.004	1.12	67.1	136	4.0	2.0	2.8	0.71	0.5	0.9

Tab. 5-8: Set C: Coupled transport of phenanthrene and TS G50 through RNA (grain size: 1.0 mm - 2.0 mm): Column properties and results. The phenanthrene influent concentration in all experiments was 100 µg L^{-1}.

C_{surf} [mM] (Exp. #)	L [cm]	ρ_b [g cm^{-3}]	n [-]	D_L [cm^2 s^{-1}]	α [mm]	v_x [m day^{-1}]	Pe [-]	t_{mr} [min]	$R_{0.5}$ [-]	R_d [-]	$R_{0.5} R_d^{-1}$ [-]	$K_{0.5}^{*}$ [L kg^{-1}]	K_d^{*} [L kg^{-1}]
0.00 (p20)	12.35	1.635	0.39	0.002	2.44	8.7	50	52.7	3.4	6.3	0.54	0.57	1.26
0.09 (p22)	12.35	1.635	0.39	0.002	2.14	8.1	58	56.7	5.4	9.4	0.57	1.04	2.00
0.18 (p23)	12.35	1.665	0.38	0.003	3.11	8.3	40	56.7	15.7	19.0	0.83	3.33	4.08
0.35 (p24)	12.35	1.616	0.39	0.002	2.58	8.0	48	56.1	13.6	19.4	0.70	3.08	4.50
0.35 (p25)	12.35	1.616	0.39	0.002	1.94	8.2	64	55.4	12.5	19.5	0.64	2.77	4.47
0.88 (p26)	12.35	1.635	0.39	0.003	2.61	8.3	47	55.5	5.0	6.4	0.79	0.96	1.28
1.76 (p27)	12.35	1.681	0.37	0.003	2.93	8.8	42	54.2	2.3	4.4	0.52	0.29	0.76
3.53 (p28)	12.35	1.633	0.39	0.002	2.04	8.5	60	54.2	1.7	2.1	0.81	0.17	0.27

6 Discussion

6.1 Surfactant Adsorption

Adsorption Kinetics

The adsorption kinetics can be explained by results of Chen et al. (1992) who used X-ray photoelectron spectroscopy (XPS) to analyze the mechanisms and kinetics of the self-assembly of surfactant monolayers and bilayers. They examined the sorption of the cationic surfactant HDTMA onto negatively charged mica surfaces and reported following results: (i) the various stages of surfactant adsorption or self-assembly are different above and below the CMC, i.e. bilayers are not formed by going through the monolayer stage, but directly to the bilayer configuration; (ii) the adsorption rate is largely independent from the surfactant concentration for surfactant concentrations well above the CMC, but it appears that the adsorption rate is fastest at the CMC and slower at concentrations both above and below the CMC; (iii) the adsorption rate for the bilayer formation is much slower than for monolayers formation below the CMC; (iv) micelles collapse in a fast adsorption step within about 100 s onto the surface ("splash") and merge quickly into a loosely packed bilayer with an adsorption density that is about 30 % below the final density reached in the equilibrium bilayer; (v) a slow process follows where the surfactant molecules reach via surface diffusion ("surface hopping") surfaces in intraparticle pore spaces and establish by reorientation ("flip flop") a homogenous bilayer. This slow process may also include the incorporation of additional surfactant monomers - but not micelles - and movement of the hydrophilic headgroups across the hydrophobic region of the bilayer. The slow approach to equilibrium may endure up to weeks. They expect that nonionic surfactants may adsorb in a state much closer to equilibrium right from the start since the electric field constraints are not as strong as for the self-assembly of ionic surfactant and their counterions.

Influence of Temperature on Surfactant Adsorption

The temperature seems to have no significant effect on the surfactant adsorption, although the opposite would be expected since the adsorption is an exothermal process which should be favoured by lower temperatures. However, some of the $K_{d, mn}$ and q_{max} values are even smaller for adsorption isotherms measured at lower temperatures. Similar observations were made by Nayyar et al. (1994) who studied the adsorption of SDS at different temperatures. They did not report a temperature effect on the SDS adsorption even below its Krafft temperature.

Adsorption Isotherms

All measured surfactant adsorption isotherms are inverse L-shaped, which are quite often described by a Langmuir model (Yeom et al., 1995; Burris and Antworth, 1992; Wagner et al., 1994; Li and Bowman, 1997; Nayyar et al., 1994). However, they seem to be better described by two different pseudo-linear segments: The first segment through the origin represents the surfactant monomer adsorption below the CMC which can be described by the linear relation $q = K_{d, mn} C_{eq}$. This linear relationship was also used in several other studies to describe the adsorption of surfactant monomers for sub-CMC concentrations (Edwards et al. 1994a, 1994b, 1994c; Rouse et al. 1996a; Nivas et al. 1996; Rouse et al. 1996b). This first segment (see Fig. 2-2) seems to corresponds to zone 2 of the typical adsorption isotherm (West and Harwell, 1992) indicating the adsorption of surfactant monomers, the formation of surfactant monolayers and hemimicelles, respectively. The adsorption of very low surfactant concentrations was not coverd by measurements in this study. Thus, zone 1 of the typical adsorption isotherm characterized by a smaller slope than zone 2 was generally not observed. Brownawell and coworkers (1997) studied the adsorption of alcohol ethoxylated

surfactants in a very low concentration range (below 10 µM) and found nonlinear isotherms that could be described by a Freundlich relationship.

The second linear segment paralled to the x-axis corresponds to zone 4 of the typical surfactant adsorption isotherm and starts at the CMC indicating the maximum surfactant adsorption q_{max}. No further increase of surfactant adsorption was observed even for high surfactant concentrations (e.g Fig. 5-1). This indicates that a complete bilayer or at least a complete monolayer should be established. In contrast, Abdul and Gibson (1991) reported Langmuir-type isotherms but with a further increase of the adsorbed concentration for higher surfactant concentration. Most of the isotherms show a sharp transition between the two linear segments. However, some of them are linked by a more or less established intermediate region, which could correspond to the zone 3 of the typical adsorption isotherm (West and Harwell, 1992).

The isotherms could also be interpreted as Langmuir-isotherms which are truncated by reaching the CMC in the aqueous phase. In this case the observed q_{max} would be smaller than the maximum surface area accessible by the surfactants. Surfactants with a higher CMC, e.g. the anionic surfactants, should have a higher q_{max} than the nonionic surfactants. This could also explain the high q_{max} values of SDS (see below).

SDS Adsorption

In opposite to the other surfactants examined the isotherms of SDS were measured without $CaCl_2$ present in the batch systems (see 4.4.2). The first steep segment of the SDS adsorption isotherm (Fig. 5-13) shows an apparent intercept with the x-axis. It can be postulated that the data show a typical isotherm, but the first segment of the isotherm corresponding to zone 1 was not covered by measurements. A similar shape of a SDS isotherm was reported by Holsen et al. (1991), who examined the adsorption of SDS on ferrihydrite. However, the isotherms of the bulk sample and the lithocomponents of the RNA (grain size frac-

tion > 1 mm) do not show an apparent x-axis intercept.

The adsorption maximum q_{max} of SDS is about a factor 5 larger compared to the isotherm of the grain size fraction 2.5 mm - 1.0 mm (Tab. 5-3). This be may due to the high percentage of quartz in the grain size fraction 0.25 mm - 1.0 mm and the significant lower maximum sorption of SDS onto the natural quartz of RNA (Fig. 5-15) compared to the adsorption of TS G50 onto the same quartz (Fig. 5-3). The surface area, which is covered by the surfactant is about a factor 10 (quartz), 33 (Triassic limestones) and 23 (Jurassic limestones, sandstones) larger compared to the area which is covered by the nonionic TS G50. The percentages of the SDS covered areas compared to the BET surface are in between about 40 % for the bulk sample and values significantly above 100 % (quartz: 111 %, Triassic limestones: 171 %). Since this observation is hardly possible under the given assumptions the formation of multiple SDS layers or the precipitation of SDS have to be considered. The formation of SDS multilayers is not likely because the comparison of the areas covered by SDS with the areas covered by TS G50 did not yield a constant factor representing the number of additional layers. Thus, the surface induced precipitation of SDS may be an explanation of the observed phenomenon (Stumm, 1992).

Similarly, adsorption isotherms of SDS onto natural aquifer materials were reported by Jafvert and Heath (1991) who also mentioned the occurrence of precipitation in their batch systems. Also Rouse et al. (1996) reported high adsorption of SDS onto natural aquifer material (CRA) due to precipitation in the presence of Ca^+ added to their batch systems. In the absence of Ca^+ they did not give a distribution coefficient for the found steep segment of the isotherm since they could not fit a linear regression through the origin. For the maximum sorption q_{max} they reported a value of about 25 mmol kg^{-1}. Nayyar et al. (1994) studied the adsolubilization of nonpolar, polar and ionizable organic compounds onto alumina coated with SDS above and below its Krafft temperature (precipitated to the surface) in batch systems. They found a typically 4 region SDS adsorption

isotherm which was not changed by lowering the temperature below the Krafft temperature. They postulated that such a surfactant system, which was derived from the admicellar chromatography, could be suitable to minimize the surfactant bleeding in a surfactant based in-situ sorption zone.

The values of q_{max} correlate to $K_{d, mn}$ yielding the CMC_e as the slope of the regression line, i.e. a high affinity of the surfactant monomers correlates to a high adsorption maximum. The correlations are shown for TS G50 and SDS in Fig. 6-1 and Fig. 6-2, respectively. Thus, the complete surfactant adsorption isotherm can be described and q_{max} can be calculated if the CMC_e and $K_{d, mn}$ is known.
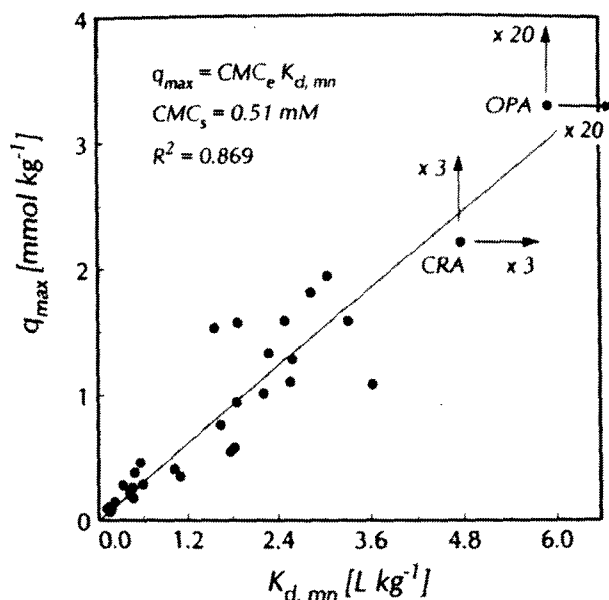

Fig. 6-1: Correlation of q_{max} and $K_{d, mn}$ of TS G50 (data in Tab. 5-1 and Tab. 5-2, x and y values of OPA and CRA were divided by 20 and 3, respectively, to be presented). The slope of the regression line yields the CMC_e.

Change of the CMC in Different Systems

The CMC of the surfactants was found to be a not constant value, but dependent on the presence of electrolytes or hydrocarbons in the aqueous phase. The CMC_e obtained from the adsorption isotherms ($CMC_e = q_{max} K_{d, mn}^{-1}$) differs significantly from the CMC_{st} determined by the surface tension method. It decreases for the nonionic TS G50, TS G80 and the di-anionic DF 8390, but increases for TX-100. This may be due to the presence of electrolyte (0.01 M $CaCl_2$) compared to the CMC_{st}. The CMC_e of SDS is almost unchanged since no electrolyte was present in these batch systems. The decrease of the CMC_{st} for the anionic surfactants may be due to the thickness of the ionic atmosphere surrounding the ionic head groups in the presence of additional electrolyte and the consequent decreased electrical repulsion between them in the micelle (Rosen, 1989). The change of the CMC_e of the nonionic surfactants in the presence of electrolytes may be attributed to a "salting out" of the hydrophobic moieties of the surfactant molecules (Rosen, 1989). TX-100 is an exception, since it is the only surfactant of which the CMC_e was increased by a factor of about 3. Similarly, Edwards et al. (1994a) reported that q_{max} of TX-100 onto Lincoln fine sand was

reached after an intermediate region between the CMC_{st} and 3 times the CMC_{st}. Also Sun et al. (1995) reported an increase of the CMC_{st} of TX-100.

A further decrease of the CMC of TS G50 was observed during the column experiments, where phenanthrene was spiked to the aqueous phase from a methanol stock solution. This may be due to the presence of hydrocarbons (Rosen, 1989). The CMC_{st} was apparently changed from 0.88 mM in the electrolyte free water system to about 0.24 mM in the system containing phenanthrene and methanol (Fig. 4-6). Only a very small volume of methanol was present in the aqueous phase (between 0.05 ‰ and 0.1 ‰), which should have no influence on the transport behavior of phenanthrene (Nkedi-Kizza et al., 1987). However, on a mol basis about 1.25 mM (2.5 mM) methanol, 0.3 μM (0.6 μM) phenanthrene, 0 mM - 3.5 mM surfactant and about 55 M water molecules were present within one liter of aqueous solution. Thus, it could be postulated that the decrease of the CMC is caused by the methanol since it is present in the same order of magnitude within the system like the surfactant.
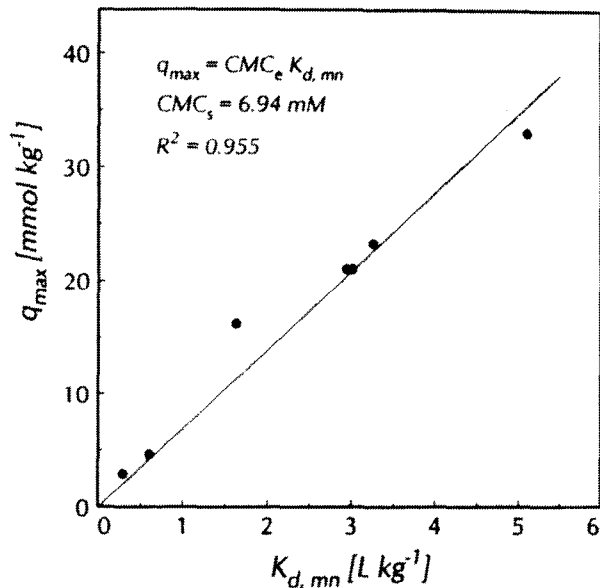
Fig. 6-2: Correlation of q_{max} and $K_{d, mn}$ of SDS (data in Tab. 5-3). The slope of the regression line yields the CMC_e.

Surfactant Specific Interfacial Area A_{surf}

The surfactant specific interfacial area A_{surf} was calculated from q_{max} according to equation (3-9) in order to compare it with the external interfacial area of the solid grains and with the BET interfacial area. It was assumed that the area per molecule is the same as at the air/water interface and a complete bilayer is established. It should be noted that small, discontinous patches or islands of surfactant bilayers are also reported for maximum adsorption of nonionic surfactants (Edwards et al., 1994b). In this case A_{surf} should be somewhat larger since the same adsorbed surfactant mass is distributed over a larger area. However, a very recent study using atomic force microscopy to examine the adsorption of nonionic surfactants indicates that a bilayer is really established at the solid/water interface (Copitzky et al., 1998). A_{surf} does also depend on the ionic strength of the aqueous phase in the batch systems. However, a comparison of A_{surf} of the different aquifer materials should be possible since all (except SDS) were measured in the presence of 0.01 M $CaCl_2$ to provide constant ionic strength. The A_{surf}-value in natural systems at lower electrolyte concentration may be somewhat smaller due to looser packing of the surfactant bilayer at the solid/water interface.

Influence of the Organic Carbon and Calcium Carbonate Content on Surfactant Adsorption

The plots of the surfactant covered interfacial area A_{surf} versus the organic carbon content f_{oc} and the calcium carbonate content $CaCO_3$ are shown in Fig. 6-3 and Fig. 6-4, respectively. No influence on the surfactant adsorption could be observed both for the f_{oc} and the $CaCO_3$.

External Surface Area A_{ext} - Influence of the Grain Size

Generally, the $A_{ext} A_{surf}^{-1}$ ratios of the natural aquifer materials range between 0.44 % and about 6 % with the lowest values for the sandstones and the highest values for the quartzes. This indicates that the external surface area of the grains A_{ext} does not control the surfactant adsorption, i.e. A_{surf} does not only depend on A_{ext} (Fig. 6-5). However, higher values of A_{surf} were found for corresponding higher values of A_{ext} for the silty clay OPA with an average grain size of about 0.003 mm (grain radius: 0.0015 mm). Even higher $A_{ext} A_{surf}^{-1}$ ratios between 9 % and about 100 % were found for the artifically broken Quartz minerals and Triassic limestones, which exhibit freshly created unweathered surfaces. In this case A_{ext} should have an influence on q_{max}. This was found for TL_{br} (Fig. 6-6), but not significantly for the industrial quartz. However, the surface area to volume ratio according to equation (3-10) had to be multiplified by an empirical factor of about 3 to fit the data. A_{ext} shows a tremendous increase with decreasing grain size for radii smaller about 0.003 mm. Thus, A_{ext} may influence the surfactant adsorption for grain sizes with radii smaller than that (Fig. 6-6). In opposite, no relationship between q_{max} and the the grain radius was observed for the Rhät sandstones (Rh-SS, Fig. 6-7).

The $A_{ext} A_{surf}^{-1}$ ratios increase with decreasing grain size (see Tab. 5-2), i.e. the external surface has more influence on surfactant adsorption for the smaller grain sizes. This could be due to fissures being more frequently present in larger grains.
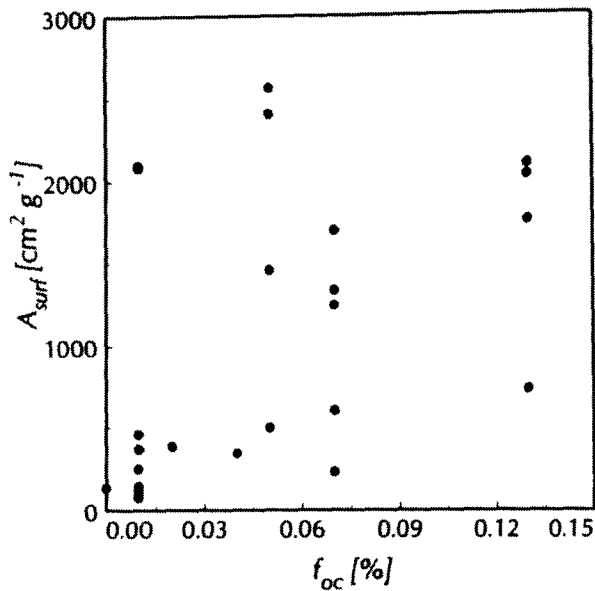
Fig. 6-3: Plot of the surfactant specific interfacial area A_{surf} versus the organic carbon content f_{oc} of the solids. No relationship could be observed between A_{surf} and f_{oc}.
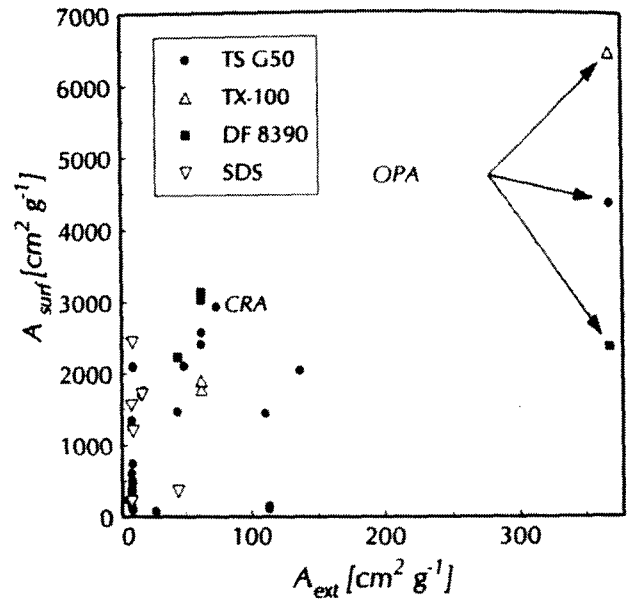
Fig. 6-5: Interfacial area covered by surfactants A_{surf} vs. external surface area of the grains A_{ext}. (x and y values of OPA and CRA were divided by 20 and 3, respectively, y values of SDS were divided by 20 to be presented in the diagramm).
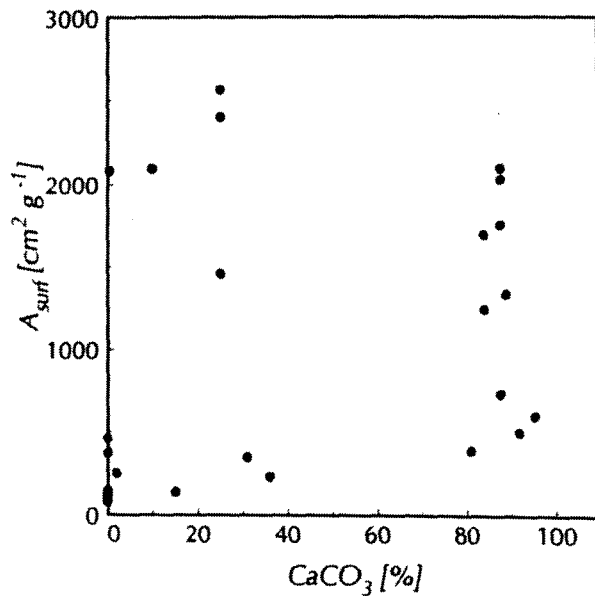
Fig. 6-4: Plot of the area covered by surfactants A_{surf} versus the calcium carbonate content $CaCO_3$ of the solids. No relationship could be observed between A_{surf} and $CaCO_3$.
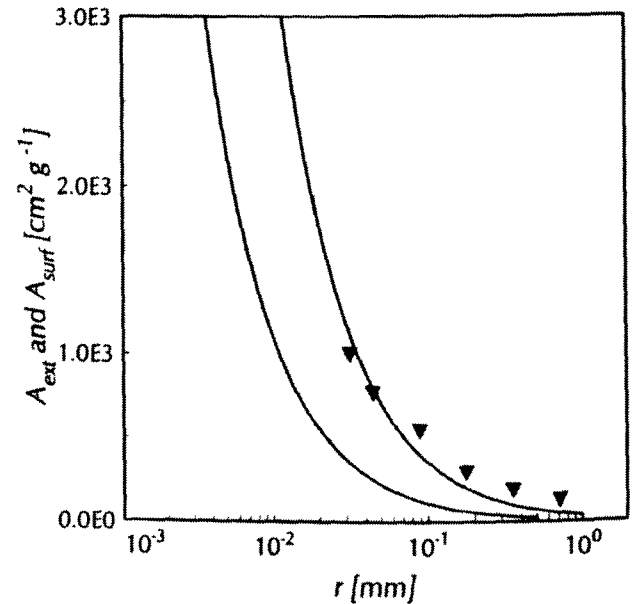
Fig. 6-6: External surface area of the solid grains A_{ext} depending on the grain radius r. A_{ext} increases tremendously for grain radii smaller about 0.003 mm, which is in the range of the clay examined. The data of A_{surf} of the artificially broken Triassic limestones are included for comparison. The surface area to volume ratio according to equation (3-10) had to be multiplified by an empirical factor 3 to fit the data.
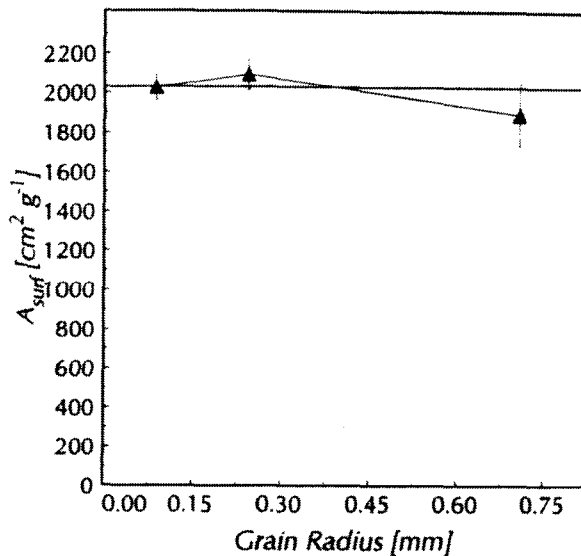
Fig. 6-7: A_{surf} derived from TS G50 adsorption isotherms using artificial broken sandstones of different grain sizes. Different grain radii yield the same value of A_{surf}.
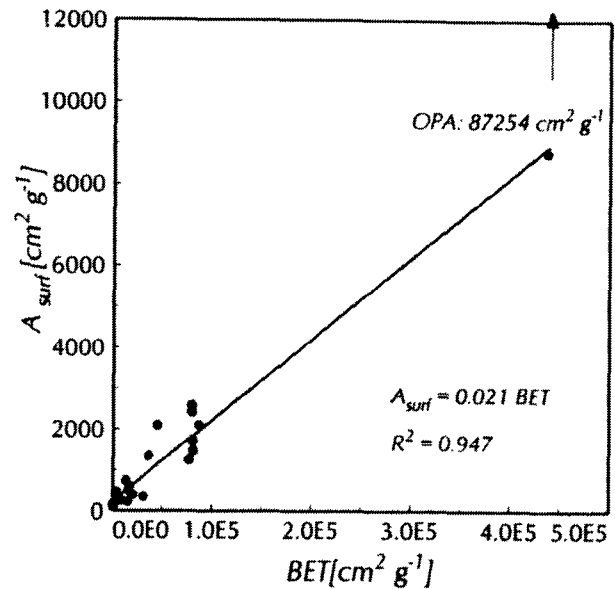
Fig. 6-8: Correlation of A_{surf} versus BET for all samples investigated by TS G50 adsorption. In average the surfactants cover about 2 % of the BET interfacial area.

A_{surf} versus BET

Assuming that the surfactants reach the same surface area as nitrogen (BET), the surface area covered by one molecule (a_{surf}^*) could be calculated according to equation (3-8). The values obtained in that way would range between 2000 $Å^2$ and 4000 $Å^2$ per molecule. These values seem to be far too large for a single surfactant molecule, even if its hydrophobic tail is completely extended.

However, if A_{surf} iscompared to the BET surface area to determine the percentage of the BET surface which can be reached by the surfactant. Between 1.1 % and 15 % of the BET surface area seems to be accessible by the surfactants. In average the surfactants cover about 2 % of the BET interfacial area (Fig. 6-9). The highest percentages were found for the quartzes since they exhibit the smallest amount of intraparticle porosity. The fairly constant $A_{surf} BET^{-1}$ ratio may indicate a relationship between mesopores and macropores accessible by the surfactants and the BET interfacial area. This indicates that a complete bilayer coverage could be established since this correlation would not occur if the surfactants adsorb at q_{max} in patchy islands of admicelles.

Surfactant Accessible Pore Diameter

A_{surf} of the different lithocomponents of RNA were compared to the respective cummulative interfacial areas obtained by combined nitrogen adsorptio and mercury intrusion data (see chapter 4). The pore diameters which have to be entered by the surfactant to cover the measured value of A_{surf} can be determined in that way (Tab. 5-1). The identified pore diameters were (49 ± 2) nm, (54 ± 4) nm, and (107 ± 9) nm for the Triassic Limestones, the Jurassic limestones and the sandstones, respectively (Fig. 6-12). This indicates that surfactant molecules can enter mesopores and macropores and the adsorption mainly occurs in these pores (Tab. 4-3). It is surprising that the surfactants can enter pores of 50 nm diameter within the limestones but about only 100 nm within the sandstones. Actually, one would expect that the same pore diameter should be accessible for the surfactant, independently from the lithocomponent. Perhaps the higher q_{max} values which result in higher A_{surf} values and thus to smaller pore diameter of the limestones is due to net positively charged calcite of the limestones at neutral pH (Stumm, 1992), which causes a higher attraction of the hydrophilic headgroup compared to the sandstones. If surfactants could access surfaces within pores of a diameter of

about 50 nm the area they should reach within the sandstones should be significantly larger. On the other hand, if they reach only surfaces within pores larger than 110 nm the Jurassic limestones and Triassic limestones should have significant rougher surfaces on the nm-scale compared to the sandstones. This observations may be also explained by surface induced precipitation within the limestones.

Assuming the length of a SDS molecule with a completely stretched alkyl chain between 1.7 nm - 2.5 nm (Lee et al. 1990; Wu et al., 1987) the molecule length of TS G50 should range between 5 nm and 8 nm (for size considerations see Fig. 4-1). Then, a complete TS G50 bilayer should have a thickness between 10 nm and 16 nm. If now a bilayer is established on both the opposite walls of a pore, e.g the diameter of a macropore (50 nm) is reduced to 30 nm or 18 nm, respectively. This seems to be sufficient to prevent further surfactant monomers to enter that particular pore. Maybe it is more likely that this effect occurs were the opposite walls of a macropores narrow to a bottle neck. The influence of structured water at the interfaces may be neglected since the thickness of structured water should be one order of magnitude smaller compared to the surfactant layers (Israelachvili, 1996).

Comparison of Surfactant Adsorption Data with Literature Data

The results of adsorption experiments with non-ionic and anionic surfactants are in good agreement with data reported in the literature which are summarized in Tab. 6-1. The $K_{d, mn}$ values range between 3.1 L kg^{-1} and 8.3 L kg^{-1}. The maximum adsorption q_{max} range between 1.4 mmol kg^{-1} and 10 mmol kg^{-1} for natural aquifer materials. It should be mentioned that sodium dodecyl benzene sulfonate (SDBS, SDS containing one benzene ring) (32.71 mmol kg^{-1}) and SDS (33.92 mmol kg^{-1}) show higher adsorption maxima, which differ by a factor of 3 from the other values using the same aquifer material. Similar observations were made within this study showing even a
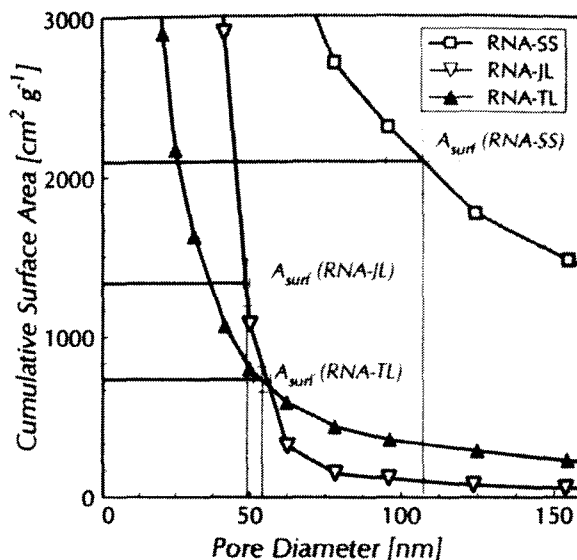
Fig. 6-9: Surface areas within the intraparticle porosity depending on the pore diameters of the lithocomponents of RNA.

larger difference between SDS adsorption and other surfactants examined (factor 2 - 20). The adsorption of the di-anionic surfactants onto aluminum oxide (AlOx) show significant higher adsorption maxima between about 50 mmol kg^{-1} and 180 mmol kg^{-1} due to highly porous aggregates.

The surfactant specific interfacial area A_{surf} was calculated with the same assumptions as in this study (complete bilayer, same area per molecule at the solid/liquid interface and at the liquid/air interface) using the area per molecule reported in these studies or if not available using the area per molecule values from this study. The calculated areas which are covered by the surfactants range between about 4000 cm^2 g^{-1} and almost 55 000 cm^2 g^{-1} where SDS and SDBS again produced the highest values. Even higher values were calculated from the data of Sun and Jaffe (1996) for the aluminum oxide (180 000 cm^2 g^{-1} - 340 000 cm^2 g^{-1}). The percentage of A_{surf} compared to the BET surface area range from 1 % to 60 %. The external surface area A_{ext} of the porous media assuming the grains as ideal spheres range between 0.1 % and 6 %. As observed in this study A_{ext} seems not to play a significant role in surfactant adsorption. Exceptions are very small grain size such as silt and clay.

Tab. 6-1: Comparison of adsorption data of nonionic and anionic surfactants reported in the literature.

Surfactant (type)	Solid	BET [m²g⁻¹]	Grain Size [mm]	MW_{surf} [g mol⁻¹]	a_{surf} [Å²]	$K_{d,mn}$ [L kg⁻¹]	q_{max} [mmol kg⁻¹]	A_{surf} [cm² g⁻¹]	$A_{surf} BET^{-1}$ [%]	$A_{surf} A_{ext}^{-1}$ [%]	Source
SDS (anionic)	CRA	36	0.1	288	53	-	25.03	39 951	11.10	0.6	Rouse et al. (1996)
CS 130[b] (anionic)	CRA	36	0.1	346	64	8.3	8.38	16 151	4.49	1.4	Rouse et al. (1996)
CS 230[c] (anionic)	CRA	36	0.1	382	48	6.3	3.30	4 767	1.32	4.7	Rouse et al. (1996)
CS 330[d] (anionic)	CRA	36	0.1	442	66	4.6	2.08	4 136	1.15	5.5	Rouse et al. (1996)
SDS (anionic)	CRA	36	0.1	288	53	6.33	33.92	54 136	15.04	0.4	Nivas et al. (1996)
DF 8390 (di-anionic)	CRA	36	0.1	642	117[a]	-	1.40	4 922	1.37	4.6	Nivas et al. (1997)
AOT (anionic)	CRA	36	0.1	445	-	5.57	6.75	-	-	-	Nivas et al. (1998)
SDBS (anionic)	CRA	36	0.1	349	-	8.3	32.71	-	-	-	Rouse et al. (1993)
C12-DPDS (di-anionic)	CRA	36	0.1	575	-	3.1	2.78	-	-	-	Rouse et al. (1994)
DF 8390 6Cl (di-anionic)	Al Ox	155	3	474	117[a]	-	51.63	181 897	11.74	0.1[e]	Sun and Jaffe (1996)
DF 8390 3B2 (di-anionic)	Al Ox	155	3	542	117[a]	-	97.01	341 766	22.05	0.1[e]	Sun and Jaffe (1996)
DF 8390- (di-anionic)	Al Ox	155	3	642	117[a]	-	181.67	640 014	41.29	0.0[e]	Sun and Jaffe (1996)
TX-100 (nonionic)	Lincoln fine sand	3	< 1	625	60[a]	-	10.00	18 066	60.22	0.1	Edwards et al. (1994a)
TX-100 (nonionic)	Lincoln fine sand	3	< 1	625	60[a]	-	6.00	10 840	36.13	0.2	Adeel and Luthy (1995)

[a] Surface area per molecule taken from this study. [b] Sodium lauryl ether sulfate, same molecule structure as SDS but with a different number of ethoxygroups EO: CS 130 (1 EO) has the same structure as Marlinat used within this study. [c] 2 EO. [d] 3 EO. [e] Assuming a density of Al Ox of 0.1 g cm⁻³. "-" Not reported.

6.1.1 Comparison of Surfactant Adsorption with Rhodamin WT Adsorption

The adsorption behavior of TS G50 was compared to adsorption data of the fluorescence dye rhodamin WT (Rh-WT). In Fig. 6-10 the TS G50 maximum adsorption q_{max} onto lithocomponents of the Horkheim aquifer material is compared to q_{max}-values of Rh-WT, which were measured by Strobel (1996). The Rh-WT isotherms had been fitted by a Langmuir adsorption model. Both compounds show the same pattern with the highest q_{max}-values for the sandstones, followed by Triassic and Jurassic limestones and the lowest adsorption for the quartz minerals. It should be noted that the q_{max}-values of Rh-WT is in the μmol kg^{-1} range (left y-axis) while the q_{max}-values of TS G50 is in the mmol kg^{-1} range (right y-axis). The transport of Rh-WT was studied by Shiau et al. (1993). Also Soerens and Sabatini (1994) reported linear isotherms in the μmol kg^{-1} range for Rh-WT adsorption onto CRA, which may be the linear part of Langmuir isotherms. Although Rh-WT has almost the same molecular weight as TS G50 and the pattern of the maximum sorption of the lithocomponents is also very similar, the adsorption is a factor 1000 smaller on a mol basis. This could indicate that Rh-WT does not form bilayers (as expected) and that Rh-WT may cover a signifantly larger surface area per molecule a_{surf}. It could also indicate that Rh-WT is only adsorbed onto the external surfaces or in larger macropores which are accessible to Rh-WT compared to TS G50. In the later case the macropore distribution (or the surface area within these macropores) would mirror the surface area which is accessible for the TS G50. An additional indication that Rh-WT is mainly adsorbed to the external surfaces of the grains could be the observations of Strobel (1996), who found an increasing Rh-WT adsorption with decreasing grain size.
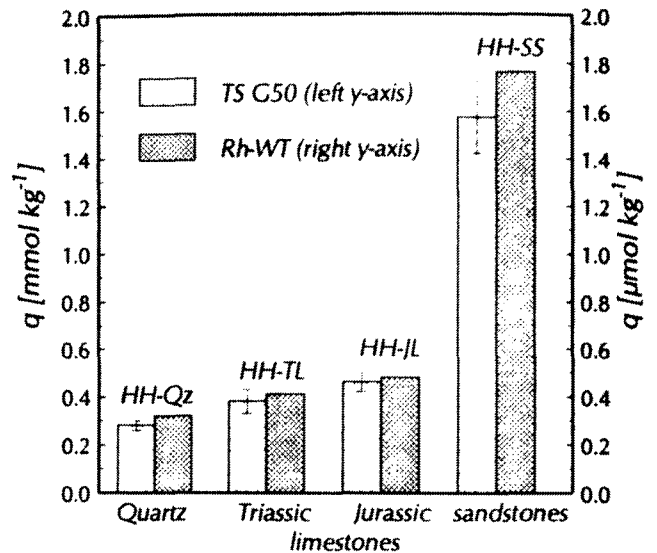
Fig. 6-10 Comparison of the maximum sorption of TS G50 (left y-axis, this study) and Rhodamin WT (right y-axis, Strobel, 1996; master thesis) onto different lithocomponents of Horkheim aquifer material (HH).

Adsorption of the Cationic HDTMA

The adsorption of the cationic surfactant HDTMA is mainly controlled by the effective cation exchange capacity ECEC (Wagner et al. 1994). The ratio of the amount of HDTMA adsorbed to the ECEC of the aquifer material should be 2 : 1 for a complete bilayer coverage (Li and Bowman, 1997). The ECEC was 12.8 meq kg^{-1} for RNA and 8.7 meq kg^{-1} for RRA using a method which is suitable for soils containing carbonates (Drechsel, 1992). The comparison of the ECEC with q_{max} indicates that the bilayer coverage should be most complete for RNA while for RRA the coverage should be slightly more than a monolayer. This difference may be due to the charge density since also in the literature the values of the maximum adsorption range from 1 to 2 times the ECEC (Tab. 6-2).

Tab. 6-2: Adsorption of the cationic surfactant HDTMA onto RNA and RRA: Comparison with the effective cation exchange capacity *ECEC* of these aquifer materials and with literature data.

Aquifer Material	Counter -ion	$K_{d, mn}$ [L kg^{-1}]	K_L [mM^{-1}]	q_{max} [mmol kg^{-1}]	ECEC [meq^{a} kg^{-1}]	q_{max} $ECEC^{-1}$	Source
RNA	Br$^-$	77.1	6	28.9	12.8	2.3	this study
RRA (Kehl)	Br$^-$	21.9	8	9.6	8.7	1.1	this study
Columbus AFB	Cl$^-$	-	-	27.78	25 - 28	1.1 -1.0	Burris and Antworth (1992)
Zeolite	Br$^-$	-	27	208	110	1.9	Li and Bowman (1997)
Zeolite	Cl$^-$	-	30	151	110	1.4	Li and Bowman (1997)
Kaolinite	Br$^-$	-	16	63	20 - 40	3.2 - 1.6	Li and Bowman (1997)
Kaolinite	Cl$^-$	-	12	48	20 - 40	2.4 - 1.2	Li and Bowman (1997)

[a] Milli-equivalent charge (mmol$_{charge}$).

6.2 Surfactant Column Experiments

The $R_d R_{eq}^{-1}$ and $R_{0.5} R_d^{-1}$ ratios close to 1 indicate that the transport of TS G50 in the column systems is close to equilibrium and that the retardation can be reasonably well predicted from the surfactant adsorption isotherms. The mean residence time of flow velocities below 10 m day^{-1} seems to be sufficient to reach local adsorption equilibrium of the surfactant.

The surfactant adsorption seems to be completely reversible since the adsorbed and desorbed surfactant masses of the breakthrough and elution curves are almost the same. However, the columns have to be flushed by a significant number of pore volumes to desorb the total surfactant mass. This results agree well with results of Abdul and Gibson (1991) as well as Adeel and Luthy (1995) who conducted column elution tests using nonionic surfactants and natural aquifer material.

Surfactant Transport Above the CMC$_e$

The surfactant breakthrough curves above and below the CMC$_e$ show a completely different shape. This may be due to the different equilibrium states and the different kinetics of surfactant monomer and micelle adsorption. The final equilibrium state for surfactant concentrations above the CMC is a bilayer while for concentrations below the CMC the adsorption does not exceed the monolayer stage (Rosen, 1989).

The breakthrough curves above the CMC$_e$ may be explained by the adsorption mechanism of a bilayer formation from a micellar solution: while monomers and micelles are present in the influent solution, the latter have a greater affinity to the surface (Chen et al., 1992). The number of pore volumes that must be exchanged until the whole accessible solid/water interfacial area is covered by a loosely packed but continuous bilayer depends on the surfactant influent concentration. Thus the breakthrough of the higher surfactant influent concentrations can be observed earlier. After this fast adsorption stage the loose bilayer changes into a more densely packed bilayer. This slow process includes overturning of surfactant molecules, lateral diffusion and exchange of surfactant molecules with those in the bulk solution (Chen et al., 1992). It should be noted that only monomers are incorporated in that more and more dense packed bilayer over a long period. This effect may cause the significant tailing observed in the breakthrough curves. Another reason may be the non-linear shape of the surfactant adsorption isotherm.

Surfactant Transport Below the CMC_e

The lower $R_{0.5} R_d^{-1}$ ratios of the column systems with influent concentrations below the CMC_e indicate, that the monomer adsorption seems to be slower compared to the adsorption of micelles above the CMC_e, i.e. an earlier breaktrough can be observed in the effluent concentration. However, the adsorption of monomers proceeds until a complete monolayer coverage is reached. This may cause the unusual shape and the tailing of the surfactant breakthrough curves below the CMC_e.

Similar observations were reported by Abdul and Gibson (1991) who conducted experiments with a nonionic alkyl ethoxylate surfactant (Witconol SN 70) in columns packed with natural aquifer material. They found regular sigmoidal breakthrough curves and the retardation factor as well as the skewness of the breakthrough curves increased with decreasing surfactant concentration. Okuda et al. (1996) used TX-100 and glass beads for breakthrough experiments and reported regular sigmoidal breakthrough curves with almost no retardation for surfactant concentrations > 1 wt %. Higher retardation factors and fairly skew breakthrough curves were reported for lower surfactant concentrations and the elution curves showed no significant tailing (Okuda et al., 1996). Schüth (1994) conducted column experiments using TX-100 and different natural aquifer materials including RNA. He reported regular sigmoidal breakthrough curves for surfactant concentrations well above and well below the CMC. At concentrations close to the CMC he observed highly skewed breakthrough curves showing a large tailing. From the column data he constructed nonlinear adsorption isotherms which showed the highest adsorption for surfactant concentration close to the CMC and less adsorption both above and below the CMC. These isotherms could not been described by conventional adsorption isotherms. These observations may be explained by the relatively short residence time of the surfactant within the columns and very fast adsorption kinetics for surfactant concentrations close to the CMC as described above (Chen et al., 1992).

Very unusual breakthrough curves were reported by Adeel and Luthy (1995) who conducted column and batch experiments to examine sorption and transport kinetics of TX-100 and natural aquifer material. They described the adsorption of TX-100 onto the aquifer material as a Langmuir type isotherm. The surfactant influent concentrations used for the column experiments were relatively high (15 - 150 times the CMC). A first increase after one pore volume up to a relative concentration C/C_0 between 0.2 and 0.4 was followed by a plateau-like region parallel to the x-axis for 1 - 7 pore volumes depending on the surfactant influent concentration. The plateau region persisted up to an "inflection point" from which a second stage breakthrough curve started with reduced effluent values of the plateau. The second stage breakthrough curves were sigmoidal and approached the influent concentration between 0.5 and more than 4 pore volumes depending on C_0. The extent of retardation as well as the skewness of the second-stage breakthrough curves was reported to be increasing with decreasing values of C_0. The elution curves of their column studies showed a rapid drop in the reduced effluent concentration within the first two pore volumes displaced and an asymptotical approach to zero. The elution curves did not show the two-step shape as observed in the breakthrough curves. The mass of surfactant desorbed during the elution process was much smaller compared to the total mass adsorbed due to the limited duration of the elution test. The observations were described by different adsorption and desorption rate constants within the different phases of the surfactant breakthrough. However, precipitation, liquid crystal formation or degradation processes were not considered to explain the observed phenomena.

Hydraulic Conductivity

No decrease of the hydraulic conductivity was observed during the column experiments. This may be due to the properties of the aquifer material used and the relatively low surfactant concentrations. However, other lab scale studies indicate that the application of surfactants can reduce the aquifer permeability by more than an order of magnitude by increasing the volume

fraction of clay (Renshaw et al., 1997; Crawford et al., 1997; Imhoff and Miller, 1996; Imhoff et al., 1996). Furthermore, permeability reductions are mainly reported from mobilization experiments either in the lab (Haegel, 1997) or in the field (Muntzer, 1997). Since in those experiments extremely high surfactant concentrations were used the permeability reduction may be due to the formation of liquid crystals (Shiau et al., 1995).

6.3 Adsolubilization

The potential of the hydrophobic surfactant pseudophases to solve HOCs can be quantified by the partitioning coefficients. TX-100 has the highest potential, followed by TS G80, TS G50 and SDS according to Tab. 5-5. This may be due to molecular structure of TX-100 containing an aromatic ring. The values determined in this study agree well with partitioning coefficients reported in the literature (Tab. 6-4). The comparison of the partitioning coefficients to the adsorbed surfactants normalized to their carbon content yields K_{oc} values which can be compared to K_{oc} values in natural systems, i.e. without surfactant. K_{oc} values inidicate the HOC adsorption potential, e.g. the quality of the organic matter derived during the sedimentation of the aquifer material or sediments of the source rocks. The calculated values indicate that the adsorbed surfactants have even a greater potential to (ad-) solubilize HOC than the intrinsic organic matter. Additionally, the adsorbed surfactant pseudophases should be good accessible since they are located within the macropores.

The partitioning coefficients K_{vol} of phenanthrene between the aqueous phase and the adsorbed TS G50 surfactant phases range from 4400 to 4740 below and from 12935 to 14197 above a surfactant aqueous concentration of about 0.15 mM, i.e. they differ by a factor of about 3. This difference may be due the more effective phenanthrene partitioning into surfactant bilayers compared to monolayers in the equilibrium system (Sun and Jaffé, 1996). The identified monolayer (K_{ml}) and bilayer (K_{bl}) partitioning coeffi-

cients were about 4600 and 14000, respectively. This indicates that the surfactant bilayers are about 3 times more effective than monolayers as a sorptive phase for phenanthrene. Due to the lower partitioning coefficient K_{ml} below a surfactant concentration of about 0.15 mM (corresponding to an adsorbed surfactant concentration of about 0.35 mmol kg^{-1}) a monolayer should be established at the solid/water interface. The monolayer adsorption maximum ($q_{ml, max}$) should be reached for adsorbed surfactant concentrations between 0.334 mmol kg^{-1} and 0.721 mmol kg^{-1} due to the increase of the partitioning coefficient within this concentration range. The partitioning coefficient identified for this range should be a mixture of K_{ml} and K_{bl} since monolayers and bilayers coexist.

A mass balance model equation (2-13) according to Sun and Jaffé (1996) was fitted to the measured distribution coefficients K_d^* in order to identify the unknown parameters K_{mn} and K_{mic}. The input parameters as well the identified parameters are summarized in Tab. 6-3. The respective adsorbed surfactant concentration (monolayer and bilayer) was calculated from the surfactant adsorption isotherm ($q = K_{d, mn} C_{eq}$) using the following scheme (modified from Sun and Jaffé, 1996):

$$q_{ml} = q \text{ and } q_{bl} = 0$$

$$\text{for } q \leq q_{ml, max}$$

$$q_{ml} = q\left(1 - \frac{q - q_{ml, max}}{q_{max} - q_{ml, max}}\right) \text{ and } q_{bl} = q - q_{ml}$$

$$\text{for } q_{ml, max} < q < q_{max}$$

$$q_{ml} = 0 \text{ and } q_{bl} = q_{max}$$

$$\text{for } q \geq q_{max}$$

Similarly, the respective aqueous surfactant concentrations (monomers and micelles) were calculated according to:

$$C_{mn} = C_{eq} \text{ and } C_{mic} = 0$$

$$\text{for } C_{eq} \leq CMC_e$$

$$C_{mn} = CMC_e \text{ and } C_{mic} = C_{eq} - CMC_e$$
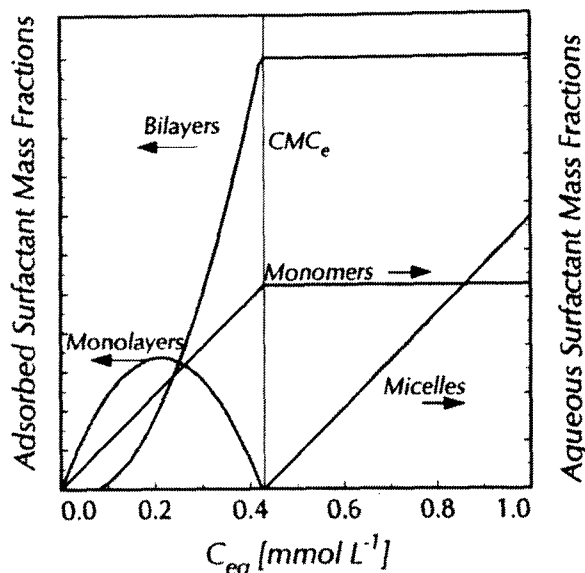
$$\text{for } C_{eq} > CMC_e$$

Fig. 6-11: Conceptual model of dimensionless mass fractions of surfactant pseudophases in the mobile water (monomers and micelles) and associated to the immobile solids (Monolayers and Bilayers) versus the aqueous surfactant concentration (modified from Sun and Jaffé, 1996).

Fig. 6-12: Apparent distribution coefficient K_d^* of phenanthrene versus surfactant equilibrium concentration C_{eq}. The measured data of K_d^* were fitted by the thermodynamic model according to equation (2-13) using $K_{mi} = 4600$ and $K_{bi} = 14000$ as known parameters (Tab. 5-5) in order to fit the monomer and micelle partitioning coefficients ($K_{mn} = 3000$, $K_{mic} = 10000$).

The different surfactant pseudophases depending on the surfactant aqueous concentration are shown as dimensionless mass fractions in Fig. 6-11.

Sun et al. (1995) also proposed a transitional model to describe the increase of K_{mn} to K_{mic} due to sequential micellization in the aqueous phase according to:

$$K_{tr} = K_{mn} + \left(C_{eq} - C_L\right)\frac{K_{mic} - K_{mn}}{C_U - C_L} \qquad (6-1)$$

where K_{tr}, C_L and C_U denote the partitioning coefficient of the transition region, the surfactant concentration at the lower and the upper boundary of the transitional region. They found that the transitional region starts at surfactant concentrations of 0.8 times the CMC and ends at concentrations of about 2 times the CMC in a system containing p,p'-DDT and the nonionic surfactant TX-100.

The two unknowns were identified by using a non-linear curve fitting procedure minimizing the sum of the squared deviations. The values were 4600 (K_{mn}) and 14000 (K_{mic}), respectively, which are very similar to the corresponding partitioning coefficients in the immobile surfactant pseudophase. However, the adsorbed surfactant phases seem to be more effective as the surfactant
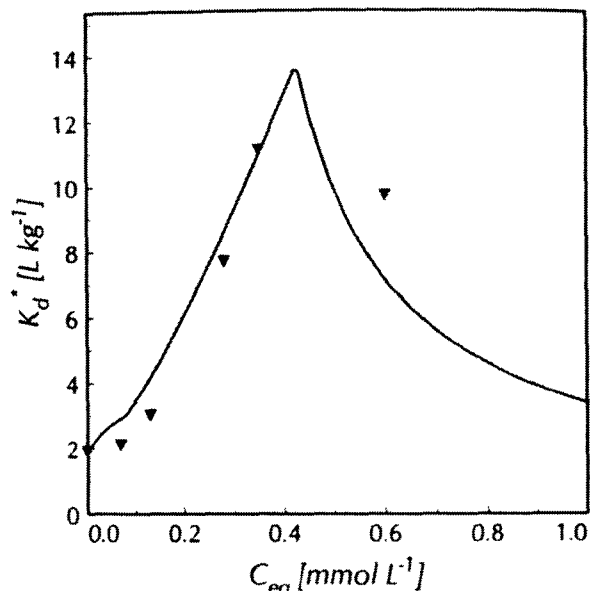
pseudophases in water. The surfactant monolayer is 1.5 times more effective than its counterpart in the aqueous phase (monomers). Analogue the adsorbed bilayer is 1.4 times more effective compared to the micelles in the aqueous phase. Similar results are reported by Sun and Jaffé (1996) who used alumina coated with di-anionic surfactants (DOWFAX) for adsolubilization studies. They see a possible reason for the observed difference in the hydration of the ionic surfactant molecules in the aqueous solution: while the hydration layer is mainly around the charged hydrophilic ionic headgroup of the surfactant molecule it could also extend in part to the hydrophobic moiety (alkyl chain) causing a partially reduced interaction with HOC in the solution (Kile and Chiou, 1989). Sun and Jaffé (1996) expect an increased radius of the hydration layer, because they used double charged di-anionic surfactants. They postulated that the hydration layer would be eliminated or significantly reduced after the surfactant molecul is adsorbed to the alumina surface by static attraction or ion exchange and its charges become neutralized. This would favor hydrophobic interactions with phenanthrene molecules. The results of this study show the

same behavior of phenanthrene partitioning using a nonionic surfactant. Maybe the findings can be also explained by an elimination or reduction of the hydration layer that surrounds a nonionic surfactant molecule, even if its extent is smaller. Another explanation according to Loyek (1997) could be a lower activity coefficient of phenanthrene within the admicelle compared to the micelle. Maybe the admicelles can expand more by dissolving phenanthrene and are therefore a more attractive pseudophase than the micelles. The volume increase due to the incorporation of an additional phenanthrene molecule results in a volume increase of the micelle as well as of the admicelle. Thus, the interface between hydrophobic surfactant moieties and water would increase in the case of spherical micelles, but not in the case of the two-dimensional admicelles.

The measured partitioning coefficients are in the range of values published in the literature. They are summarized including K_{ow}-values and literature data in Tab. 6-3. Earlier work has been done by Kile and Chiou (1989) who measured the water solubility enhancement of DDT and Trichlorobenzene (TCB) by some surfactants below and above the CMC. They used some nonionic surfactants of the Triton series and Brij 35 as well as the anionic SDS and a cationic surfactant. They determined monomer and micelle partitioning coefficients for DDT and TCB. Rouse et al. (1995) studied the influence of hydrocarbons of varying polarity solubilized into the core or the palisade layer of a micelle on further solubilization of HOCs. Sun et al. (1995) examined in batch experiments the adsorption of HOC (DDT, TCB, PCB) in a soil-water system containing TX-100. They quantified the sorption of TX-100 onto soil and the monomer partitioning coefficient to be smaller than the micelle partitioning coefficient. They formulated a model for

the apparent distribution coefficient of HOC in the presence of different surfactant concentrations considering monomers and micelles and treated adsorbed surfactant as soil organic matter. The measured distribution coefficient showed the highest values for supra-CMC concentration in the batch systems. They also introduced the transitional model for the concentration range close to the CMC as mentioned above. Edwards et al. (1991) determined the solubilization of selected PAHs by nonionic surfactants (polyethoxylated alcohols). The measured micelle partitioning coefficient showed a good correlation to the octanol/water partitioning coefficient on a log scale. Edwards et al (1994a) studied the distribution of phenanthrene and the nonionic surfactant TX-100 in a sediment/aqueous system. They found that the intrinsic distribution coefficient K_d of phenanthrene can be increased by a factor of 10 due to the adsorbed surfactant pseudophase below the CMC. On a carbon normalized basis, the surfactant was found to be more effective than organic matter. Above the CMC an enhanced solubilization of phenanthrene was observed resulting in desorption of phenanthrene from the sediment. A screening study for the selection of surfactant for the removal of petroleum products from shallow sandy aquifers had been conducted by Abdul and coworkers (1990, 1992). They found that an ethoxylated alcohol surfactant was the most effective since it showed good solubilization and mobilization of the petroleum product, but caused low soil colloid dispersion. Jafvert (1991) and Jafvert et al. (1994) studied the partitioning of PAHs and SDS. They correlated the micelle partitioning coefficient to the octanol/water partitioning coefficient and found a relationship of $K_{mic} = 0.15\, K_{ow}$. They concluded that on a carbon normalized basis the SDS micelles and the natural media used in these studies had almost the same affinity or sorption potential for PAHs.

Tab. 6-3: Summary of experimental measured monolayer and bilayer partitioning coefficients K_{ml} and K_{bl} and fitted K_{mn} and K_{mic} for sorption of phenanthrene onto RNA in the presence of the nonionic surfactant TS G50; the results of Sun and Jaffé (1996) are included for comparison (they used phenanthrene and aluminum oxide coated with di-anionic DOWFAX surfactants characterized by alkyl chains of C6 (DF-6CL), C10 (DF-3B2) and C16 (DF-8390)).

Surfactant	Adsorbed Surfactant Phase				Aqueous Surfactant Phase				
	K_{ml} [-]	K_{bl} [-]	$q_{ml, max}$ [mmol kg^{-1}]	q_{max} [mmol kg^{-1}]	K_{mn} [-]	K_{mic} [-]	CMC [mM]	$K_{ml} K_{mn}^{-1}$	$K_{bl} K_{ml}^{-1}$
TS G50[a]	4600	14000	0.2	1.1	3000	10000	0.43	1.5	1.4
DF-6CL[b]	2580	16600	16.9	59.1	765	-[c]	-[c]	3.4	-
DF-3B2[b]	5550	28350	20.9	104.0	1815	4015	1.17	3.1	7.1
DF-8390[b]	11950	32100	23.5	181.2	5200	11200	0.86	2.3	2.9

[a] This study, [b] data from Sun and Jaffé (1996), partially converted in units used within this study (multiplied with the carbon weight fraction f_{carbon} of the surfactants), [c] not reported

Tab. 6-4: HOC partitioning coefficients between aqueous phase and surfactant pseudophases compared to the octanol/water partitioning coefficients K_{ow} (selected literature data, partially converted into units used within this study).

Surfactant	MW_{surf} [g mol^{-1}]	HOC	log K_{ow}	log K_{mic}	K_{mic} K_{ow}^{-1}	log K_{mn}	K_{mn} K_{ow}^{-1}	log K_{bl}	K_{bl} K_{ow}^{-1}	log K_{ml}	K_{ml} K_{ow}^{-1}	Source
SDS	265	naphthalene	3.36	2.92	0.36	-	-	3.49	1.36	-	-	Nayyar et al. (1994)
SDS	265	ANSA	0.17	1.78	40.93	-	-	2.28	129.4	-	-	Nayyar et al. (1994)
SDS	265	naphtol	2.69	2.33	0.44	-	-	2.39	0.50	-	-	Nayyar et al. (1994)
DF 8390	643	phenanthrene	4.57	4.05	0.30	3.72	0.14	4.51	0.86	4.08	0.32	Sun and Jaffé (1996)
DF 6CL	474	phenanthrene	4.57	-		2.88	0.02	4.22	0.45	3.41	0.07	Sun and Jaffé (1996)
DF 3B2	542	phenanthrene	4.57	3.60	0.11	3.26	0.05	4.45	0.76	3.74	0.15	Sun and Jaffé (1996)
TX-100	625	p,p'-DDT	6.36	6.15	0.62	4.26	0.01	-	-	-	-	Kile and Chiou (1989)
Brij35	1198	p,p'-DDT	6.36	5.75	0.25	4.18	0.01	-	-	-	-	Kile and Chiou (1989)
SDS	265	p,p'-DDT	6.36	5.38	0.10	2.68	0.00	-	-	-	-	Kile and Chiou (1989)
Brij 30	363	phenanthrene	4.57	4.27	0.50	-	-	-	-	-	-	Edwards et al. (1991)
Igepal CA 720	735	phenanthrene	4.57	4.07	0.32	-	-	-	-	-	-	Edwards et al. (1991)
Tergitol NP-10	683	phenanthrene	4.57	4.14	0.37	-	-	-	-	-	-	Edwards et al. (1991)
TX-100	625	phenanthrene	4.57	4.16	0.39	-	-	-	-	-	-	Edwards et al. (1991)
TX-100	625	phenanthrene	4.57	4.39	0.66	-	-	-	-	-	-	Yeom et al. (1995)
TX-100	625	pyrene	5.22	4.98	0.58	-	-	-	-	-	-	Yeom et al. (1995)
TX-100	625	B(a)P [a]	6.50	6.20	0.50	-	-	-	-	-	-	Yeom et al. (1995)
Brij 35	1198	phenanthrene	4.57	4.20	0.43	-	-	-	-	-	-	Yeom et al. (1995)
Brij 35	1198	pyrene	5.22	4.71	0.31	-	-	-	-	-	-	Yeom et al. (1995)
Brij 35	1198	B(a)P [a]	6.50	5.98	0.30	-	-	-	-	-	-	Yeom et al. (1995)
Tween 80	1310	phenanthrene	4.57	4.39	0.65	-	-	-	-	-	-	Yeom et al. (1995)
Tween 80	1310	pyrene	5.22	4.93	0.51	-	-	-	-	-	-	Yeom et al. (1995)
Tween 80	1310	B(a)P [a]	6.50	6.12	0.42	-	-	-	-	-	-	Yeom et al. (1995)

[a] Benzo(a)pyrene. "-" = Not reported

6.4 Coupled Transport of Phenanthrene and Surfactant

The transport behavior of phenanthrene depends strongly on the surfactant concentration. The phenanthrene retardation increases with increasing adsorbed surfactant concentration (enhanced retardation). Similar results of column experiments are reported for the transport of PAHs in the presence of dissolved organic matter by Danzer et al. (1993) and Totsche et al. (1997). A facilitated transport, i.e. faster transport compared to the column system without surfactant was observed for surfactant concentrations well above the CMC. The retardation factors determined from the breakthrough curves were converted into phenanthrene distribution coefficients K_d^* and $K_{0.5}^*$ according to the equations (3-39) to (3-42). In that way the results of column experiments showing some variations in bulk density, porosity or flow velocities can be compared to each other and to equilibrium batch data. The measured distribution coefficients were compared to the predicted distribution coefficient according to equation (2-13) (mass balance model). The input parameters are summarized in Tab. 6-5. The partitioning coefficients and the surfactant adsorption data were determined in indepently equilibrium batch experiments as described above. The phenanthrene distribution coefficient K_d was determined by a column experiment in the absence of surfactant. In the time frame of the column experiments K_d has to be considered as an apparent distribution coefficient.

The phenanthrene distribution coefficients versus the surfactant concentration are plotted in Fig. 6-13 and Fig. 6-14. In both cases K_d^* can be reasonably well predicted by the presented mass balance model. Sensitivity analysis were carried out in order to identify the influence of the single input parameters on the mass balance model: The apparent distribution coefficient of phenanthrene is the most significant input parameter throughout the whole surfactant concentration range.
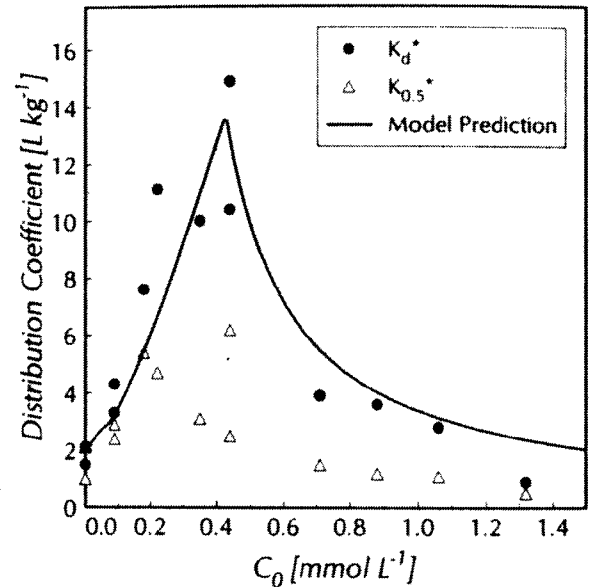

Fig. 6-13: Apparent distribution coefficient K_d^* of phenanthrene onto RNA for different TS G50 surfactant influent concentrations C_0 (Column experiments set B, column length: 7 cm or 9 cm, grain size: 0.25 mm - 1.0 mm, the results were given in Tab. 5-7).
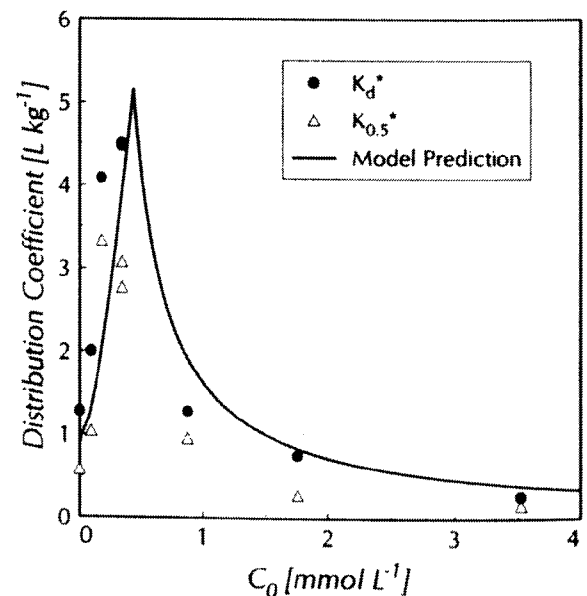

Fig. 6-14: Apparent distribution coefficient K_d^* of phenanthrene onto RNA for different TS G50 surfactant influent concentrations C_0 (Column experiments set C, column length: 12.35 cm, grain size: 1.0 mm - 2.0 mm, the results were given in Tab. 5-8)

The model is also very sensitive with respect to K_{bl} and K_{mic} while K_{ml} and K_{mn} are less important.

However, a higher adsorption of phenanthrene is observed for surfactant concentration even below the CMC. Lower retardation factors and distribution coefficients were observed as expected, if the 50 % breakthrough is considered.

Tab. 6-5: Input parameters for the mass balance model equation (2-13) for the description of the apparent distribution coefficients K_d^* determined in column experiments, results are shown for the experimental Set B in Fig. 6-13 and Set C in Fig. 6-14, respectively.

Parameter	Batch	Column
K_d [L kg^{-1}]	1.1	3.6 1.1
$K_{d,\,mn}$ [L kg^{-1}]	2.6	2.6 [a] 2.7 [b]
CMC_e [mM]	0.42	0.42
$q_{max,\,ml}$ [mmol kg^{-1}]	0.20	0.20 [a] 0.23 [b]
$q_{max,\,bl}$ [mmol kg^{-1}]	1.1	1.1 [a] 1.2 [b]
K_{ml} [-]	4600 [c]	4600 [c]
K_{bl} [-]	14000 [c]	14000 [c]
K_{mn} [-]	3000 [d]	3000 [e]
K_{mic} [-]	10000 [d]	10000 [e]

[a] Column experiments Set B, grain size: 0.25 mm - 1.0 mm. [b] Column experiments Set C, grain size: 1.0 mm - 2.0 mm. [c] Measured. [d] Fitted. [e] Determined in equilibrium batch experiments.

7 Conclusions

Batch and column experiments were performed in order to study the adsorption of different surfactants onto natural aquifer material and the coupled transport of phenanthrene in the presence of a nonionic surfactant at different concentrations. Following conclusions can be drawn:

- The CMC_{st} determined by a surface tension method generally decreased (exception: TX-100) to CMC_e in the batch and column systems due to the presence of electrolytes or cosolvent hydrocarbons.

- The surfactant adsorption can be described simply by an isotherm with a linear relationship for the surfactant monomers ($q = K_{d,mn} C_{eq}$) and an adsorption maximum q_{max} above the CMC.

- The adsorption maximum q_{max} can be calculated according to $q_{max} = K_{d,mn} CMC_e$ if $K_{d,mn}$ and CMC_e are known.

- A surfactant specific surface area A_{surf} can be calculated assuming that the area per molecule is the same at the solid/water and water/air interface and that a complete bilayer is established at q_{max}.

- The external interfacial area A_{ext} of the aquifer grains assumed as ideal, non-porous spheres has only a percentage between 0.5 % and 6 % of A_{surf}. Thus A_{ext}, i.e. the grain size (> 0.003 mm) of the natural aquifer material has only minor influence on the surfactant adsorption.

- In average 2 % of the BET interfacial area is covered by surfactants (A_{surf}). This indicates a relationship between macropores and mesopores (maybe micropores) in natural aquifer material.

- Only macropores are accessible by the nonionic surfactant studied (from comparison of A_{surf} with N_2 adsorption (BET) and Hg intrusion porosimetry data).

- Surfactant transport can be reasonably well predicted by the equilibrium adsorption isotherm. The surfactant adsorption is completely reversible.

- The phenanthrene partitioning into adsorbed surfactant pseudophases such as monolayers or bilayers (adsolubilization) can be quantified by a partitioning coefficient. The coefficients of the phenanthrene partitioning into monolayers amd bilayers are in the same order of magnitude as monomers and micelles, respectively. Howerver, there are indications that adsorbed surfactant pseudophases are more effective for phenanthrene partitioning compared to surfactants in the mobile aqueous phase.

- The coupled tranport of phenanthrene and surfactant: the retardation of phenanthrene increases with increasing surfactant concentration to the CMC_e (enhanced retardation). Above the CMC_e the retardation decreases until the same retardation as in the system without surfactant is reached for surfactant concentrations of about 3 times the CMC_e. Above that concentration a facilitated transport of phenanthrene can be observed.

- The coupled transport of phenanthrene and surfactant can be reasonably well predicted by a mass balance model with input parameters (partitioning coefficients, surfactant adsorption) determined in independent equilibrium batch experiments.

Implications for Surfactant Enhanced Subsurface Remediation (SESR)

Two different scenarios have to be discussed for SESR implications with respect to the results of this study:

(i) Solubilization coupled with facilitated transport of HOCs.

(ii) Adsolubilization resulting in an enhanced retardation of the HOCs (sorption barrier, reactive wall).

The efficiency of each of that schemes can be estimated by the retardation factor given in equation (2-21). This was calculated for the surfactants examined and is shown in Fig. 7-1. Since HOCs partition coefficients into the surfactant pseudophases are similar for different surfactants the HOC retardation depends mainly on the adsorption behavior of the surfactant. Facilitated transport can be obtained by high surfactant concentrations and relative minor adsorption of the surfactant onto the aquifer material. The retardation decreases with increasing surfactant concentration. This remediation system is limited by the mass transfer of HOCs from the NAPL or the desorption from the aquifer material (Grathwohl, 1998; Loyek 1998). It should be noted that the surfactant concentration can not be be increased infinitely since the hydraulic conductivity may decrease due to high surfactant concentrations. It should be noted that the *CMC* could also decrease in the natural subsurface environment due to the presence of electrolytes and (e.g. cosolvent) hydrocarbons, especially in an contaminated aquifer. The surfactant loss during SESR can be reasonably well predicted from the surfactant adsorption isotherms. Only surfactants should be selected which show no precipitation or other phase behavior (e.g. formation of gels or liquid crystals) in the subsurface environment.

On the other hand enhanced HOCs retardation can only obtained by surfactants which adsorb strongly onto natural aquifer material, e.g. HDTMA. The application of surfactant modified zeolites as an alternative to the in-situ modification of aquifer material was proposed by Li and Bowman (1997). The surfactants used within this
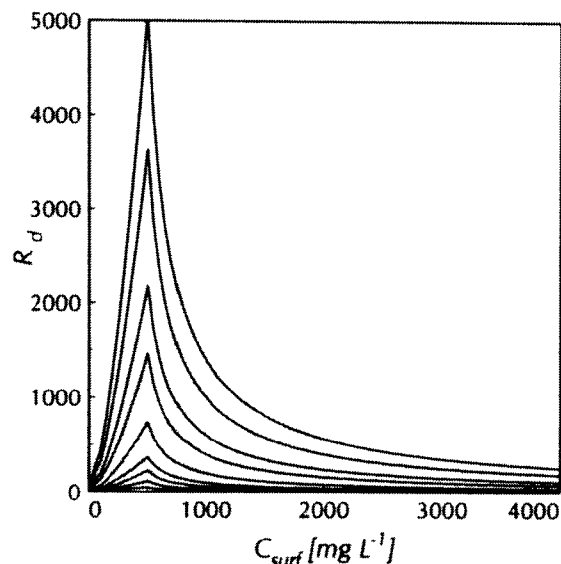

Fig. 7-1: Calculated retardation factors (equation 2-21) of phenanthrene depending on the surfactant concentration. Partition coefficients determined within this study were used as well as surfactant adsorption coefficients $K_{d\ mn}$ ranging from 0.6 L kg^{-1} for DF 8390 and about 70 L kg^{-1} for HDTMA.

study - except HDTMA - seem to be not suitable for an enhanced retardation of HOCs since for more hydrophobic HOCs than phenanthrene the distribution coefficients and the retardation factors, respectively, of these compounds are higher than the respective values of the surfactants. In this case the surfactant based reactive zone in the subsurface would move faster than the contaminants which should be adsorbed.

Since the solubilization takes place on a molecular level it is far less effctive than mobilization which is able to remove NAPLs in bulk using an appropriate surfactant system, e.g. middle phase microemulsion. An overview of field tests mainly performed in the US both for solubilization and mobilization schemes are given by the AADTF (1997) or Fountain (1997). Economic considerations of SESR implementations are given by Krebs-Yuill (1995).

The detection of solid/water or NAPL/water interfaces may be another application of surfactants. Maybe, surfactants can be also used as environmental more friendly compound compared to mercury in order to detect macropores in the laboratory. However, more research is necessary to support this hypothesis.

8. References

AATDF, The advanced technology demonstration facility program (1997), AATDF Technology practices manual for surfactants and cosolvents, *AATDF Report TR-97-2*, Houston, Texas, US.

Abdul, A.S., Gibson, T.L. (1991), Laboratory studies of surfactant-enhanced washing of polychlorinated biphenyl from sandy material, *Environmental Science and Technology, 25*, 665-671.

Abdul, A.S., Gibson, T.L., Ang., C.C., Smith, J.C., Sobczynski, R.E. (1992), In situ surfactant washing of polychlorinated biphenyls and oils from a contaminated site, *Groundwater, 30*, 219-231.

Abdul, A.S., Gibson, T.L., Rai, D.N. (1990), Selection of surfactants for the removal of petroleum products from shallow sandy aquifer, *Groundwater, 28*, 920-926.

Aboul-Kassim, T.A., Simoneit, B.R.T. (1993), Detergents: A review of the nature, chemistry, and behavior in the aquatic environment. part i. chemical composition and analytical techniques, *Critical Reviews in Environmental Science and Technology, 23*, 325-376.

Abriola, L.M., Pennell, K.D., Pope, G.A., Dekker, T.J. Luning-Prak, D.J. (1995), Impact of surfactant flushing on the solubilization and mobilization of dense non-aqueous phase liquids, chapter 2 in *Surfactant-enhanced subsurface remediation*, Sabatini, D. A., Knox, R. C., Harwell, J. H. (Eds.), ACS Symposium Series 594, American Chemical Society, Washington, USA.

Adamson, A.W. (1990), Physical chemistry of surfaces, John Wiley and Sons, New York, USA.

Adeel, Z., Luthy, R.G. (1995), Sorption transport kinetics of a nonionic surfactant through an aquifer sediment, *Environmental Science and Technology, 29*, 1032-1042.

Aronstein, B.N., Calvillo, Y.M., Alexander, M. (1994), Effect of surfactants at low concentrations on the desorption and biodegradation of sorbed aromatic compounds in soil, *Environmental Science and Technology, 25*, 1728-1731.

Bai, G.Y., Brusseau, M.L., Miller, R.M. (1997), Biosurfactant-enhanced removal of residual hydrocarbon from soil. *Journal of Contaminant Hydrology, 25*, (1-2), 157-170.

Brownawell, B.J., Chen, H., Zhang, W., Westall, J.C. (1997), Sorption of nonionic surfactants on sediment material, *Environmental Science and Technology 31*, 1735-1741.

Brunner, P. H., Capri, S., Marcomini, A., Giger, W. (1988), Occurence and behavior of linear alkylbenzene sulphonates, oxylates in sewage and sewage sludge treatment, *Water Res. 22*, 101-113

Burris, D.R., Antworth, C.P. (1992), In situ modification of an aquifer material by a cationic surfactant to enhance retardation of organic contaminants, *Journal of Contaminant Hydrology* 10, 325-337.

Chen, Y.L., Chen, S., Frank, C., Israelachvili, J. (1992), Molecular mechanisms and kinetics during self assembly of surfactant layers, *J. Coll. Interf. Sci.* 153, 221-242.

Clemens, W. D., Haegel, F. H., Nolte, P., Stickdorn, K., Webb, L. (1993), Microemulsions for soil remediation, in: Arendt, F., Annokkée, G. J., Bosman, R., van den Brink, W. J. (Eds.), Contaminated soils '93, Vol. II, 1375-1376, Kluwer Academic Publishers, Dordrecht

Copitzky, T., Laszlo, K., Koglin, E., Schwuger, M.J. (1998), Rasterkraftmikroskopische Untersuchungen zur Adsorption von nichtionischen Tensiden an Mineraloberflächen, in *Horizonte 2000, Kurzfassung der Vorträge und Poster, 6. Wolfgang-Ostwald-Kolloquium der Kolloid-Gesellschaft, 3. Nachwuchstage der Kolloid- und Grenzflächenforschung*, Haegel, F.-H., Lewandowski, H., Krahl-Urban, B. (Hrsg.), Jülich, S. 53.

Crawford, S.C., Bruell, C.J., Ryan, D.K., and Duggan, J.W. (1997), Effects of emulsion viscosity during surfactant-enhanced soil flushing in porous media, *J.Soil Contam.* 6(4), 355-370, 1058-8337.

Danzer, J., Grathwohl, P. (1998), Coupled transport of PAH and surfactant in natural aquifer material, *Phys. Chem. Earth.* 23, 237-243.

Danzer J., Totsche K. U., Kögel-Knabner I. (1993), Cotransport polyzyklischer aromatischer Kohlenwasserstoffe und gelöster organischer Substanz (DOM) in Laborbodensäulen; Mitt. Deutsch. Bodenk. Ges. 72, 81-84.

Danzer, J., Wu, B., Grathwohl, P., Sabatini, D.A. (1998), Surfactant enhanced attenuation/mobilization of tar oil and lubricating oil, in *Horizonte 2000, Kurzfassung der Vorträge und Poster, 6. Wolfgang-Ostwald-Kolloquium der Kolloid-Gesellschaft, 3. Nachwuchstage der Kolloid- und Grenzflächenforschung,* Haegel, F.-H., Lewandowski, H., Krahl-Urban, B. (Hrsg.), Jülich, S. 99.

Delshad, M., Pope, G.A., Sepehrnoori, K. (1996), A compositional simulator for modeling surfactant enhanced aquifer remediation .1. Formulation. *Journal of Contaminant Hydrology, 23,* (4), 303-327.

Di Corcia, A., Samperl, R., Marcomini, A. (1994), Monitoring aromatic surfactants and their biodegradation intermediates in raw and treated sewages by solid-hase extraction chromatography, *Environmental Science and Technology,* 28, 850-858.

Di Toro, D.M., Dodge, L.J., Hand, V.C. (1990), A Model for Anionic Surfactant Sorption. *Environmental Science and Technology,* 24, 1013-1020.

Dow Chemicals (1994) Safety Data Sheet.

Dow Chemicals (1996), Safety Data Sheet.

Drechsel, (1992), KAK-Bestimmung von karbonathaltigen Böden, Praktikumsscript Bodenanorganik, Lehrstuhl für Bodenkunde, Uni Bayreuth, unpublished.

Eberhard, Ch. (1995), Freisetzung von polyzyklischen aromatischen Kohlenwasserstoffen aus Teer und Kreosot, Diploma Thesis, unpublished, Applied Geology, University of Tuebingen.

Edwards, D.A., Adeel, Z., Luthy, R.G. (1994a), Distribution of Nonionic Surfactant and Phenanthrene in a Sediment/Aqueous System, *Environmental Science and Technology* 28, 1550-1560.

Edwards, D.A., Laha, S., Liu, Z., Luthy, R.G. (1992), Solubilisation and biodegradation of hydrophobic organic compounds in soil-aqueous systems with nonionic surfactants.- In: Transport and remediation of subsurface contaminants. Sabatini, D.A., Knox, R.C. (Eds.) American Cheical Society, Symposium Series 491, 124-132.

Edwards, D.A., Liu, Z., Luthy, R.G. (1994b), Experimental data and modeling for surfactant micelles, hocs, and soil, *Journal of Environmental Engineering,* 120, 23-41.

Edwards, D.A., Liu, Z., Luthy, R.G. (1994c), Surfactant solubilization of organic compounds in soil/aqueous systems, *Journal of Environmental Engineering,* 120, 5-22.

Edwards, D.A., Luthy, R.G., Liu, Z. (1991), Solubilization of Polycyclic Aromatic Hydrocarbons in Micellar Nonionic Surfactant Solution, *Environmental Science and Technology,* 25, 127-133.

Fetter, C.W. (1992), Contaminant Hydrogeology, Macmillan Publishing Company, New York, 458 p.

Finkel Michael (1999), Quantitative Beschreibung des Transports von polyzyklischen aromatischen Kohlenwasserstoffen (PAK) und Tensiden in porösen Medien, . *Tübinger Geowissenschaftliche Arbeiten* TGA C47, 98 p.

Fountain, J.C. (1997), The role of field trials in development and feasibility assessment of surfactant-enhanced aquifer remediation. *Water Environ Res, 69,* (2), 188-195.

Freundlich, H. (1909), Kapillarchemie, Akademische Verlagsgesellschaft m.b.H., Leipzig.

Gauthier, T.D., Seitz, W.R., Grant, C.L. (1987), Effects of structural and compositional variations of dissolved humic materials on pyrene K_{oc} values, *Environmental Science and Technology,* 21, 243-248.

Gauthier, T.D., Shane, E.C., Guerin, W.F., Seitz, W.R., Grant, C.L. (1986), Fluorescence quenching method for determining equilibrium constants for polycyclic aromatic hydrocarbons binding to dissolved humic materials, *Environmental Science and Technology,* 20, 1162-1166.

Grathwohl, P. (1998), Diffusion in natural porous media: Contaminant transport, sorption/desorption and dissolution kinetics, Kluwer Academic Publishers, Norwell, Massachusetts, USA.

Grathwohl, P., Reinhard, M. (1993), Desorption of trichloretylene in aquifer material: Rate limitation at the grain scale, *Environmental Science and Technology*, 27, 2360-2366.

Gregg, S.J., Sing, K.S.W. (1982), Adsorption, Surface Area and Porosity, Second Edition, Academic Press, New York, 303 p.

Haegel, F.H., 1997, personal communication.

Hayworth, J.S., Burris, D.R. (1997), Nonionic surfactant-enhanced solubilization and recovery of organic contaminants from within cationic surfactant-enhanced sorbent zones: 1. Experiments, *Environmental Science and Technology*, 31(5), 1277-1283.

Holsen, T.M., Taylor, E.T., Seo, Y.C., Anderson, P.R. (1991), Removal of sparingly soluble organic chemicals from aqueous solutions with surfactant-coated ferrihydrite, *Environmental Science and Technology*, 25, 1585-1589.

Hunter, R.J. (1989), Foundations in colloid science, Volume 2, Oxford Science Publications, Oxford, UK.

Imhoff, P.T., Miller, C.T. (1996), Dissolution fingering during the solubilization of nonaqueous phase liquids in saturated porous media . 1. Model predictions. *Water Resour Res* 32(7), 1919-1928.

Imhoff, P.T., Thyrum, G.P., Miller, C.T. (1996), Dissolution fingering during the solubilization of nonaqueous phase liquids in saturated porous media: 2. Experimental observations, *Water Resour Res*, 32(7), 1929-1942.

Israelachvili, J., Wennerström, H. (1996), Role of hydration and water structure in biological and colloidal interactions, *Nature* 379, 219-225.

Jafvert, C.T. (1991), Sediment- and Saturated-Soil-Associated Reactions Involving an Anionic Surfactant (Dodecylsulfate), 2. Partition of PAH Compounds among Phases. *Environmental Science and Technology*, 25, 1039-1045.

Jafvert, C.T., Heath, J.K. (1991), Sediment- and Saturated-Soil-Associated Reactions Involving an Anionic Surfactant (Dodecylsulfate), 1. Precipitation and micelle formation, *Environmental Science and Technology*, 25, 1031-1038.

Jafvert, C.T., Van Hoof, P.L., Heath, J.K. (1994), Solubilization of non-polar Compounds by non-ionic surfactant micelles. *Water Resources Research*, 28, 1009-1017.

Karickhoff, S.W., Brown, D.S., Scott, T.A. (1979), Sorption of hydrophobic pollutants on natural sediments.- Water Res., 13, 241-248.

Kile, D.E., Chiou, C.T. (1989), Water Solubility Enhancement of DDT and Trichlorbenzene by Some Surfactants Below and Above the Critical Micelle Concentration. *Environmental Science and Technology*, 23, 832-838.

Kile, D.E., Chiou, C.T. (1990), Effect of Some Petroleum Sulfonate Surfactants on the Apparent Water Solubility of Organic Compounds. *Environmental Science and Technology*, 24, 205-208.

Klein, R. (1998), Mechanische Bodenlockerungsverfahren zur Verbesserung der Sanierungseffizienz bei In-situ-Maßnahmen, . *Tübinger Geowissenschaftliche Arbeiten* TGA C37, 106 p.

Kleineidam, S. (1998), Der Einfluß von Sedimentologie und Sedimentpetrographie auf den Transport gelöster organischer Schadstoffe im Grundwasser - Laborversuche, *Tübinger Geowissenschaftliche Arbeiten* TGA C41, 80 p.

Kleineidamm, Sybille (1997), Applied Geology, University of Tübingen, personal communication.

Kleiner, Birgit (1994), Dow Europe, Horgen, Switzerland, personal communication.

Kleiner, Birgit (1996), Dow Europe, Horgen, Switzerland, personal communication.

Klier, J., Suarez, R.S., Green, D.P., Kumar, A.M., Hoffman, M., Tucker, C.J., Landes, B., Redwine, D. (1997), Cleaning properties of single-phase hydrocarbon-based microemulsion systems, *J Amer Oil Chem Soc*, 74(7), 861-867.

Kosswig , K., Stache, H. (1993), Die Tenside - Carl Hanser Verlag, München, Wien, 510 p.

Krebs-Yuill, B., Harwell, J.H., Sabatini, D.A., Knox, R.C. (1995), Economic considerations in surfactant enhanced pump-and-treat remediation, chapter 19 in *Surfactant-enhanced subsurface remediation*, Sabatini, D. A., Knox, R. C., Harwell, J. H. (Eds.), ACS Symposium Series 594, American Chemical Society, Washington, USA.

Lee, C. Yeskie, M.A., Harwll, J.H., O'Rear, E.A. (1990), Two-site adsolubilization model of incorporation of alcohols into adsorbed surfactant aggregates, *Langmuir*, 6, 1758-1762.

Lemp, Elvira, (1996), Versuche zur Auswirkung der mechanischen Bodenlockerung/ -homogenisierung auf die hydraulischen Parameter, Diploma Thesis, unpublished, Applied Geology, University of Tuebingen.

Li, Z.H., Bowman, R.S. (1997), Counterion effects on the sorption of cationic surfactant and chromate on natural clinoptilolite, *Environmental Science and Technology*, 31(8), 2407-2412.

Lösch, T. (1997), Bestimmung hydraulischer und hydrogeochemischer Parameter in fluvioglazialen Sanden, Diploma Thesis, unpublished, Applied Geology, University of Tuebingen.

Loyek, Diana (1997), Applied Geology, University of Tübingen, personal communication.

Loyek, D., Grathwohl, P. (1998a), Ermittlung und Reduzierung der Schadstoffemission bei teer- und teerölkontaminierten Böden. 1. Schadstoff-Freisetzung im Kontaminationsherd. Abschlußbericht zum PWAB-Projekt PD 94 159, Projekt Wasser-Abfall-Boden (PWAB), Kernforschungszentrum Karlsruhe.

Loyek, Diana (1998b), Löslichkeit und Lösungskinetik von polyzyklischen aromatischen Kohlenwasserstoffen (PAK) aus der Teerphase, *Tübinger Geowissenschaftliche Arbeiten* TGA C44, 81 p.

Mackay, D., Shiu, W.J. (1977), Aqueous solubility of polynuclear hydrocarbons, *J Chem. Eng. Data*, 22, 399-402.

Martin, P. (1997), Transportverhalten von Phenanthren an durch Tensidadsorption modifiziertem Aquifermaterial-Laboruntersuchungen, Diploma Thesis, unpublished, Applied Geology, University of Tuebingen.

Merkel, P. (1996), Desorption and release of polycyclic aromatic hydrocarbons (PAHs) from contaminated aquifer materials, *Tübinger Geowissenschaftliche Arbeiten*, TGA C32, Tübingen, Germany.

Menzie, C.A., Potocki, B.B., Santodonato, J. (1992), Exposure to carcinogenic PAHs in the environment, *Environ. Sci. Technol.*, 26, 1278-1284.

Miller, M.M., Wasik, S., Huang, G-L., Shiu, W-Y., Mackay, D.M. (1985), Relationship between octanol-water partition coefficient and aqueous solubility, *Environmental Science and Technology*, 19 (6), 522-529.

Muntzer, P. (1997), IFARE, Straßburg, personal communication.

Nayyar, S.P., Sabatini, D.A., Harwell, J.H. (1994), Surfactant adsolubilisation and modified admicellar sorption of nonpolar, polar, and ionizable organic contaminants, *Environmental Science and Technology* 28, 1874-1881.

Nivas, B.T., Sabatini, D.A., Shiau, B.-J., Harwell, J.H. (1996), Surfactant enhanced remediation of subsurface chromium contamination, *Water Resources*, 30, 511-520.

Nkedi-Kizza, P., Rao, P.S.C., Hornsby, A.G. (1987), Influence of Organic Cosolvents on Leaching of Hydrophobic Organic Chemicals through Soils, *Environmental Science and Technology*, 21, 1107-1111.

Ogata, A., Banks, R.G. (1961), A solution of the differential equation of longitudinal dispersion in porous media.- U.S Geological Survey Professional Paper 411 A, Washington D.C.

Okuda, I., Mcbride, J.F., Gleyzer, S.N., Miller, C.T. (1996), Physicochemical transport processes affecting the removal of residual DNAPL by nonionic surfactant solutions. *Environmental Science and Technology*, 30(6), 1852-1860.

Park, J.W., Jaffe, P.R. (1993), Partitioning of three nonionic organic compounds between adsorbed surfactants, micelles, and water, *Environmental Science and Technology*, 27, 2559-2565.

Penell, K.D, Pope, G.A., Abriola, L.M. (1996) Influence of viscous and buoyancy forces on the mobility of residual tetrachloroethylene during surfactant flushing, *Environmental Science and Technology* 30, 1328-1335.

Pennell, K.D., Adinolfi, A.M., Abriola, L.M., Diallo, M.S. (1997), Solubilization of dodecane, tetrachloroethylene, and 1,2-dichlorobenzene in micellar solutions of ethoxylated nonionic surfactants. *Environmental Science and Technology*, 31, (5), 1382-1389.

Pennell, K.D., Jin, M., Abriola, L.M., Pope, G.A. (1994), Surfactants enhanced remediation of soil columns contaminated by residual tetrachloroethylene. *Journal of Contaminant Hydrology, 16*, 35-53.

Pyka, W. (1994), Freisetzung von Teerinhaltsstoffen aus residualer Teerphase in das Grundwasser: Laboruntersuchungen zur Lösungsrate und Lösungsvermittlung, *Tübinger Geowissenschaftliche Arbeiten*, TGA C21, 76 p.

Renshaw, C.E., Zynda, G.D., Fountain, J.C. (1997), Permeability reductions induced by sorption of surfactant. *Water Resour Res, 33*, (3), 371-378.

Rosen, M. J. (1989), Surfactants and interfacial phenomena, 2nd Edition, John Wiley & Sons, New York.

Rouse, J.D., Sabatini, D.A. (1993), Minimizizing Surfactant Losses Using Twin-Head Anionic Surfactants in Subsurface Remediation, *Environmental Science and Technology*, 27, 2072-2078.

Rouse, J.D., Sabatini, D.A., Brown, R.E., Harwell, J.H. (1996), Evaluation of ethoxylated alkylsulfate surfactants for use in subsurface remediation, *Water Environment Research*, 68, 162-168.

Rouse, J.D., Sabatini, D.A., Deeds, N.E., Brown, E., Harwell, J.H. (1995), Micellar solubilization of unsaturated hydrocarbon concentrations as evaluated by semiequilibrium dialysis, *Environmental Science and Technology*, 29, 2484-2489.

Rouse, J.D., Sabatini, D.A., Suflita, J.M., Harwell, J.H. (1994), Influence of surfactants on microbial degradation of organic compounds. *Critical Reviews in Environmental Science and Technology*, 24(4),325-370.

Rügner, H. (1998), Einfluß der Aquiferlithologie auf die Sorption organischer Schadstoffe. *Tübinger Geowissenschaftliche Arbeiten* TGA, C39, 78 p.

Sabatini, 1997, personal communication.

Sabatini, D.A., Austin, T.Al (1991), Charakteristics of Rhodamine WT and Fluorescein as Adsorbing Ground-Water Tracers, *Ground Water* Vol.29, No 3, 341-349.

Sahoo, D., Smith, J.A. (1997), Enhanced trichloroethene desorption from long-term contaminated soil using Triton X-100 and pH increases. *Environmental Science and Technology, 31*, (7), 1910-1915.

Saripalli, K.P., Kim H., Rao, P.S.C., Annable, M.D. (1997), Measurement of specific fluid-fluid interfacial areas of immiscible fluids in porous media, *Environmental Science and Technology*, 31(3), 932-936.

Schiau, B.-J., Sabatini, D.A., Harwell, J.H. (1993), Influence of Rhodamine WT Properties on Sorption and Transport in Subsurface Media, *Ground Water* 31(6), 913- 920.

Schüth, Ch. (1994), Sorptionskinetik und Transportverhalten von polyzyklischen aromatischen Kohlenwasserstoffen (PAK) im Grundwasser-Laborversuche, *Tübinger Geowissenschaftliche Arbeiten*, TGA C19, 80 p.

Schwarzenbach, R.P., Gschwend, P.M., Imboden, D.M. (1993), Environmental organic chemistry.- John Wiley & Sons, New York, USA, 681 S.

Shiau, B.-J., Sabatini, D.A. (1995), Properties of food grade (edible) surfactants affecting subsurface remediation of chlorinated solvents, *Environmental Science and Technology*, 29, 2929-2935.

Shiau, B.-J., Sabatini, D.A., Harwell, J.H. (1994), Solubilization and microemulsification of chlorinated solvents using direct dood additive (edible) surfactants. *Groundwater* 32, 561-569.

Shiau, B.-J., Sabatini, D.A., Harwell, J.H., Vu D.Q. (1996), Microemulsion of mixed chorinated solvents using food grade (edible) surfactants, *Environmental Science and Technology*, 30, 97-103.

Siegenthaler, Ch., Huggenberger, P. (1992), in Best, J., Bristow, Ch. (Eds), Braided Rivers, 147-162.

Sims, R.C., Overcash, M.R. (1983), Fate of polynuclear aromatic compounds (PNA) in soil-plant systems, *Residue Reviews*, 88, Springer Verlag N.Y. Inc, 1-68.

Soerens, T.S., Sabatini, D.A. (1994), Cosolvency Effects on Sorption of a Semipolar, Ionogenic Compound (Rhodamine WT) with Subsurface Materials.- Environ. Sci. Technol., Vol 28, No. 6, 1010-1014.

Strobel, Helmut (1996), Sorption eines reaktiven Tracers (Rhodamin WT) in heterogenem Aquifermaterial vom Testfeld "Horkheimer Neckarinsel", Diploma Thesis, unpublished, Applied Geology, University of Tuebingen.

Stumm, W. (1992), Chemistry of the solid-water interface, John Wiley & Sons, New York, USA, 428 p.

Sun, S., Boyd, S.A. (1993), Sorption of organic compounds in soil-water systems containig petroleum sulfonate-oil surfactants, Environmental Science and Technology 27, 1340-1346.

Sun, S., Inskeep, W.P., Boyd, S.A. (1995), Sorption of nonionic organic compounds in soil-water systems containing a micelle-forming surfactant, Environmental Science and Technology, 29, 903-913.

Sun, S., Jaffe, P.R. (1996), Sorption of phenanthrene from water onto alumina coated with dianionic surfactants, Environmental Science and Technology, 30, 2606-2913.

Terton, H. (1994), Auswirkungen der lithologischen Zusammensetzung des Horkheimer Aquifermaterials auf die Sorption von Phenanthren, Diploma Thesis, unpublished, Applied Geology, University of Tuebingen.

Teutsch, G., Kobus, H. (1990), The environmental research field site "Horkheimer Neckarinsel", IAHR Journal of Hydraulic Research, 28, 491-501.

Tiehm, A., Stieber, M., Werner, P., Frimmel, F.H. (1997), Surfactant-enhanced mobilization and biodegradation of polycyclic aromatic hydrocarbons in manufactured gas plant soil. Environmental Science and Technology, 31(9), 2570-2576.

Totsche, K.U., Danzer, J., Kogel-Knabner, I. (1997), Dissolved organic matter-enhanced retention of polycyclic aromatic hydrocarbons in soil miscible displacement experiments. J Environ Qual, 26, (4), 1090-1100.

Wagner, J., Chen, H., Brownawell, B.J., Westall, J.C. (1994), Use of Cationic Surfactants to Modify Soil Surfaces to Promote Sorption and Retard Migration of Hydrophobic Organic Compounds. Environmental Science and Technology, 28, 231-237.

West, C.C., Harwell, J.H. (1992), Surfactants and Subsurface Remediation. Environmental Science and Technology, 26, 2324-2330.

Wu, J., Harwell, J.H., O'Rear, E.A. (1987), Two dimensional reaction solvents: Surfactant bilayers in the formation of ultrathin films. Langmuir, 3, 531-537.

Yalkowsky, S.H.,Valvani, S.C. (1979), Solubilities and partitioning - 2. Relationships between aquoeus solubilities, partition coefficients and molecular surface areas of rigid aromatic hydrocarbons, J. Chem. Eng. Data, 24, 127-129.

Yeom, I.T., Ghosh, M.M., Cox, C.D., Robinson, K.G. (1995), Micellar solubilization of polynuclear aromatic hydrocarbons in coal tar-contaminated soils, Environmental Science and Technology, 30, 3015-3021.

In der Reihe C der Tübinger Geowissenschaftlichen Arbeiten (TGA) sind bisher erschienen:

Nr. 1: Grathwohl, Peter (1989): Verteilung unpolarer organischer Verbindungen in der wasserungesättigten Bodenzone am Beispiel der leichtflüchtigen aliphatischen Chlorkohlenwasserstoffe. 102 S.

Nr. 2: Eisele, Gerhard (1989): Labor- und Felduntersuchungen zur Ausbreitung und Verteilung leichtflüchtiger chlorierter Kohlenwasserstoffe (LCKW) im Übergangsbereich wasserungesättigte/wassergesättigte Zone. 84 S.

Nr. 3: Ehmann, Michael (1989): Auswirkungen atmogener Stoffeinträge auf Boden- und Grundwässer sowie Stoffbilanzierungen in drei bewaldeten Einzugsgebieten im Oberen Buntsandstein (Nordschwarzwald). 134 S.

Nr. 4: Irouschek, Thomas (1990): Hydrogeologie und Stoffumsatz im Buntsandstein des Nordschwarzwaldes. 144 S.

Nr. 5: Sanns, Matthias (1990): Experimentelle Untersuchungen zum Ausbreitungsverhalten von leichtflüchtigen Chlorkohlenwasserstoffen (LCKW) in der wassergesättigten Zone. 122 S. **(Vergriffen!)**

Nr. 6: Seeger, Thomas (1990): Abfluß- und Stofffrachtseparation im Buntsandstein des Nordschwarzwaldes. 154 S.

Nr. 7: Einsele, Gerhard & Pfeffer, Karl-Heinz (Hrsg.) (1990): Untersuchungen über die Auswirkungen des Reaktorunfalls von Tschernobyl auf Böden, Klärschlamm und Sickerwasser im Raum von Oberschwaben und Tübingen. 151 S.

Nr. 8: Douveas, Nikon G. (1990): Verwitterungstiefe und Untergrundabdichtung beim Talsperrenbau in dem verkarsteten Nord-Pindos-Flysch (Projekt Pigai-Aoos, NW-Griechenland). 165 S.

Nr. 9: Schlöser, Heike (1991): Quantifizierung der Silikatverwitterung in karbonatfreien Deckschichten des Mittleren Buntsandsteins im Nordschwarzwald. 93 S.

Nr. 10: Köhler, Wulf-Rainer (1992): Beschaffenheit ausgewählter, nicht direkt anthropogen beeinflußter oberflächennaher und tiefer Grundwasservorkommen in Baden-Württemberg. 144 S.

Nr. 11: Bundschuh, Jochen (1991): Der Aquifer als thermodynamisch offenes System. - Untersuchungen zum Wärmetransport in oberflächennahen Grundwasserleitern unter besonderer Berücksichtigung von Quellwassertemperaturen (Modellversuche und Geländebeispiele). 100 S.

Nr. 12: Herbert, Mike (1992): Sorptions- und Desorptionsverhalten von ausgewählten polyzyklischen aromatischen Kohlenwasserstoffen (PAK) im Grundwasserbereich. 111 S.

Nr. 13: Sauter, Martin (1993): Quantification and forecasting of regional groundwater flow and transport in a karst aquifer (Gallusquelle, Malm, SW-Germany. 150 S.

Nr. 14: Bauer, Michael (1993): Wasserhaushalt, aktueller und holozäner Lösungsabtrag im Wutachgebiet (Südschwarzwald). 130 S.

Nr. 15: Einsele, Gerhard & Ricken, Werner (Hrsg.) (1993): Eintiefungsgeschichte und Stoffaustrag im Wutachgebiet (SW-Deutschland). 215 S.

Nr. 16: Jordan, Ulrich (1993): Die holozänen Massenverlagerungen des Wutachgebietes (Südschwarzwald). 132 S.

Nr. 17: Krejci, Dieter (1994): Grundwasserchemismus im Umfeld der Sonderabfalldeponie Billigheim und Strategie zur Erkennung eines Deponiesickerwassereinflusses. 121 S.

Nr. 18: Hekel, Uwe (1994): Hydrogeologische Erkundung toniger Festgesteine am Beispiel des Opalinustons (Unteres Aalenium). 170 S.

Nr. 19: Schüth, Christoph (1994): Sorptionskinetik und Transportverhalten von polyzyklischen aromatischen Kohlenwasserstoffen (PAK) im Grundwasser - Laborversuche. 80 S.

Nr. 20: Schlöser, Helmut (1994): Lösungsgleichgewichte im Mineralwasser des überdeckten Muschelkalks in Mittel-Württemberg. 76 S.

Nr. 21: Pyka, Wilhelm (1994): Freisetzung von Teerinhaltsstoffen aus residualer Teerphase in das Grundwasser: Laboruntersuchungen zur Lösungsrate und Lösungsvermittlung. 76 S.

Nr. 22: Biehler, Daniel (1995): Kluftgrundwässer im kristallinen Grundgebirge des Schwarzwaldes – Ergebnisse von Untersuchungen in Stollen. 103 S.

Nr. 23: Schmid, Thomas (1995): Wasserhaushalt und Stoffumsatz in Grünlandgebieten im württembergischen Allgäu. 145+ 92 S.

Nr. 24: Kretzschmar, Thomas (1995): Hydrochemische, petrographische und thermodynamische Untersuchungen zur Genese tiefer Buntsandsteinwässer in Baden-Württemberg. 142 S.

Nr. 25: Hebestreit, Christoph (1995): Zur jungpleistozänen und holozänen Entwicklung der Wutach (SW-Deutschland). 88 S.

Nr. 26: Hinderer, Matthias (1995): Simulation langfristiger Trends der Boden- und Grundwasserversauerung im Buntsandstein-Schwarzwald auf der Grundlage langjähriger Stoffbilanzen. 175 S.

Nr. 27: Körner, Johannes (1996): Abflußbildung, Interflow und Stoffbilanz im Schönbuch Waldgebiet. 206 S.

Nr. 28: Gewald, Thomas (1996): Der Einfluß der Desorptionskinetik bei der Freisetzung von Trichlorethen (TCE) aus verschiedenen Aquifersanden. 67 S.

Nr. 29: Schanz, Ulrich (1996): Geophysikalische Untersuchungen im Nahbereich eines Karstsystems (westliche Schwäbische Alb). 114 S.

Nr. 30: Renner, Sven (1996): Wärmetransport in Einzelklüften und Kluftaquiferen - Untersuchungen und Modellrechnungen am Beispiel eines Karstaquifers. 89 S.

Nr. 31: Mohrlok, Ulf (1996): Parameter-Identifikation in Doppel-Kontinuum-Modellen am Beispiel von Karstaquiferen. 125 S.

Nr. 32: Merkel, Peter (1996): Desorption and Release of Polycyclic Aromatic Hydrocarbons (PAHs) from Contaminated Aquifer Materials. 76 S.

Nr. 33: Schiedek, Thomas (1996): Auftreten und Verhalten von ausgewählten Phthalaten in Wasser und Boden. 112 S.

Nr. 34: Herbert, Mike & Teutsch, Georg (Hrsg.) (1997): Aquifersysteme Südwestdeutschlands - Eine Vorlesungsreihe an der Eberhard-Karls-Universität Tübingen. 162 S.

Nr. 35 Schad. Hermann (1997): Variability of Hydraulic Parameters in Non-Uniform Porous Media: Experiments and Stochastic Modelling at Different Scales. 233 S.

Nr. 36 Herbert. Mike & Kovar. Karel (Eds.) (1998): GROUNDWATER QUALITY 1998: Remediation and Protection - Posters - - Proceedings of the GQ'98 conference, Tübingen, Sept. 21-25, 1998, Poster Papers. 146 S.

Nr. 37 Klein, Rainer (1998): Mechanische Bodenbearbeitungsverfahren zur Verbesserung der Sanierungseffizienz bei In-situ-Maßnahmen. 106 S.

Nr. 38 Schollenberger, Uli (1998): Beschaffenheit und Dynamik des Kiesgrundwassers im Neckartal bei Tübingen. 74 S.

Nr. 39 Rügner. Hermann (1998): Einfluß der Aquiferlithologie des Neckartals auf die Sorption und Sorptionskinetik organischer Schadstoffe. 78 S.

Nr. 40 Fechner. Thomas (1998): Seismische Tomographie zur Beschreibung heterogener Grundwasserleiter. 113 S.

Nr. 41 Kleineidam, Sybille (1998): Der Einfluß von Sedimentologie und Sedimentpetrographie auf den Transport gelöster organischer Schadstoffe im Grundwasser. 82 S.

Nr. 42 Hückinghaus, Dirk (1998): Simulation der Aquifergenese und des Wärmetransports in Karstaquiferen. 124 S.

Nr. 43 Klingbeil, Ralf (1998): Outcrop Analogue Studies - Implications for Groundwater Flow and Contaminant Transport in Heterogeneous Glaciofluvial Quaternary Deposits. 111 S.

Nr. 44 Loyek. Diana (1998): Die Löslichkeit und Lösungskinetik von polyzyklischen aromatischen Kohlenwasserstoffen (PAK) aus der Teerphase. 81 S.

Nr. 45 Weiß, Hansjörg (1998): Säulenversuche zur Gefarhrenbeurteilung für das Grundwasser an PAK-kontaminierten Standorten. 111 S.

Nr. 46 Jianping Yan (1998): Numerical Modeling of Topographically-closed Lakes: Impact of Climate on Lake Level, Hydrochemistry and Chemical Sedimentation. 144 S.

Nr. 47 Finkel, Michael (1999): Quantitative Beschreibung des Transports von polyzyklischen aromatischen Kohlenwasserstoffen (PAK) und Tensiden in porösen Medien. 98 S.

Nr. 48 Jaritz, Renate (1999): Quantifizierung der Heterogenität einer Sanbsteinmatrix (Mittlerer Keuper, Württemberg). 106 S.